AD-A075 390 SCIENCE APPLICATIONS INC EL SEGUNDO CALIF F/G 4/2
RAIN ATTENUATION OVER EARTH-SATELLITE PATHS.(U)
MAY 79 N E FELDMAN
UNCLASSIFIED SAI-171-80-573-LA N00039-79-C-0136
NL

1 OF 2
AD A075390

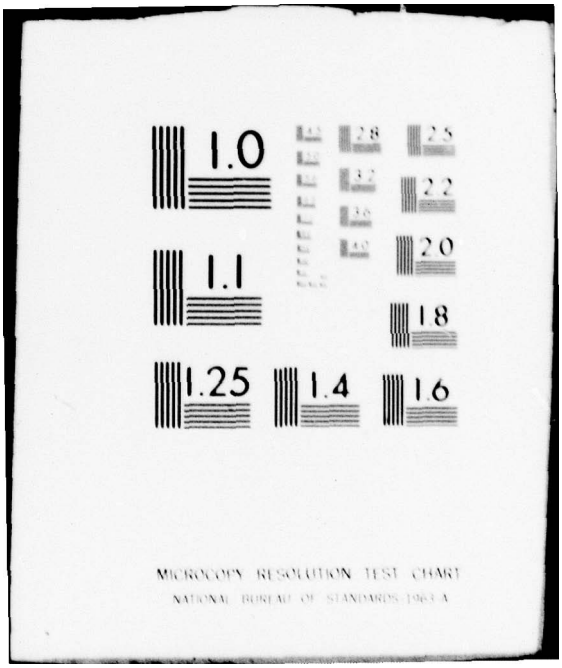
1.0
1.1
1.25
1.4
1.6
2.8
2.5
2.2
2.0
1.8
MICROCOPY RESOLUTION TEST CHART
NATIONAL BUREAU OF STANDARDS 1963 A

LEVEL II

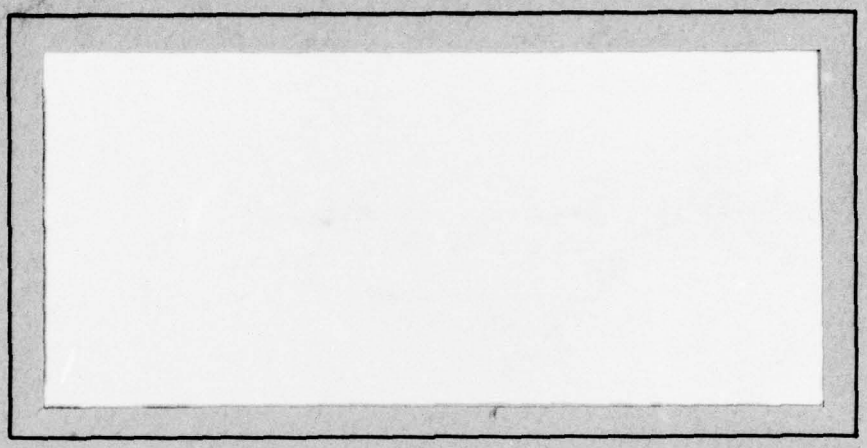

SAI

SCIENCE APPLICATIONS, INC.

UNCLASSIFIED

SECURITY CLASSIFICATION OF THIS PAGE (When Data Entered)

REPORT DOCUMENTATION PAGE

READ INSTRUCTIONS BEFORE COMPLETING FORM

1. REPORT NUMBER: SAI-171-80-573-LA
2. GOVT ACCESSION NO.:
3. RECIPIENT'S CATALOG NUMBER:

4. TITLE (and Subtitle): RAIN ATTENUATION OVER EARTH-SATELLITE PATHS.

5. TYPE OF REPORT & PERIOD COVERED: FINAL REPORT 12/27/78 to 5/25/79

6. PERFORMING ORG. REPORT NUMBER:

7. AUTHOR(s): NATHANIEL E. FELDMAN

8. CONTRACT OR GRANT NUMBER(s): N00039-79-C-0136

9. PERFORMING ORGANIZATION NAME AND ADDRESS:
Science Applications, Inc.
1801 Avenue of the Stars, Suite 1201
Los Angeles, California 90067 El Segundo

10. PROGRAM ELEMENT, PROJECT, TASK AREA & WORK UNIT NUMBERS: Satellite Communications

11. CONTROLLING OFFICE NAME AND ADDRESS:
NAVAL ELECTRONICS SYSTEMS COMMAND
Washington, D.C. 20360
Attn: ADVANCED SATCOM SYSTEMS, PME-106-15

12. REPORT DATE: May 1979 (12) 153

13. NUMBER OF PAGES: 151

14. MONITORING AGENCY NAME & ADDRESS (if different from Controlling Office): Final rept. 27 Dec 78 - 25 May 79

15. SECURITY CLASS. (of this report): Unclassified

15a. DECLASSIFICATION/DOWNGRADING SCHEDULE:

16. DISTRIBUTION STATEMENT (of this Report)

Approved for public release; distribution unlimited

DDC RECEIVED OCT 23 1979 A

17. DISTRIBUTION STATEMENT (of the abstract entered in Block 20, if different from Report)

18. SUPPLEMENTARY NOTES

To be published as a paper entitled "Rain Attenuation Over Earth-Satellite Paths: A Seasonal, Oceanic Model" at the AIAA 8th Communications Satellite Systems Conference.

19. KEY WORDS (Continue on reverse side if necessary and identify by block number)

seasonal, oceanic rain model
precipitation attenuation
rain outage duration

20. ABSTRACT (Continue on reverse side if necessary and identify by block number)

This analysis of precipitation-attenuation over earth-satellite paths extends R.K. Crane's model by correcting for measured total rainfall and frequency of occurrence. The authors convert Crane's model to a seasonal one and extend it up to 36 percent of the time. Four seasonal world maps show the location of the nine precipitation rate regions and another four show mean freezing height. A method for estimating the outage duration distribution is proposed and used to determine the mean daily outage duration and the number of outages per day.

DD FORM 1 JAN 73 1473 EDITION OF 1 NOV 65 IS OBSOLETE S/N 0102-LF-014-6601

UNCLASSIFIED 407 842

SECURITY CLASSIFICATION OF THIS PAGE (When Data Entered)

Science Applications, Inc.
One Continental Plaza, Suite 310
101 Continental Boulevard
El Segundo, California 90245

RAIN ATTENUATION OVER EARTH-SATELLITE PATHS

CONTRACT N00039-79-C-0136

FINAL REPORT
SAI-171-80-573-LA
MAY 1979

PREPARED FOR:

DEPARTMENT OF THE NAVY
NAVAL ELECTRONIC SYSTEMS COMMAND
WASHINGTON, D.C. 20360

PREPARED BY:

NATHANIEL E. FELDMAN
CHIEF SCIENTIST, SYSTEMS RESEARCH OPERATION
SCIENCE APPLICATIONS, INC.
101 CONTINENTAL BLVD., SUITE 310
EL SEGUNDO, CALIFORNIA 90245

TABLE OF CONTENTS

PREFACE i
SUMMARY ii
LIST OF FIGURES viii
LIST OF TABLES xii

1.0 INTRODUCTION 1
1.1 Excess Path Attenuation 1
1.2 Why We Must Model Rain Attenuation 2
1.3 Rain Versus Precipitation 3

2.0 THE CRANE MODEL FOR RAIN ATTENUATION OVER EARTH-SATELLITE PATHS 4
2.1 Description of The Model 4
2.2 Results Based on Crane's Model 12

3.0 EXTENSIONS AND MODIFICATIONS TO THE CRANE MODEL 31
3.1 Rationale for Changes 32
3.1.1 Ocean Distribution of Climate Regions 33
3.1.2 Seasonal Variation of Climate 34
3.1.3 Variation in Mean Freezing Height 43
3.2 Proposed Seasonal Oceanic Precipitation-Rate Climate Model 43
3.2.1 Seasonal Maps of Oceanic Precipitation-Rate Regions 45
3.2.2 Seasonal Maps of Mean Freezing Height 49
3.3 Modified Precipitation-Rate Distributions 49
3.3.1 Procedure for Modifying the Distributions 60
3.3.2 Consistency of Modified Distributions with Climate Type Criteria 62

4.0 APPLICATION OF PROPOSED OCEANIC MODEL TO 13 SELECTED LOCATIONS 67
4.1 Inclusion of the Local Precipitation Rate Correction Factor, k 67
4.2 Seasonal Extremes of Attenuation - Results 68

5.0 OUTAGE DURATION STATISTICS 114
5.1 Local Precipitation Frequency Correction Factor, k' 114
5.2 Link Margin Exceedance Probabilities 116
5.3 Estimating Precipitation Durations 116

TABLE OF CONTENTS (con't)

6.0 CONCLUSIONS AND FUTURE WORK 131

6.1 Conclusions 132

6.2 Future Work 134

REFERENCES 136

PREFACE

This analysis of rain attenuation over earth-satellite paths for ocean and coastal terminals was performed for NAVELEX, Advanced SATCOM Systems, C. J. Waylan, CDR, USN, Code PME-106-15 under contract N00039-79-C-0136. Michael A. Plunkett, Code 106-1521, directed the task. Ronald B. Luftman was the Contracting Officer and Betty McWhirt was the Purchasing Office Representative for this procurement. Principal investigator at SAI was Nathaniel E. Feldman, Chief Scientist of the Systems Research Operation. The following SAI consultants were key contributors to this analysis: Ralph E. Huschke, Howland H. Bailey, and Izhak Rubin. Mr. Huschke provided the basic meteorological inputs to the study and drafted section 3.0. Dr. Bailey analyzed the equation and required inputs to the Crane precipitation-rate region model used as the starting point for this study. He selected the cases to be run, and presented and interpreted the results. Dr. Rubin generated a mathematical formulation of the approach and guided the statistical presentation of the final results so that they would constitute suitable inputs to any further analysis. Ronald V. Harper did some analysis, Michael A. Morris did the programming and numerous other SAI personnel provided research support.

SUMMARY

This report utilizes readily available meteorological data to refine the best of the existing rain models, one proposed by R.K. Crane, for attenuation over earth-satellite paths from ocean and coastal terminals. The report presents a clear, tutorial explanation of both the original and refined models. The results are expressed in detailed graphs covering all key parameters. Thus this report is a handbook which presents engineers with the best available estimates of attenuation distributions over earth-satellite paths. It should prove a valuable aid in selecting satellite constellations and in designing earth-satellite links.

Because it makes no sense to use a world-average precipitation rate when a captain knows where his ship is, we retained Crane's division of the earth's surface into precipitation-rate regions, but increased the number from eight to nine regions. Since the captain knows what month it is, it makes no sense to lump the rainy and dry seasons together. We have separated them. Thus the attenuations are a function of latitude, longitude and season of the year. We accounted for local variation from point to point within a climatic region by adjusting parameters to match known data at the selected locations. Frequency and elevation angle were explicitly included in Crane's original model. Although the frequencies of interest in this report are 240 and 340 MHz, 7.5, 8.2, 21, 40, 41, 43 and 45 GHz, precipitation attenuation is negligible below 1 GHz. We examined elevation angles from 10 to 90 degrees, but emphasized 10, 20, and 30 degrees. The one-minute surface point precipitation-rate distributions have been extended down to 0.1 or 0.05 mm/hr, which are values that approximate the smallest rates of observed precipitation. The extension of the surface point precipitation rates to the minimum observable amount extends the model from 2 percent to as much as 35 percent of the year region. At these percentages of the time, cloud attenuation at low elevation angles and millimeter-wave frequencies might be

as significant as the precipitation attenuation over the path, but this effect has not been quantitatively included.

Results of interest to the system designer and the system user extend beyond the cumulative outage. Thus, we examine the division of the cumulative outage -- outage duration distributions conclude this report.

The refined oceanic precipitation model developed in this study provides estimates of the slant path attenuation through the atmosphere over a wider range of frequency of occurrence and precipitation rates than has appeared in the literature. At one end of the scale, we cover extreme events which are infrequent and short-lived, i.e., which occur only 0.001 percent of the season which corresponds to a total of 1.3 minutes per season. At the other end of the scale, we cover commonplace events, i.e., light drizzles which occur about 6 to 36 percent of the season. (These percentages correspond to a total of 130 to 790 hours per season and spread uniformly throughout the season, would occur 1.4 to 9 hours per day.) These latter percentages correspond to the minimum observable or the minimum measurable precipitation rates for precipitation gauges in widespread use. This limit is about 0.05 mm/hr for snow and 0.1 to 0.25 mm/hr for rain. While only the commonplace events are the focus of this study, the entire range had to be covered to check the consistency of the model, e.g., to verify that the integrated precipitation matched the seasonally measured data.

Using this seasonal model, we find that the Sep-Nov period is the worst season in the North Atlantic, the Mar-May period is the mildest and that the difference between them is large. At 44 GHz and 20° elevation, 1.1 dB is exceeded less that 10 percent of the time in the worst season and 4 dB less than 1 percent of the time. In the Persian Gulf, however, there is little difference between the best and worst seasons of the year.

For the worst season of the year at each location, the table which follows summarizes the attenuations at 44 GHz and 20° elevation angle. The correction for total amount of precipitation is already included in the figures from which this data was taken.

Precipitation Margin Requirements for Thirteen Selected Locations (dB)

Location	Availability (percent): Cumulative Outage ("):	99.9 0.1	99.0 1.0	90.0 10.0
# 1	Mid-Atlantic	32	13	4.4
# 2	North Atlantic	13	4.1	1.1
# 3	Mediterranean	25	8.7	1.3
# 4	Persian Gulf	19	7.3	1.4
# 5	Indian Ocean	108*	40*	8.6*
# 6	W. Australia	34	13	2.2
# 7	East Indies	127*	40*	6.9*
# 8	Philippines	100*	31*	5.0*
# 9	Sea of Japan	60	22	4.6
#10	Bering Sea	12	4.8	1.3
#11	N.E. Pacific	43	15	3.5
#12	Hawaii	41	15	3.5
#13	Panama	130*	41*	6.6*

In the table, the four highest attenuation values for each cumulative outage level are marked with an asterisk. Note the dramatic change in precipitation margin depending on whether one requires 99.9 percent availability, or only 99 to 90 percent. The table which follows indicates the range of the four highest attenuation values and their design implications.

Highest Precipitation Margin Requirements
and Their Design Implications
(44 GHz, 20° elevation, worst season)

Cumulative Outage (percent)	0.1	1	10
Precipitation Margin, dB	100 to 130	30 to 40	5 to 9
Design Implications	Probably technically and economically infeasible unless there are exceptional circumstances, e.g., if greatly restricted coverage area were acceptable.	Large satellite investment required but technically feasible.	Readily achievable with current technology for a modest incremental cost.

From the above estimates, one concludes that reasonable downlink precipitation margins of 10 to 15 dB will provide availabilities over 90 percent. That such high availability could be achieved at 44 GHz and 20° elevation angle with only 10 to 15 dB margin was an unexpected conclusion. While this conclusion remains tentative because of the quick-response nature of this study, such a conclusion makes it particularly important to further refine the model.

Rather than terminate the study with these estimates of cumulative outage, we chose to go one step further and examine the outage durations which make up the cumulative outage. We computed the probability density function for the outage durations for three locations (Figures 80 to 82). To estimate, for example, the relative probability of an outage of 30 to 60 minutes duration, one need only compare the relative area under the curves. Thus one can compare a 15 dB margin to a 10 dB margin or a 30° elevation angle to a 10° angle. Using this information, we computed the mean (average) outage duration and the average number of outages per day.

As an example, consider the rainest season in a high rain rate area like the Philippines. With 10 dB margin at 44 GHz and 10^{o} elevation the average outage lasts 72 minutes, but a 15 dB margin reduces the average outage to 41 minutes. With 10 dB margin at 30^{o} elevation, however, the average outage lasts only 9 minutes. A 15 dB margin now reduces the average outage to 6 minutes. Furthermore, there would be an average of less than two such outages per day. We consider this analysis of outage durations a fitting conclusion to any discussion of precipitation outage.

LIST OF FIGURES

1.	Rain Rate Climate Regions	5
2.	Cumulative Distributions of One-Minute Surface Rain Rates for Eight Climatic Regions	7
3.	Log-Log Plot of Cumulative Distributions of Precipitation Rate	8
4.	Attenuation Distributions from Crane's Model for f = 7.5 GHz, $\theta = 10^{o}$	15
5.	" " " for f = 7.5 GHz, $\theta = 20^{o}$	16
6.	" " " for f = 7.5 GHz, $\theta = 30^{o}$	17
7.	" " " for f = 21 GHz, $\theta = 10^{o}$	18
8.	" " " for f = 21 GHz, $\theta = 20^{o}$	19
9.	" " " for f = 21 GHz, $\theta = 30^{o}$	20
10.	" " " for f = 40 GHz, $\theta = 10^{o}$	21
11.	" " " for f = 40 GHz, $\theta = 20^{o}$	22
12.	" " " for f = 40 GHz, $\theta = 30^{o}$	23
13.	Attenuation Exceeded 1% of the Year vs. Elevation Angle from Crane's Model for $C_{\Lambda = 60^{o}}$ (also for A, B)	24
14.	Attenuation Exceeded 1% of the Year vs. Elevation Angle from Crane's Model for Region D (also $C_{\Lambda=30^{o}}$, F)	25
15.	Attenuation Exceeded 1% of the Year vs. Elevation Angle from Crane's Model for Region G (also E, H)	26
16.	Attenuation Exceeded 1% of the Year vs. Frequency from Crane's Model for $\theta = 10^{o}$	28
17.	" " for $\theta = 20^{o}$	29
18.	" " for $\theta = 30^{o}$	30
19.	Superposition of Average Daily Precipitation, Precipitation Frequency and Average Cloud Cover for December-February	35
20.	" " for March-May	36

LIST OF FIGURES (con't)

21. Superposition of Average Daily Precipitation, Precipitation Frequency and Average Cloud Cover for June-August 37

22. " " " for September-November 38

23. Location of the Thirteen Points Examined 41

24. Freezing Height Variation 44

25. Precipitation Amount and Frequency Bounds for the Climatic Regions 48

26. Ocean Climate Regions for Dec. through Feb. 50

27. " " " for Mar. through May 51

28. " " " for Jun. through Aug. 52

29. " " " for Sep. through Nov. 53

30. Average Freezing Height (km) for Dec. through Feb. 54

31. " " " for Mar. through May 55

32. " " " for Jun. through Aug. 56

33. " " " for Sep. through Nov. 57

34. Cumulative Distributions of One-Minute Surface Precipitation Rates, Proposed Model 61

35. Seasonal Maximum and Minimum Attenuation exceedance Probabilities for Loc. #1, Mid-Atlantic, $\theta = 10^{o}$ 70

36. " " for Loc. #1, Mid-Atlantic, $\theta = 20^{o}$ 71

37. " " for Loc. #1, Mid-Atlantic, $\theta = 30^{o}$ 72

38. " " for Loc. #2, North Atlantic, $\theta = 10^{o}$ 73

39. " " for Loc. #2, North Atlantic, $\theta = 20^{o}$ 74

40. " " for Loc. #2, North Atlantic, $\theta = 30^{o}$ 75

41. " " for Loc. #3, Mediterranean, $\theta = 10^{o}$ 76

42. " " for Loc. #3, Mediterranean, $\theta = 20^{o}$ 77

43. " " for Loc. #3, Mediterranean, $\theta = 30^{o}$ 78

LIST OF FIGURES (con't)

44.	Seasonal Maximum and Minimum Attenuation Exceedance Probabilities for Loc. #4, Persian Gulf, $\theta = 10^{o}$	79
45.	" " for Loc. #4, Persian Gulf, $\theta = 20^{o}$	80
46.	" " for Loc. #4, Persian Gulf, $\theta = 30^{o}$	81
47.	" " for Loc. #5, Indian Ocean, $\theta = 10^{o}$	82
48.	" " for Loc. #5, Indian Ocean, $\theta = 20^{o}$	83
49.	" " for Loc. #5, Indian Ocean, $\theta = 30^{o}$	84
50.	" " for Loc. #6, W. Australia, $\theta = 10^{o}$	85
51.	" " for Loc. #6, W. Australia, $\theta = 20^{o}$	86
52.	" " for Loc. #6, W. Australia, $\theta = 30^{o}$	87
53.	" " for Loc. #7, East Indies, $\theta = 10^{o}$	88
54.	" " for Loc. #7, East Indies, $\theta = 20^{o}$	89
55.	" " for Loc. #7, East Indies, $\theta = 30^{o}$	90
56.	" " for Loc. #8, Philippines, $\theta = 10^{o}$	91
57.	" " for Loc. #8, Philippines, $\theta = 20^{o}$	92
58.	" " for Loc. #8, Philippines, $\theta = 30^{o}$	93
59.	" " for Loc. #9, Sea of Japan, $\theta = 10^{o}$	94
60.	" " for Loc. #9, Sea of Japan, $\theta = 20^{o}$	95
61.	" " for Loc. #9, Sea of Japan, $\theta = 30^{o}$	96
62.	" " for Loc. #10, Bering Sea, $\theta = 10^{o}$	97
63.	" " for Loc. #10, Bering Sea, $\theta = 20^{o}$	98
64.	" " for Loc. #10, Bering Sea, $\theta = 30^{o}$	99
65.	" " for Loc. #11, NE Pacific, $\theta = 10^{o}$	100
66.	" " for Loc. #11, NE Pacific, $\theta = 20^{o}$	101
67.	" " for Loc. #11, NE Pacific, $\theta = 30^{o}$	102

LIST OF FIGURES (con't)

68. Seasonal Maximum and Minimum Attenuation Exceedance Probabilities for Loc. #12, Hawaii, $\theta = 10^{o}$ 103

69. " " for Loc. #12, Hawaii, $= 20^{o}$ 104

70. " " for Loc. #12, Hawaii, $= 30^{o}$ 105

71. " " for Loc. #13, Panama, $= 10^{o}$ 106

72. " " for Loc. #13, Panama, $= 20^{o}$ 107

73. " " for Loc. #13, Panama, $= 30^{o}$ 108

74. Attenuation vs. Frequency for Five Selected Locations at 1% Exceedance Level, for $\theta = 10^{o}$ 110

75. " " " for $\theta = 30^{o}$ 111

76. Attenuation vs. Elevation Angle for Five Selected Locations at 1% Exceedance Level, for f = 21 GHz 112

77. " " " " for f = 44 GHz 113

78. Cumulative Precipitation Rate and Attenuation (Fade) Duration Distributions 122

79. Cumulative Precipitation Rate Duration Distributions for Various Precipitation Rate Thresholds 124

80. Outage Duration Probability Density Function for Loc. #8, Philippines, Summer 125

81. " " for Loc. #11, NE Pacific, Fall 126

82. " " for Loc. #1, Mid-Atlantic, Summer 127

LIST OF TABLES

1.	Crane's Rain-Rate Distribution Values	6
2.	Tabulation of α, β for Use in αR_p^{β}	11
3.	Revised Rain-Rate Distributions	13
4.	Monthly and Seasonal Precipitation Data for Selected Ocean Locations	40
5.	Annual Number of Thunderstorm Days Estimated by Four Different Methods	42
6.	Regional Characteristic Values of Precipitation Frequency and Average Daily Precipitation	59
7.	Cumulative Precipitation-Rate Distributions for a Proposed Oceanic Climate Model	63
8.	Comparison of Integrated Precipitation Rate with Characteristic Annual Precipitation for Each Climatic Region	66
9.	Seasonal Precipitation Rate, Climate Type, k and $\overline{FH}$ for Thirteen Selected Locations	69
10.	Exceedance times for Various Margin Levels: Loc. #8, Philippines, Jun-Aug, Rain Type H	117
11.	" " Loc. #11, NE Pacific, Sep-Nov, Rain Type C'	118
12.	" " Loc. #1, Mid-Atlantic, Jun-Aug, Rain Type C	119
13.	Mean Outage Duration and Average Number of Outages per Day for Loc. #8, Philippines, Jun-Aug	128
14.	" " for Loc. #11, NE Pacific, Sep-Nov	129
15.	" " for Loc. #1, Mid-Atlantic, Jun-Aug	130

1.0 INTRODUCTION

Frequencies of interest for this study of rain attenuation were specified as 240 and 340 MHz, and 7.5, 8.2, 21, 40, 41, 43 and 45 GHz. At frequencies below 1 GHz, rain causes negligible attenuation of electromagnetic waves propagating through the atmosphere.* Thus, no results appear at the two lowest frequencies. However, severe storms cause appreciable signal attenuation around 7.5 and 8.2 GHz, military SHF downlink and uplink frequencies. As one designs earth-satellite links for even higher frequencies, rain attenuation becomes a major design factor. Attenuation by oxygen at sea level is large by 53 GHz (1 dB/km) and increases rapidly to about 16 dB/km at the 60 GHz resonance peak.* For the next generation of MILSATCOM systems, we need to analyse the feasibility of using higher frequency links through the atmosphere. However, these links need to be well away from the oxygen absorption region. Thus the highest frequency considered was 45 GHz, which meets this condition.

1.1 Excess Path Attenuation

Measurements of signal attenuation in excess of that due to the clear atmosphere include rain and cloud effects. At the communication satellite frequencies at which most measurements have been made, the cloud effects are quite small. Since they are not separated out, clouds constitute a component of the excess path attenuation; however, attenuation is primarily caused by rain. Rain also causes such effects+ as scatter interference, a lossy layer on radomes, and polarization and phase changes in the electromagnetic wave[2] and degrades the signal to noise ratio by adding noise to the receiver.[2,3] In this study, we have focused on just the rain attenuation effect. After more than 40 years of study,

---

* See reference 1, Figure 1.
+ Reference 2 contains an excellent tutorial review of the effects, a description of the measuring techniques and equipment, and an extensive bibliography.

predicting rain attenuation probabilities over a path remains a formidable problem. The point-to-point variations are known to be large. The year-to-year variations can be even larger. Dam designers have to worry about the heaviest deluge in a century or more. Communication satellite link designers do not worry about such worst case conditions, but they would like reasonable estimates for at least the next five years. Any such estimate, however, should be based on at least 15 years of past measurements.

1.2 Why We Must Model Rain Attenuation

We do not now have and will never have 15 years of data, e.g., from satellite beacon measurements, at each geographic location where we may become interested in operating a MILSATCOM terminal, at each frequency of interest and for every elevation angle that may occur with suitable satellite constellations. We have no choice but to model the rain attenuation as a function of these parameters.

If we can specify the rain rate R over each element of the earth-to-satellite path and properly characterize the rain (by drop size distribution, shape of drops, canting angle due to wind, the temperature of the water drops) at every instant, theory permits us to calculate rather accurately the resultant attenuation A as a function of frequency. Using the formula $A = aR^b$ for each element of the path, one could in principal calculate the overall path attenuation. This approach can best be described as an exact solution to a theoretical problem. Even over short terrestrial paths, it has proven prohibitively costly and complex to evaluate all the necessary parameters. Thus some surrogate must be used for some of the relevant parameters. The model recently developed by R.K. Crane is the only world-wide one for earth-satellite paths. While the model of reference 3 gives excellent results for Washington, D.C., it can not easily be extended world-wide. We started our study using Crane's model.

1.3 Rain Versus Precipitation

Most gauges throughout the world measure total precipitation. Nevertheless, it is customary to refer to the gauges used to measure precipitation as rain gauges, although they actually measure the equivalent liquid water content of all precipitation. Heated gauges do this better; snow may plug up an unheated gauge. These gauges have a least reading of 0.1 to 0.25 mm/hr. Below this, precipitation is referred to as a trace. Crane's model uses one-minute surface point precipitation-rate distributions. Although Crane refers to his model as a rain-rate model, we prefer to call it a precipitation-rate model. Crane's terminology is used for figures taken from his work; thereafter we tend to use "precipitation" rather than "rain" to remind one of the distinction.

2.0 THE CRANE MODEL FOR RAIN ATTENUATION OVER EARTH-SATELLITE PATHS

The method described here for calculating the attenuation due to rain over earth-to-satellite paths is based on the recent model proposed by Crane.[4,5]

2.1 Description Of The Model

The first step in the development of this model was the definition of eight climatological regions, i.e. eight regions characterized by distinct one-minute surface rain rate distributions, and the piecemeal allocation of the entire surface of the earth to one of these eight regions. A map delineating his region boundaries appears in Figure 1.* The second step was the determination of the curves that best fit the available one-minute surface rain rate frequency of occurrence data over a year for each region. Crane's values are given in Table 1 and his cumulative distributions are shown in Figure 2. The same data, smoothed slightly as described later, are plotted in Figure 3 using a logarithmic ordinate in order to better reveal the shape of the curves at low rain-rates. The remarkable achievement of Crane's two-step process is that the distributions for geographically adjacent climatic regions bound the expected variations (both point-to-point and year-to-year) in the rain-rate distribution for each region.

So far we have only discussed surface point rain rates. However, for the purpose of calculating earth-to-satellite path attenuation, the spatial distribution of rain rate over the propagation path represents the more relevant quantity. This involves the spatial correlation function for rain rate, which itself is a function of rain rate. For example, very high rain rates are known to have relatively short correlation distances and vice versa. In

---

* Private communications from R.W. Crane. This replaces the map in the Draft Submission to the CCIR, reference 5. It includes recent research which tentatively subdivides the ocean areas as well as the land areas.

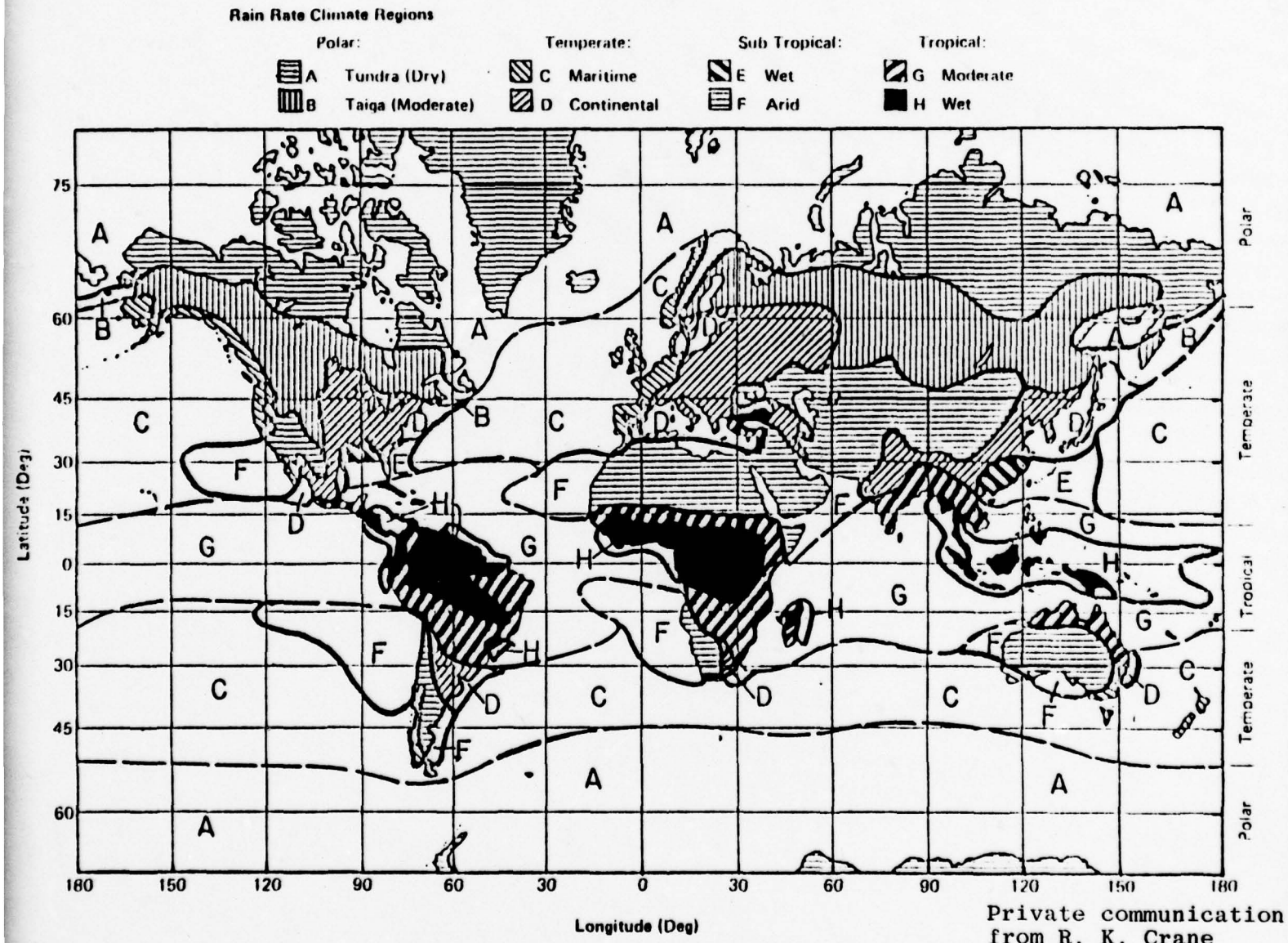

Private communication from R. K. Crane

Fig. 1. Rain rate climate regions

Table 1. CRANE'S RAIN-RATE DISTRIBUTION VALUES[a] (mm/h)

PERCENT	RAIN RATE CLIMATE REGIONS							
OF YEAR	A	B	C	D	E	F	G	H
0.001	28	54	80	102	164	66	129	251
0.002	24	40	62	86	144	51	109	220
0.005	19	26	41	64	117	34	85	178
0.01	15	19	28	49	98	23	67	147
0.02	12	14	18	35	77	14	51	115
0.05	8.0	9.5	11	22	52	8.0	33	77
0.1	6.5	6.8	7.2	15	35	5.5	22	51
0.2	4.0	4.8	6.8	9.5	21	3.8	14	31
0.5	2.5	3.0	2.8	5.2	8.5	2.4	7.0	13
1.0	1.7	1.8	1.9	3.0	4.0	1.7	4.0	6.4
2.0	1.1	1.4	1.0	1.8	2.0	1.1	1.6	2.8

[a]From Crane, reference 2. These are one-minute surface point rain rates (mm/h) which are exceeded the indicated percent of year (0.001 above means 0.001 percent, or 10^{-5} of a year). The relationship between percent of year, minutes per year and average number of minutes per day is shown below.

Percent Of Year	Minutes Per Year	Average No. Of Minutes Per Day
0.001	5.26	0.01
0.002	10.5	0.03
0.005	26	0.07
0.01	53	0.14
0.02	105	0.29
0.05	263	0.72
0.1	526	1.44
0.2	1052	2.88
0.5	2630	7.20
1.0	5260	14.4
2.0	10,520	28.8

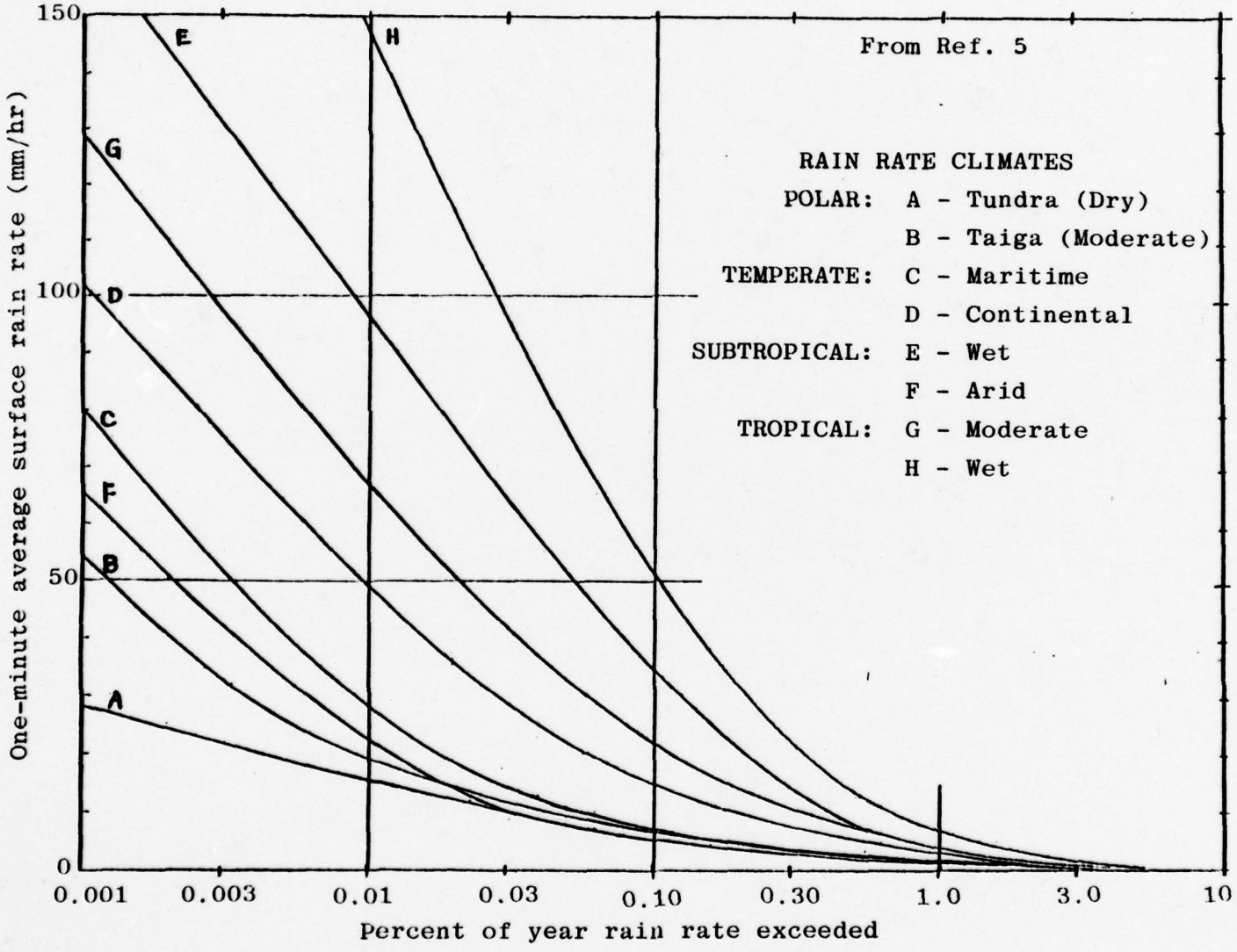

Fig. 2. Cumulative distributions of one-minute surface rain rates for eight climatic regions

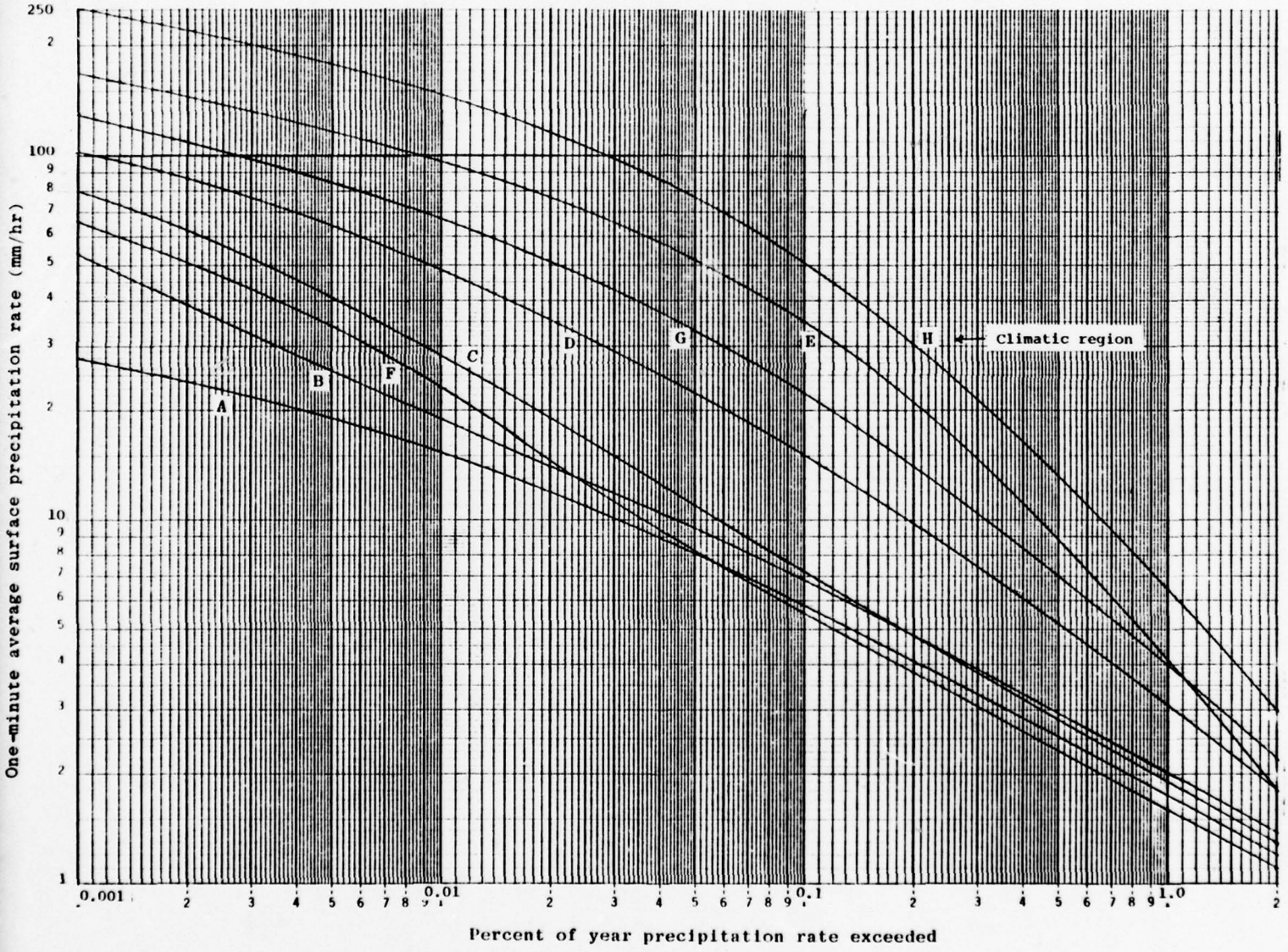

Fig. 3. Log-log plot of cumulative distributions of precipitation rate

Crane's model, the correction for spatial correlation is not made directly on rain rate, but rather as a rain rate-dependent correction to the total attenuation. This correction is of the form $\gamma(D)R_p^{-\delta(D)}$ where R_p is the one-minute surface point rain rate for a given exceedance probability (P) and γ and δ are empirical functions of D which will be discussed later. D is the surface projection of the appropriate portion of the propagation path.

Crane's model makes two additional assumptions to facilitate specific path attenuation calculations. The first is that, for the frequencies of current interest (i.e., $f < 50$ GHz), only liquid water need be considered; ice crystals and snow flakes can be neglected. It follows from this assumption that, if the mean freezing height ($\overline{FH}$) can be estimated or modeled, the path length for propagation at an elevation angle θ above the horizontal is simply $L = (\overline{FH})/\sin\theta$, and $D = (\overline{FH})/\tan\theta$. Using Crane's simple latitude-dependent model,

$$\overline{FH} \text{ (in km)} = 4.8 \text{ for } |\Lambda| \leq 30^\circ$$

$$= 7.8 - 0.1|\Lambda| \text{ for } |\Lambda| > 30^\circ.$$

The second assumption is that the "specific attenuation" in dB/km due to rain can be fitted by an expression of the form αR_p^{β} where α and β are empirical functions of the carrier frequency. Tables of α and β, based on applying logarithmic regression to Mie scattering calculations, have been given by Olsen et al[6] for five published drop-size distributions and for three different rain temperatures. The Laws and Parsons (LP) drop-size distributions are the most widely tested and the most widely used. Olsen gives two regressions, LP_L and LP_H, for "low" and "high" rain rates, and he suggests that LP_L be used for $R_p < 40$ mm/hr and LP_H be used for $R_p > 40$ mm/hr.

The regression for the Marshall-Palmer (MP) drop-size distribution lies between the two LP values at frequencies around 40 GHz. At lower frequencies, MP is slightly more pessimistic. Similar statements can be made about the Joss "thunderstorm" drop-

size distribution, while the Joss "drizzle" drop-size distribution is both less conservative in the 40 GHz region and less widely tested than the others. Accordingly, following Olsen's own recommendations, we use the LP_L and LP_H values for α and β. Graphical interpolations* between Olsen's published data were necessary to determine values at the frequencies specified for this study. However, we conservatively assumed that the values given for 1 GHz hold for all frequencies below that value. Table 2 lists the values used for α and β, interpolated where necessary. The $0^{\circ}C$ values are generally used with a few exceptions. The exceptions are the tropics (regions G and H) and the lowest latitudes of region C (within 30° of the equator) where $20^{\circ}C$ values are used. (Reference 6 discusses the range of rain temperatures.) An excursion for region E used both temperatures, in order to evaluate the magnitude of the temperature effect.

Finally, the attenuation in dB as a function of the exceedance probability P (the cumulative probability of being exceeded) expressed as percent of a year, is given by:

$$A(P) = L(\Lambda,\theta)\ \alpha(f,R_p)\ \gamma(D)\ R_p(P)^{[\beta(f,R_p)-\delta(D)]} \qquad \text{Eq. (1)}$$

Further details of the calculative procedure follow:
First, we specify

1. eight climatic regions A through H of Figure 1
2. four latitudes, $\Lambda = 0, 30, 40, 60^{\circ}$;
   i.e., for regions A and B, $\Lambda = 60^{\circ}$;
   for region C, $\Lambda = 30^{\circ}$ and 60°;
   for region D, $\Lambda = 40^{\circ}$;
   for regions E and F, $\Lambda = 30^{\circ}$;
   for regions G and H, $\Lambda = 0^{\circ}$.
3. six elevation angles, $\theta = 10, 20, 30, 45, 60, 90^{\circ}$
4. nine frequencies, f = 1.0, 7.5, 8.2, 21, 40, 41, 43, 44, 45 GHz

---

*For 7.5 and 8.2 GHz, a smooth curve was drawn through the published values at 6, 7, 8 and 9 GHz. For 21 GHz, a curve was drawn through the values at 15, 20 and 25 GHz. For the five values from 40 through 45 GHz, the interpolation was done in two steps. First the values at 25, 30, 35, 40, 50 and 60 were used to get a "good" value at 45 GHz; then the values at 35, 40, 45 and 50 were plotted at a larger scale to determine the values listed in Table 2.

Table 2. TABULATION[a] OF α, β FOR USE IN αR_p^{β}

Frequency (GHz)	$\alpha(LP_L)$	$\alpha(LP_H)$	$\beta(LP_L)$	$\beta(LP_H)$
		Temperature = 0°C		
1.0	6.41×10^{-5}	5.26×10^{-5}	0.891	0.947
7.5	5.49×10^{-3}	4.28×10^{-3}	1.1850	1.2585
8.2	6.95×10^{-3}	5.84×10^{-3}	1.1870	1.2396
21	7.05×10^{-2}	8.21×10^{-2}	1.1141	1.0728
40	0.313	0.467	0.981	0.864
41	0.330	0.490	0.973	0.857
43	0.365	0.534	0.958	0.845
44	0.382	0.555	0.951	0.840
45	0.400	0.575	0.943	0.835
		Temperature = 20°C		
1.0	3.84×10^{-5}	3.17×10^{-5}	0.889	0.945
7.5	3.52×10^{-3}	2.77×10^{-3}	1.2941	1.3644
8.2	4.72×10^{-3}	4.29×10^{-3}	1.2998	1.3322
21	7.68×10^{-2}	9.66×10^{-2}	1.1016	1.0367
40	0.312	0.452	0.972	0.864
41	0.329	0.473	0.965	0.858
43	0.363	0.515	0.951	0.846
44	0.380	0.535	0.944	0.841
45	0.397	0.555	0.936	0.836

[a]Based on Olsen et.al., reference 6; interpolated where necessary. LP refers to the Laws and Parsons drop-size distributions. The subscripts L and H refer to low and high rain rates; the transition is at about 40 mm/hr.

Second, we calculate: $\overline{FH} = 7.8 - 0.1\,|\Lambda|$ or $\overline{FH} = 4.8$ km as explained earlier, and L and D, where $L = \overline{FH}/\sin\theta$,

$$D = \overline{FH}/\tan\theta.$$

Third, we read α and β from Table 2, using both the LP low and LP high values.

Fourth, we calculate

$$\gamma(D) = 1 + (D^*/4.5) - 0.23(D^*/4.5)^2 + 0.0215(D^*/4.5)^3$$

and

$$\delta(D) = (D^*/21.5) - 0.98(D^*/21.5)^2 + 0.446(D^*/21.5)^3,$$

where

$D^* = D$ for $D \leq 22.5$ km

$= 22.5$ for $D > 22.5$ km

Fifth, we read $R_p(P)$ from Figure 3 or Table 3, noting whether $R_p < 40$ mm/hr or $R_p > 40$ mm/hr.

Sixth, we calculate A(P) in dB using the appropriate values for α and β from the two choices available (LP_L or LP_H).

Seventh, we list or plot A versus P^*,

where $P^* = P$ for $D \leq 22.5$ km

$= (D/22.5)P$ for $D > 22.5$ km,

where P is the tabulated value of percent of the year corresponding to the value of R_p used in calculating A.

2.2 Results Based On Crane's Model

A FORTRAN IV program was established for carrying out the indicated computations on an IBM 360/91 computer. The 5940 values of A, the earth-to-satellite excess path attenuation in dB, were calculated from the 10 rain rate region/latitude conditions, six elevation angles, nine RF frequencies, and the 11 exceedance percentage values. Representative results judged to be of primary interest are presented in Figures 4 through 18.

Table 3. REVISED RAIN-RATE DISTRIBUTIONS (mm/hr)

Percent of Year	Rain Rate Climate Regions							
	A	B	C	D	E	F	G	H
0.001	28.0	54	80	102	164	66	129	251
0.002	24.0	39	62	86	144	51	109	220
0.005	19.0	26	41	64	117	34	85	178
0.01	15.4	19	28	48	98	23	67	147
0.02	12.0	14	19	35	77	14	51	115
0.05	8.0	9.5	11	22	52	8.0	33	77
0.1	5.8	6.8	7.2	15	35	5.5	22	51
0.2	4.1	4.8	4.8	9.8	21	3.8	14	30
0.5	2.5	3.0	2.8	5.2	8.6	2.4	7.0	13
1.0	1.7	2.1	1.9	3.1	4.0	1.7	4.0	6.4
2.0	1.1	1.4	1.3	1.8	2.0	1.2	2.2	3.0

[a]This table is a slightly revised version of Table 1 based on the smoothed curves of Figure 3.

The first nine plots show the basic frequency of occurrence relationships, A vs. P, for three RF frequencies (7.5, 21 and 40 GHz) and three elevation angles (10, 20 and 30°). There is a curve on each plot for each one of the different climatic regions. In all cases, the attenuation at 1 GHz is less than 1 dB. Hence these values are below the scale and do not appear; this frequency is hereafter ignored. Figure 4 shows the results at 7.5 GHz for an elevation angle of 10° (the angle giving the highest attenuation over the range from 10 to 90°). Two special effects are also illustrated in Figure 4. Firstly, the sensitivity to rain temperature is shown by plotting the result of using both 0°C and 20°C values of α and β (from Table 2) for region E. The two curves differ by less than 2 dB even at the low frequency-of-occurrence high-attenuation end, and this is the largest difference found in any case. Thus temperature, which changes the dielectric constant of the rain water slightly, is considered to have a negligible effect on earth-space path attenuation. Comparing C for $\Lambda = 30°$ latitude and $\Lambda = 60°$ latitude, the effect of freezing height is seen to be major. This results because freezing height directly determines the amount of rain that the signal must pass through on any given path. Secondly, the effect of drop-size distribution is shown. The D curve in Figure 4 shows one of the largest discontinuities found at the transition from Laws and Parsons "high" to "low" drop-size distributions. We also consider this effect negligible. In all other cases throughout this report, we show a single smooth curve joining the LP_L and LP_H curves, and do not bother to show the step at 40 mm/hr. Figures 5 and 6 give the results at 7.5 GHz for 20 and 30° elevation. The results at 21 GHz appear in Figures 7, 8 and 9. Figures 10, 11 and 12 give the results at 40 GHz. The straightforward dependence on elevation angle is shown in Figure 13, 14 and 15 at the 1% frequency of occurrence. The sharp upturn in the tropical curves (climatic regions G and H) at low elevation angles is a feature of the model. We surmise that it arises from the model when the ground projection of the relevant (non-freezing) propagation path exceeds 22.5 km because there is an increased

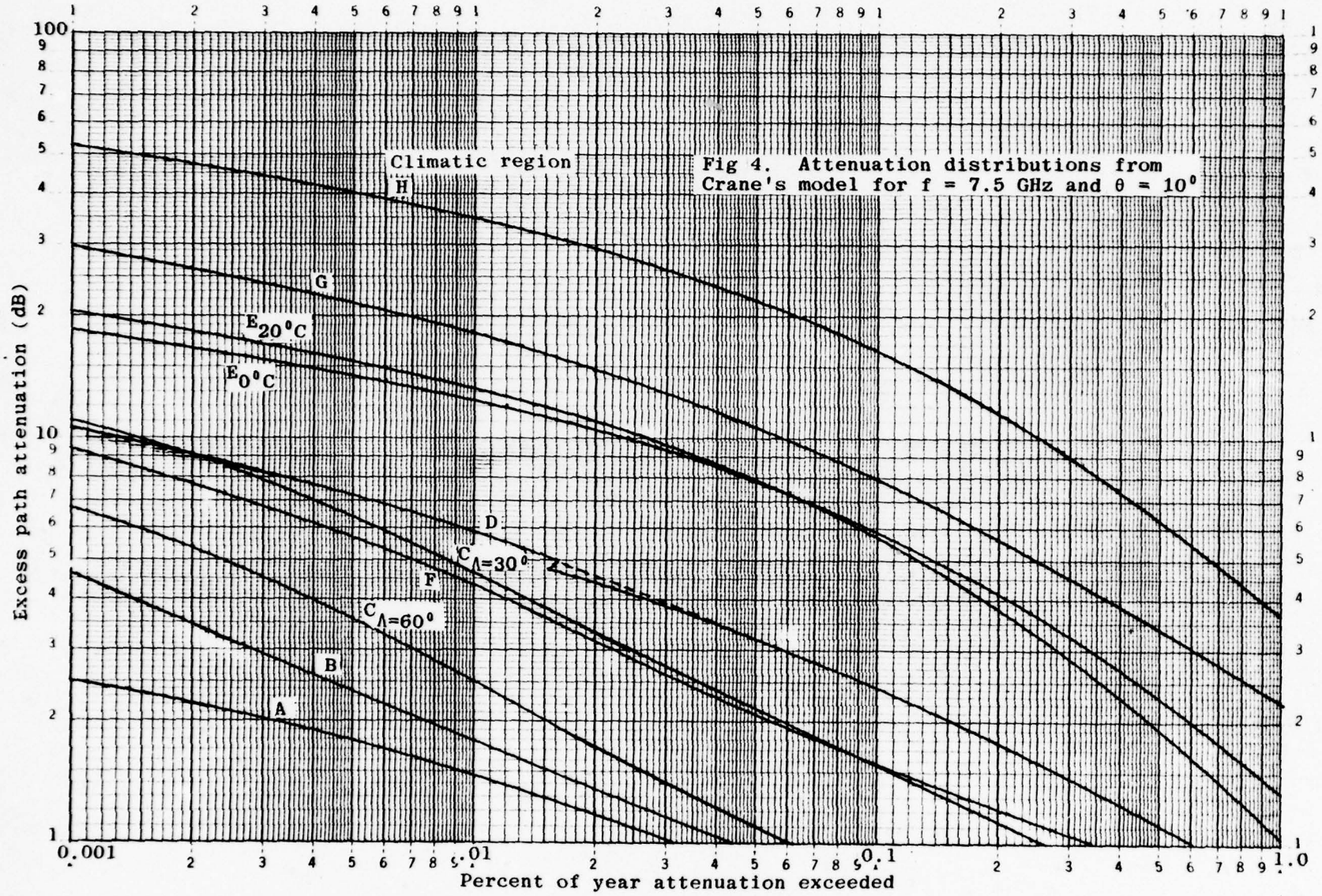

Fig 4. Attenuation distributions from Crane's model for f = 7.5 GHz and θ = 10°

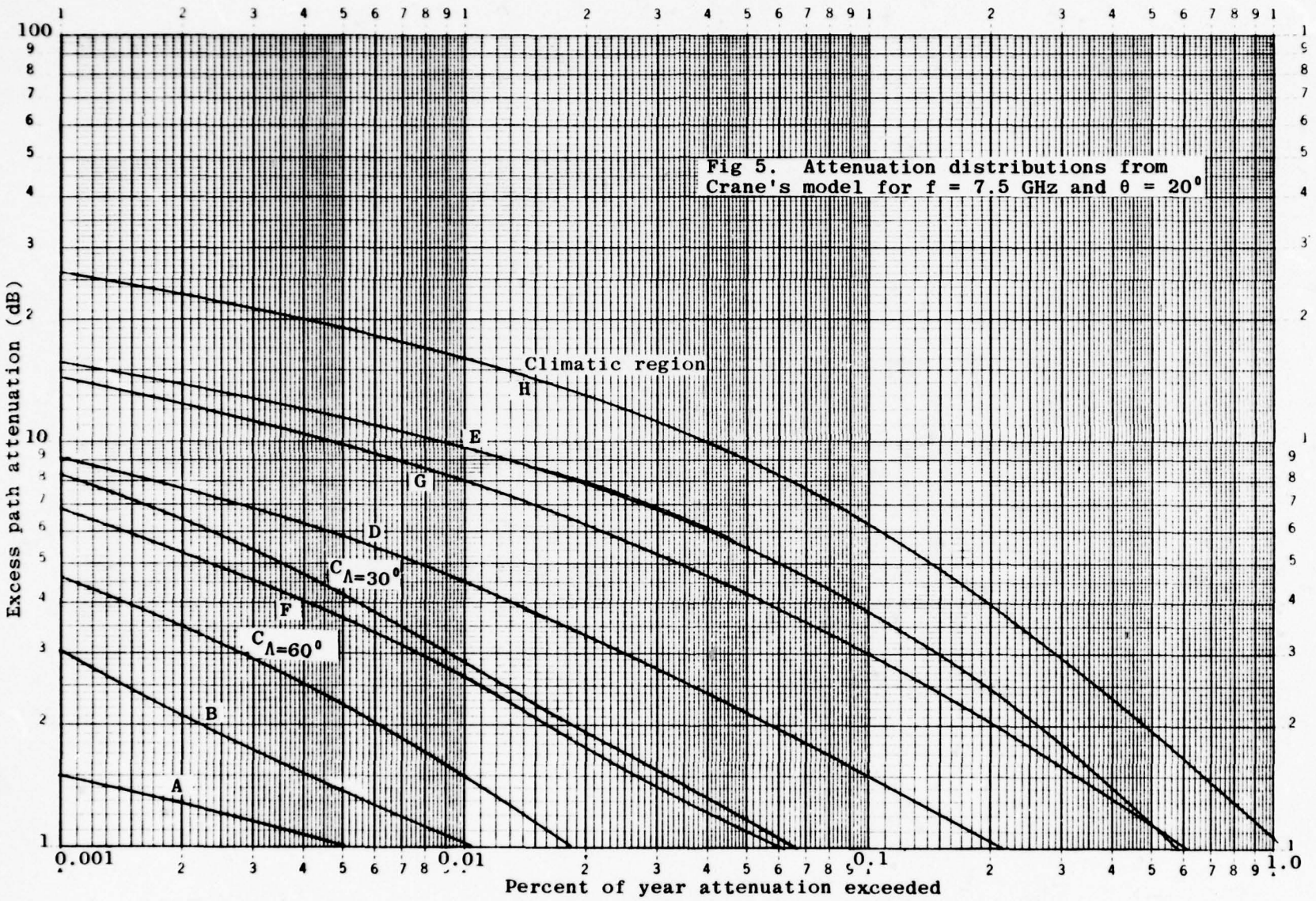

Fig 5. Attenuation distributions from Crane's model for f = 7.5 GHz and θ = 20°

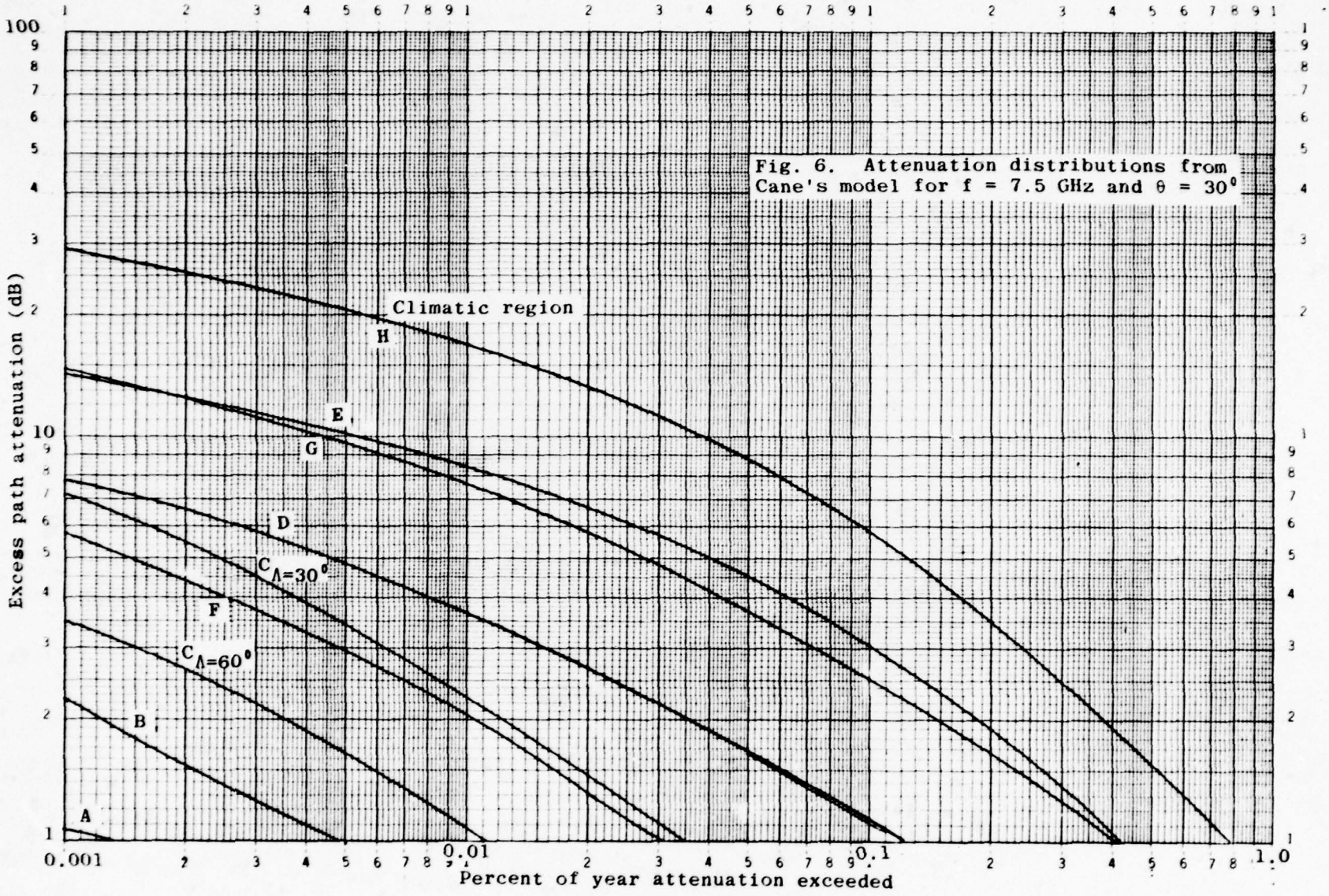

Fig. 6. Attenuation distributions from Cane's model for f = 7.5 GHz and $\theta = 30^\circ$

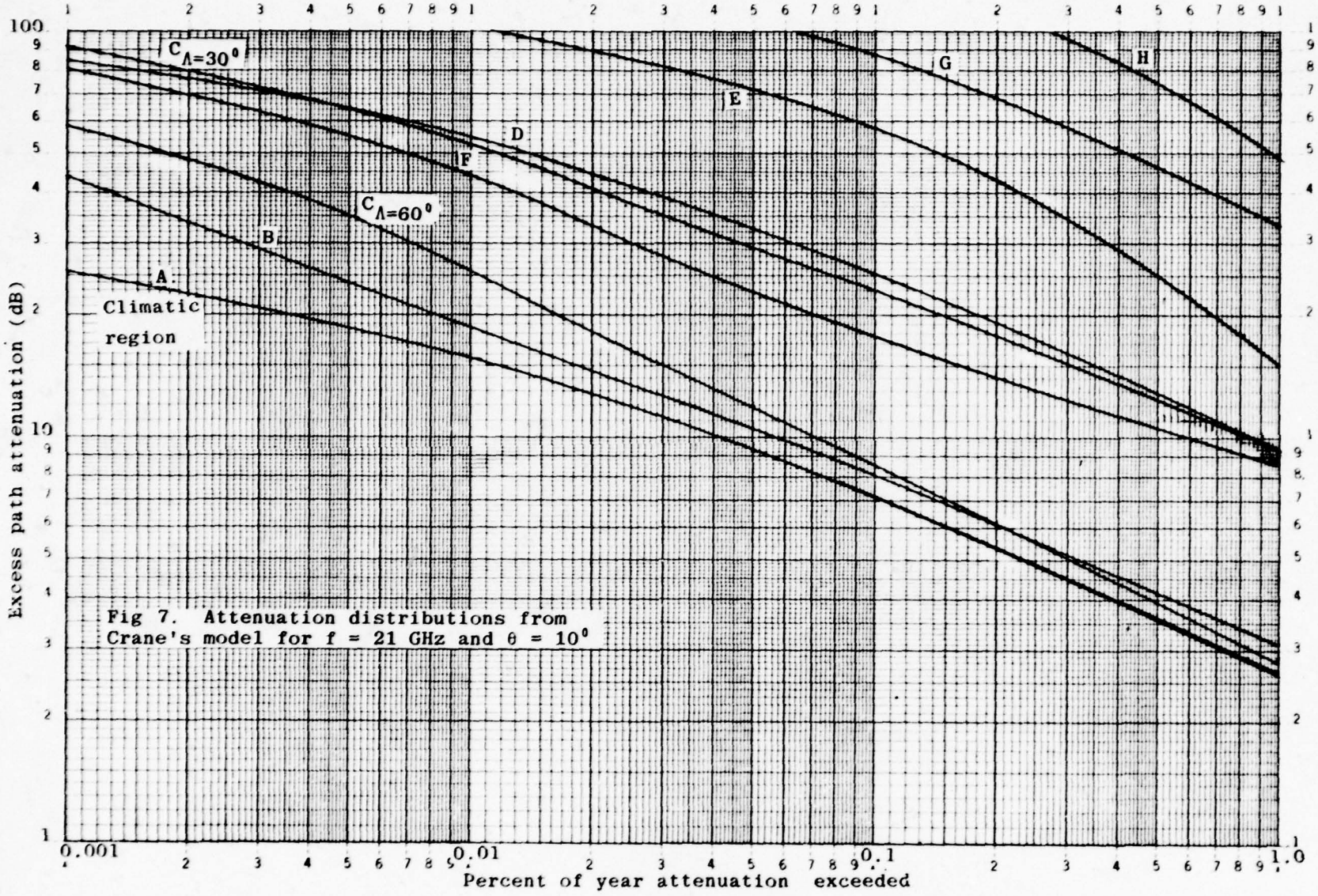

Fig 7. Attenuation distributions from Crane's model for f = 21 GHz and $\theta = 10^0$

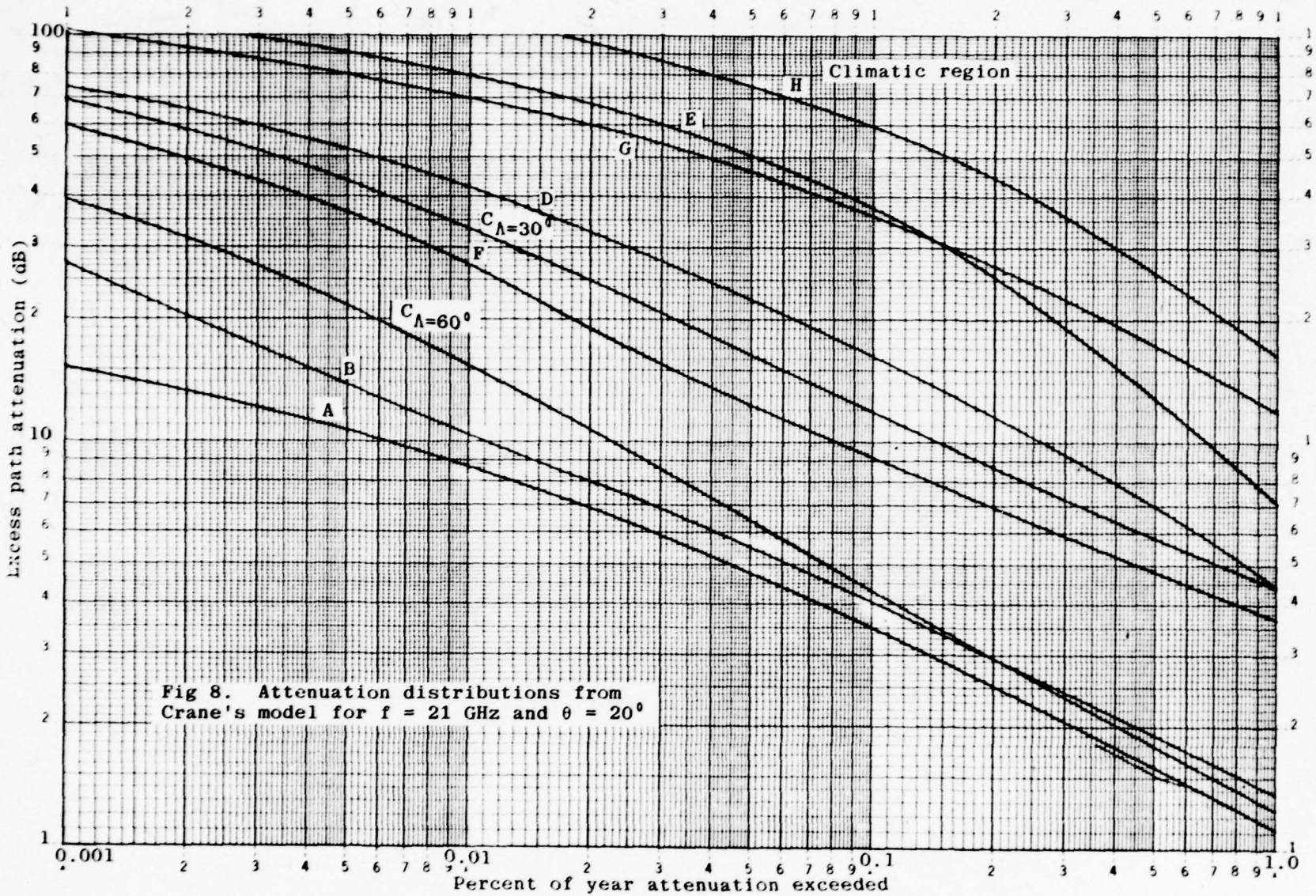

Fig 8. Attenuation distributions from Crane's model for f = 21 GHz and $\theta = 20^0$

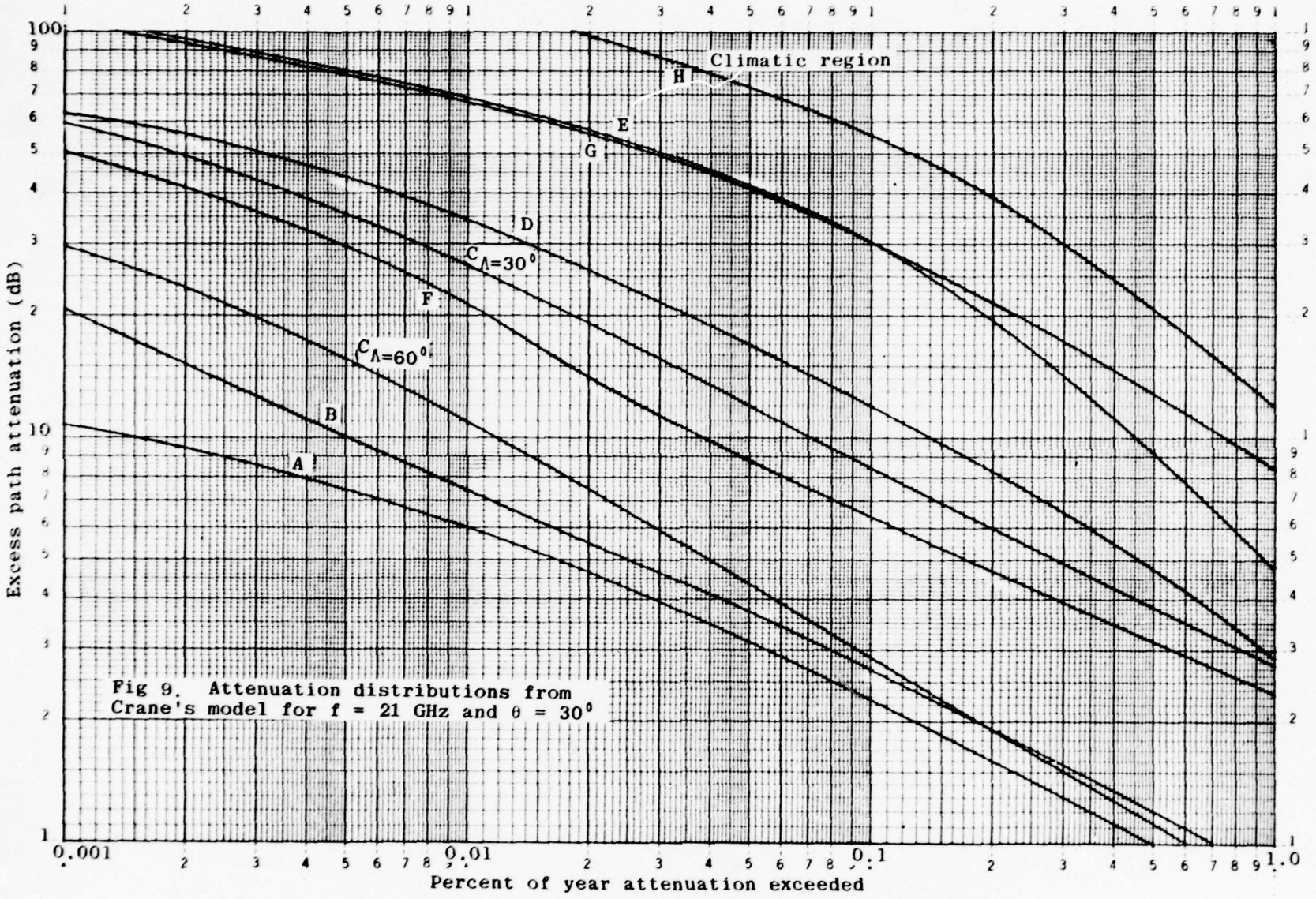

Fig 9. Attenuation distributions from Crane's model for f = 21 GHz and θ = 30°

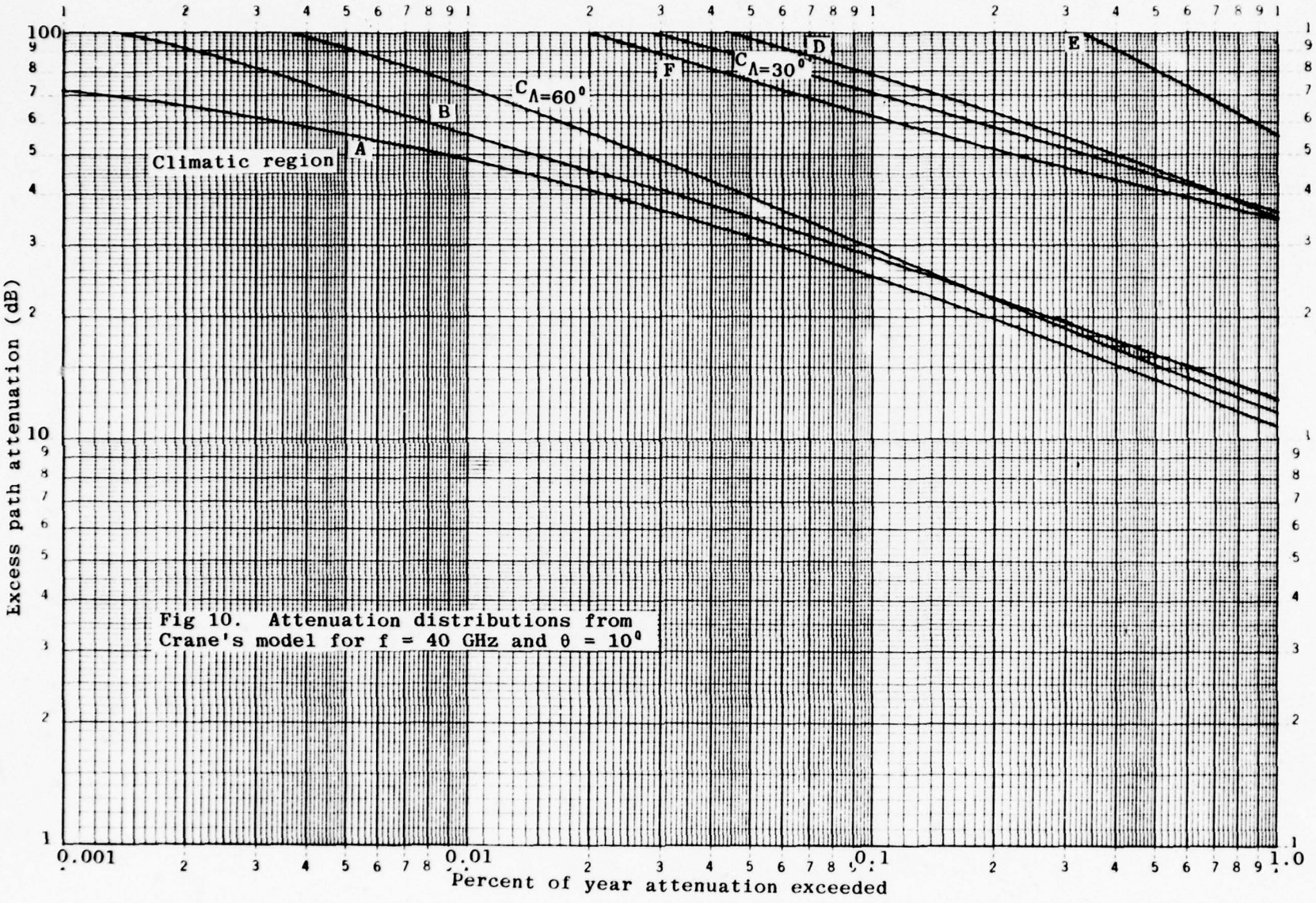

Fig 10. Attenuation distributions from Crane's model for f = 40 GHz and θ = 10°

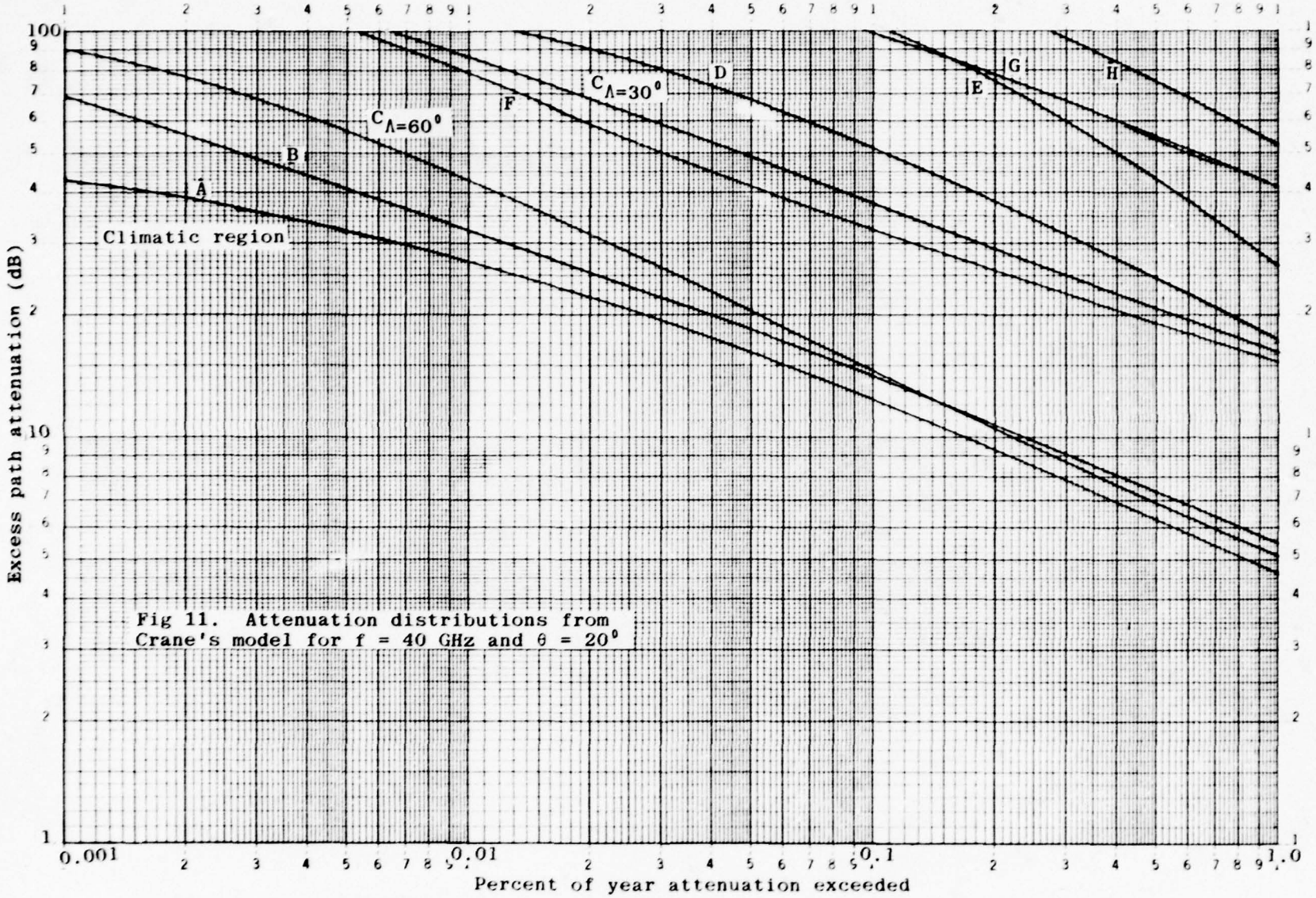

Fig 11. Attenuation distributions from Crane's model for f = 40 GHz and θ = 20°

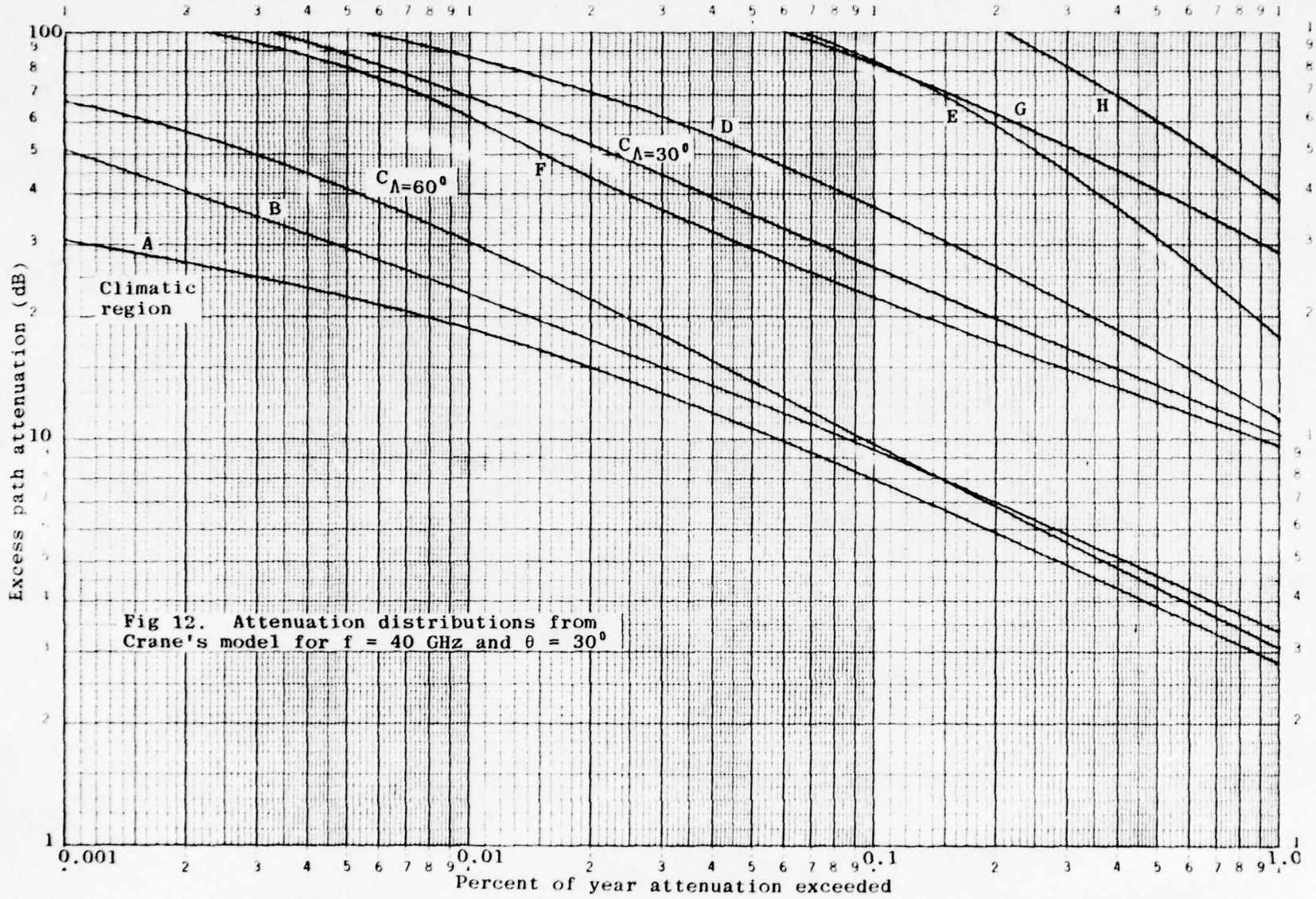

Fig 12. Attenuation distributions from Crane's model for f = 40 GHz and θ = 30°

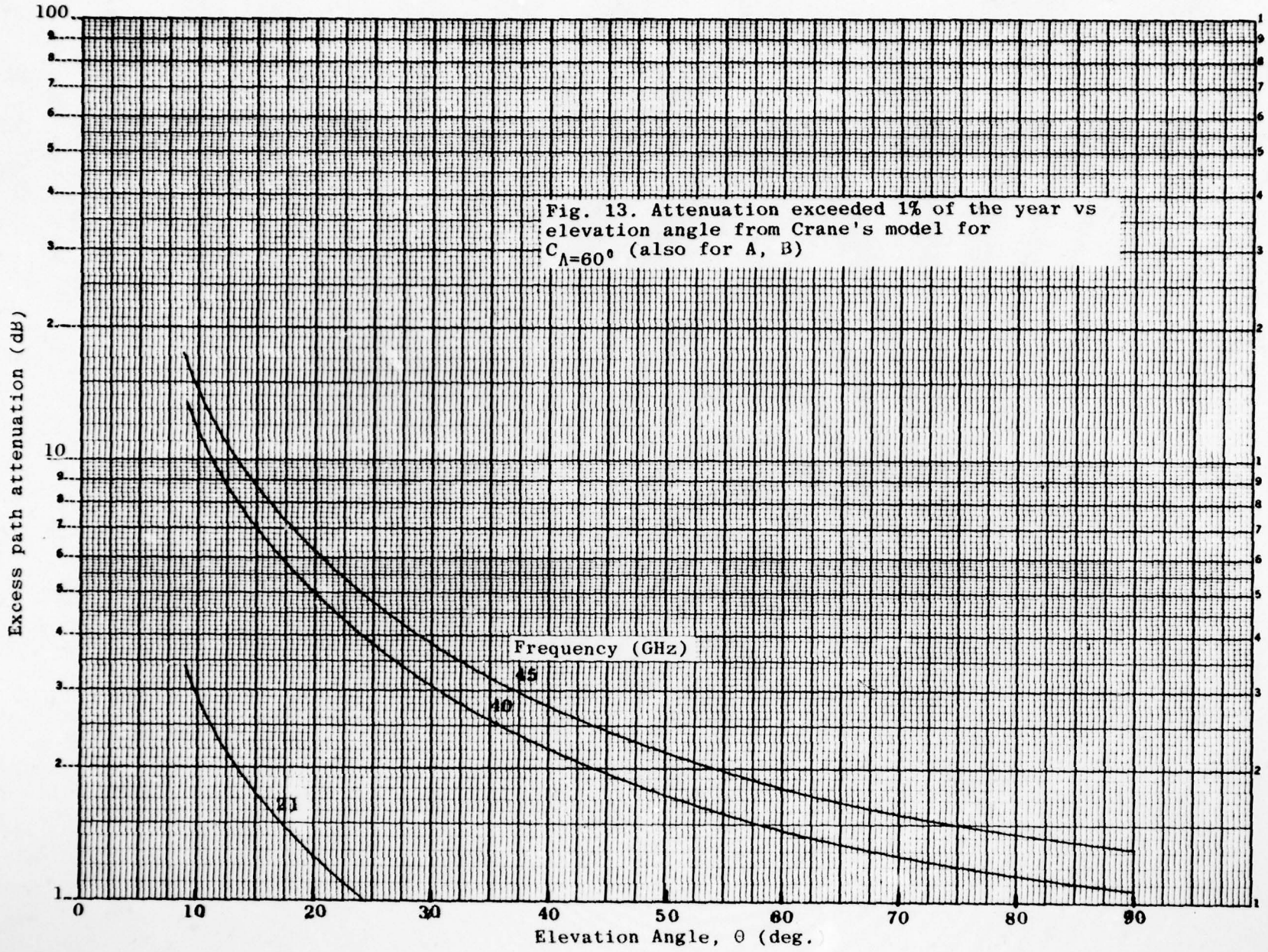

Fig. 13. Attenuation exceeded 1% of the year vs elevation angle from Crane's model for $C_{\Lambda=60^\circ}$ (also for A, B)

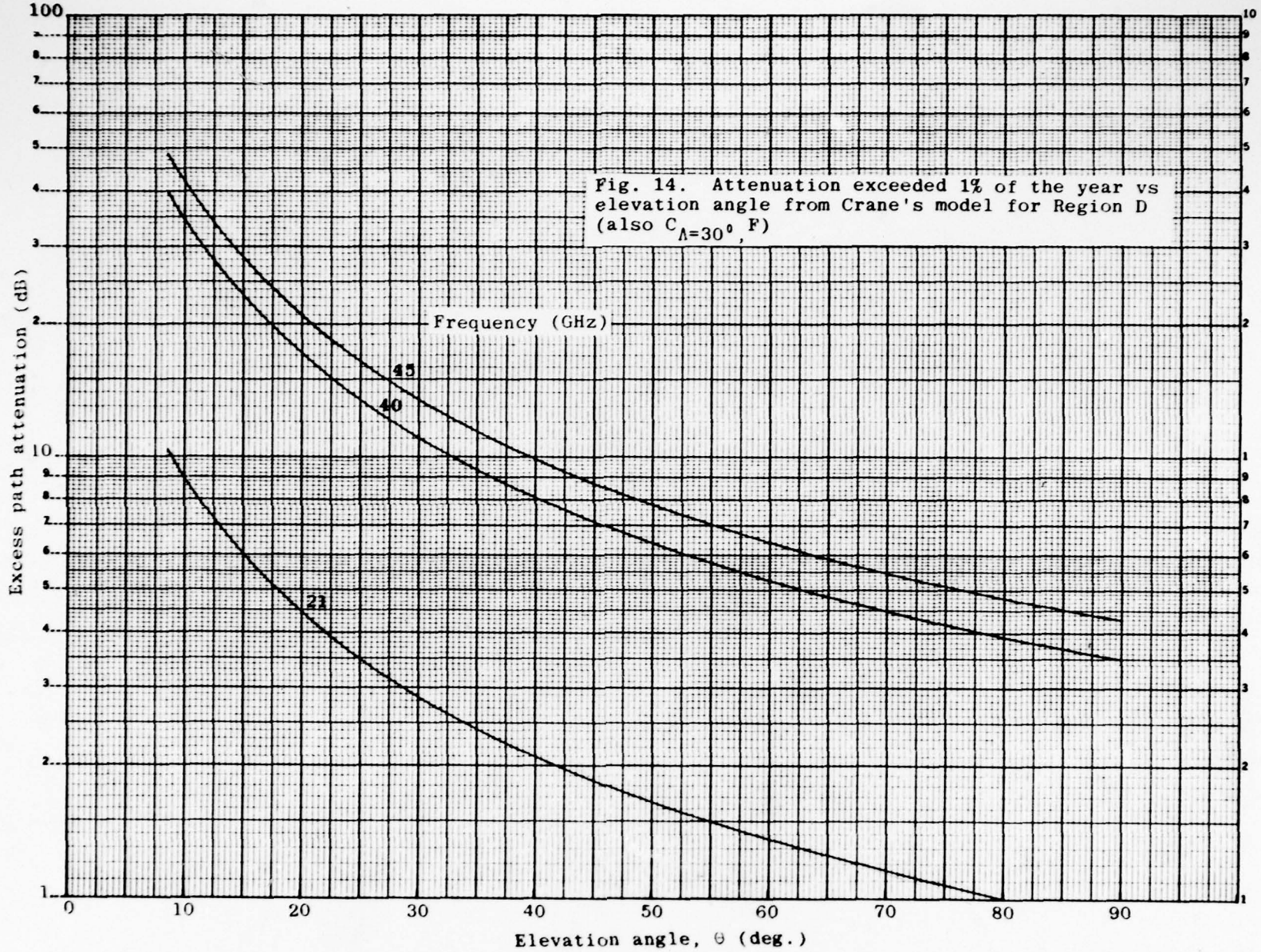

Fig. 14. Attenuation exceeded 1% of the year vs elevation angle from Crane's model for Region D (also $C_{\Lambda=30^0}$, F)

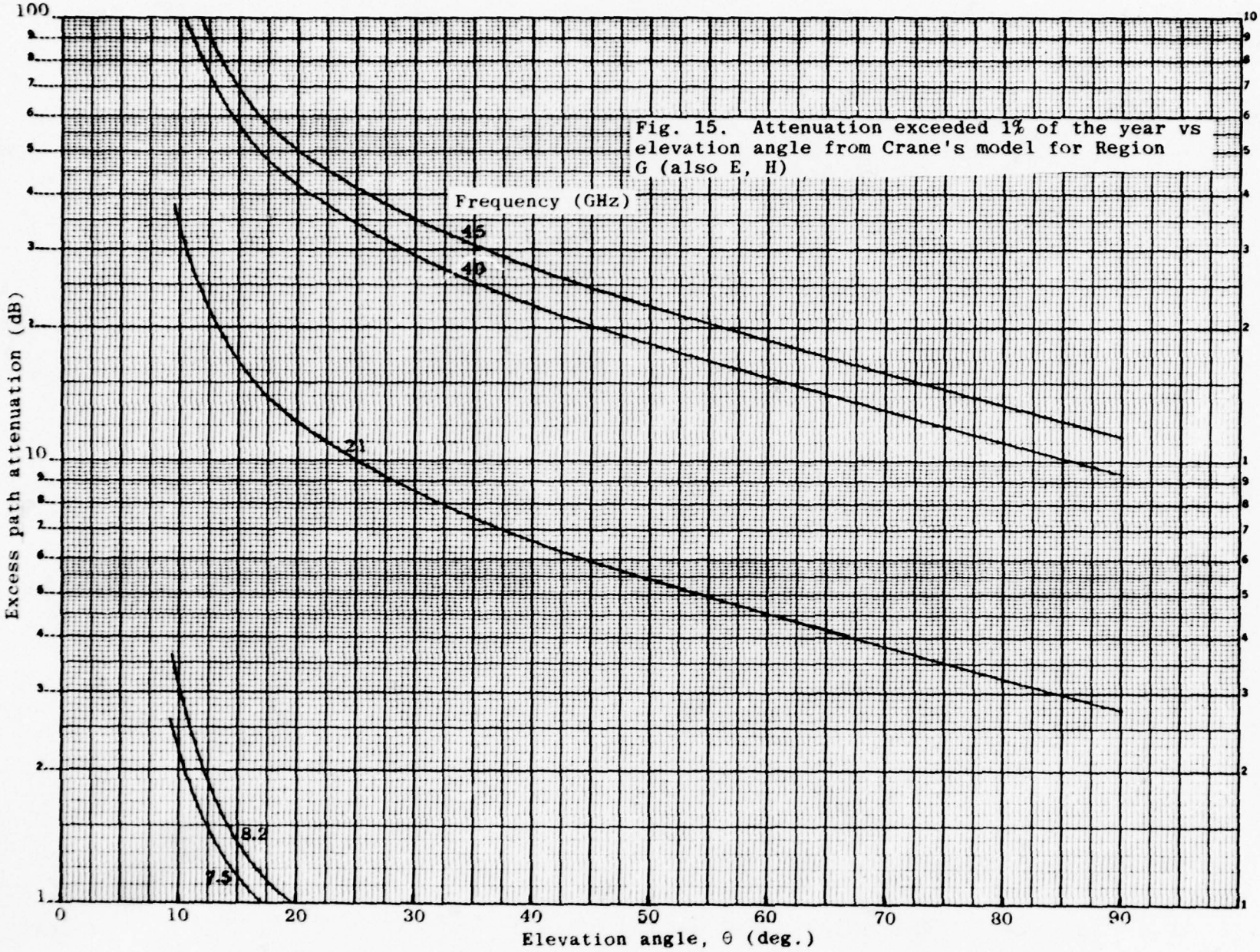

Fig. 15. Attenuation exceeded 1% of the year vs elevation angle from Crane's model for Region G (also E, H)

probability over the single-point rain probability that a dense rain cell will be encountered somewhere along the path. Cross plots of these data at the 1% frequency of occurrence are given in Figures 16, 17 and 18 to emphasise the severe frequency dependence of rain attenuation. Only five curves are shown on each plot instead of nine or ten. At 1% frequency of occurrence, the missing curves lie very close to one of the curves shown, as indicated by the parameters in parentheses. These five samples are sufficient to indicate the behavior of the larger group.

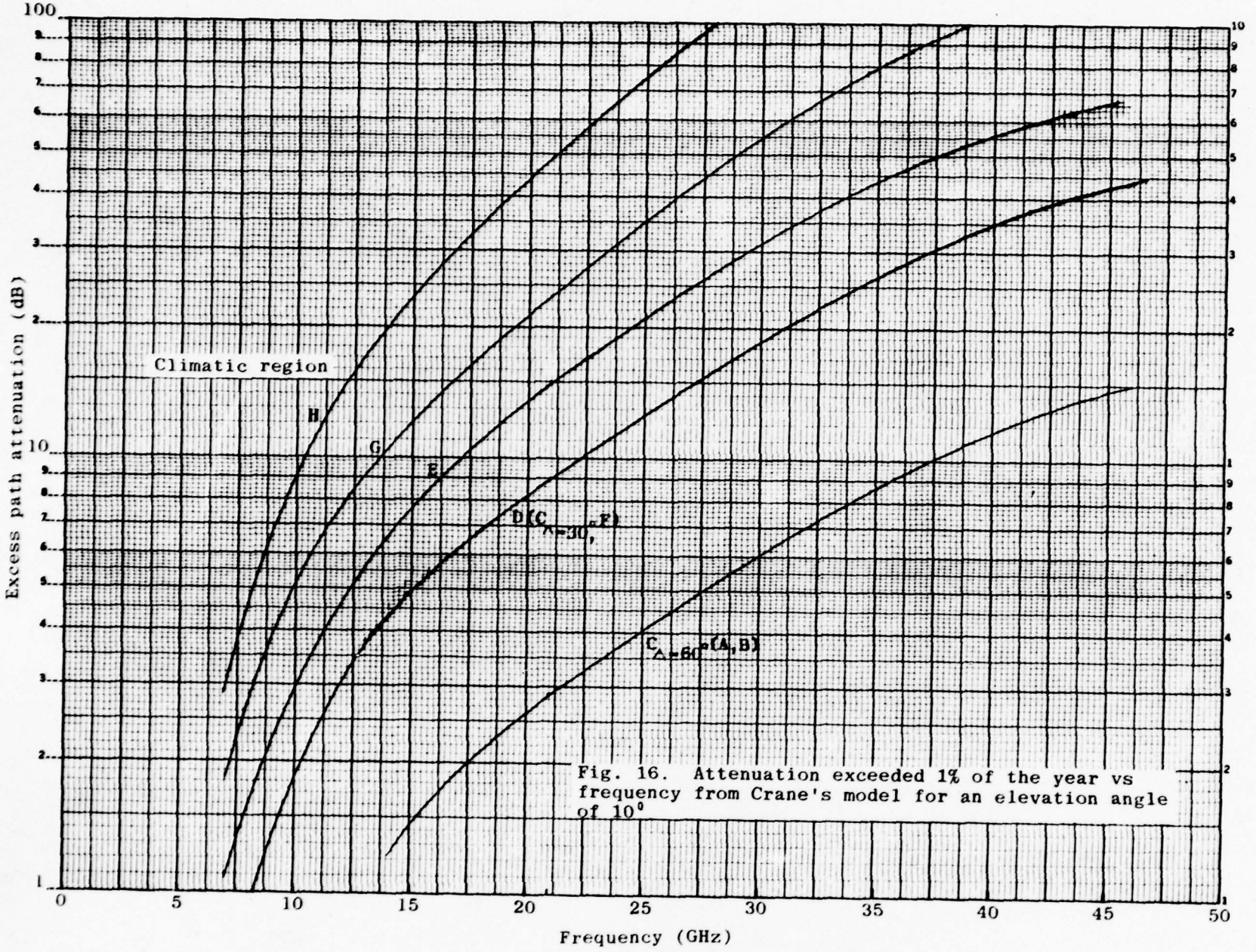

Fig. 16. Attenuation exceeded 1% of the year vs frequency from Crane's model for an elevation angle of 10^0

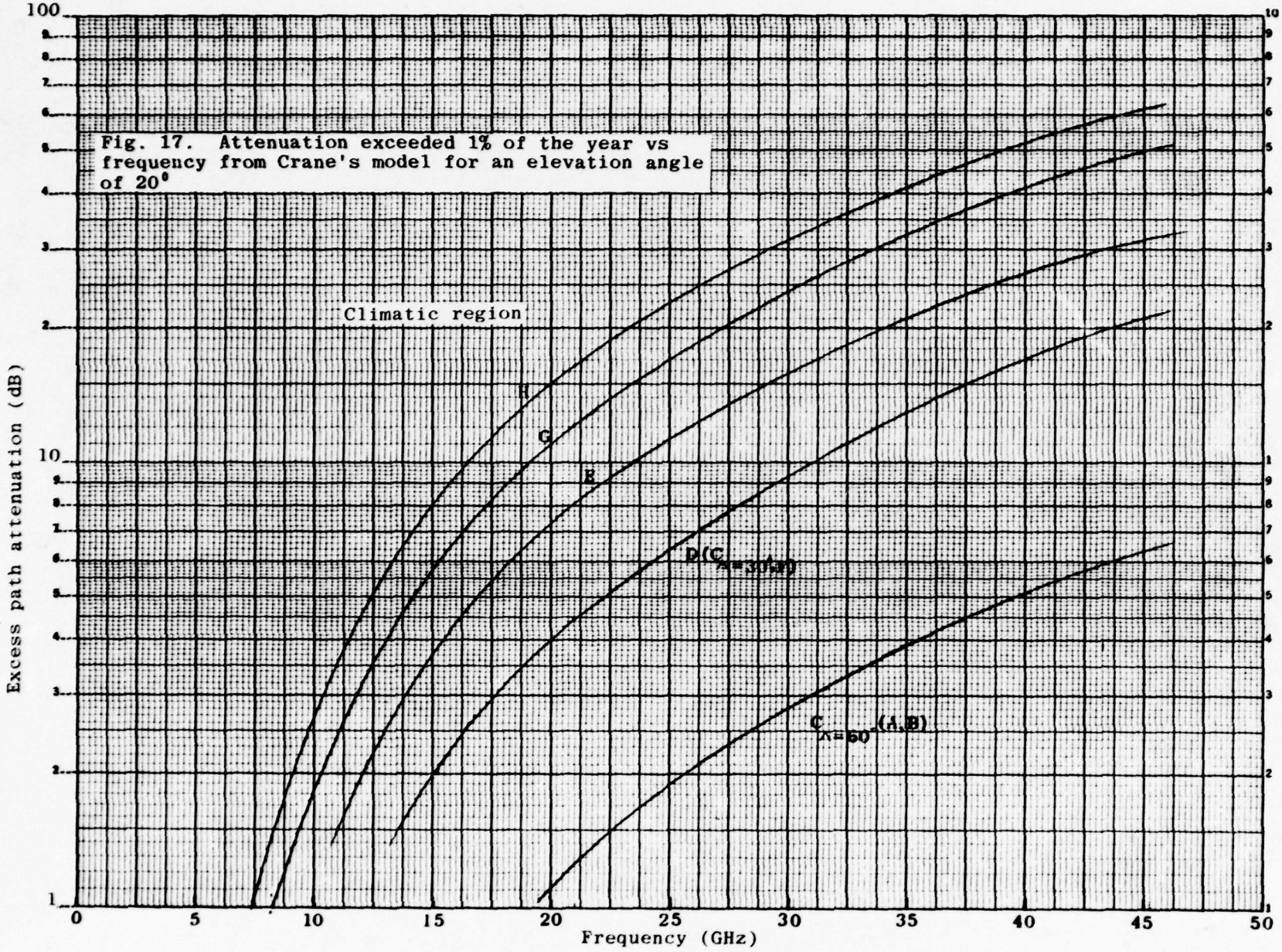
Fig. 17. Attenuation exceeded 1% of the year vs frequency from Crane's model for an elevation angle of 20°
Climatic region
H
G
E
D($C_{A=30}$, B)
$C_{A=60}$ (A, B)
Excess path attenuation (dB)
Frequency (GHz)
100
10
1
0
5
10
15
20
25
30
35
40
45
50

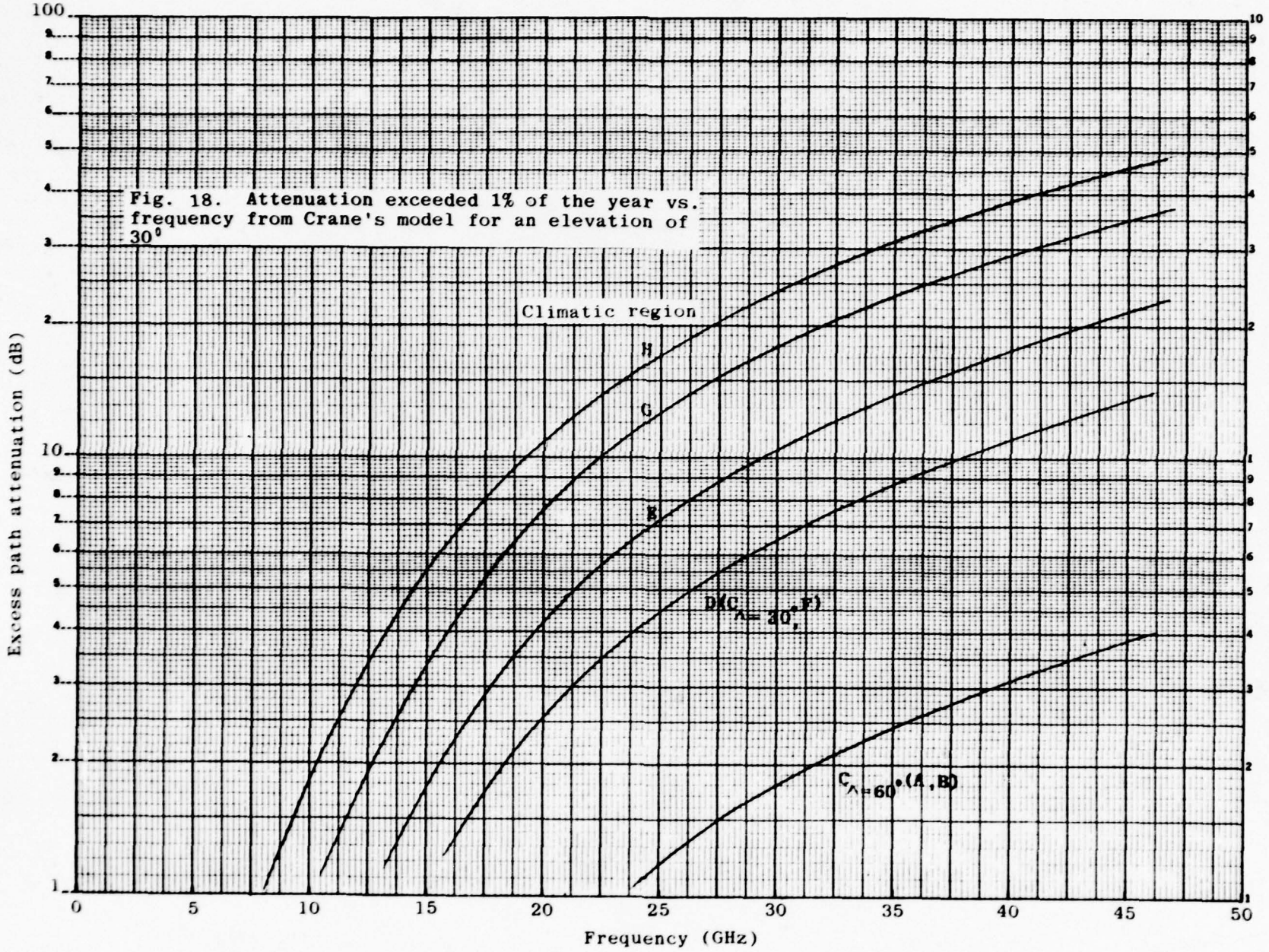

Fig. 18. Attenuation exceeded 1% of the year vs. frequency from Crane's model for an elevation of 30°

3.0 EXTENSIONS AND MODIFICATIONS TO THE CRANE MODEL

The Crane precipitation-rate model consists of (1) a map showing eight climate "types" distributed as regions over the globe, (2) an approximate expression for the zonally averaged, mean annual freezing height $\overline{FH}$ as a function of latitude, and (3) one-minute precipitation rate distributions typical of each climate type.[4,5] Crane based geographical distribution of climate types on annual precipitation amounts, annual numbers of "thunderstorm days", and general information from climate texts and other global climate classifications. Crane gathered all of the precipitation rate versus frequency-of-occurrence data he could find (mostly in the U.S. Canada and Europe), correlated the frequency distributions with annual precipitation and thunderstorm data, and defined the climate regions based on relative homogeneity among those data. He then used the published, worldwide, annual precipitation and thunderstorm information along with general climatological knowledge to extrapolate the rain-rate regions globally. According to Crane*, no rigorous objective scheme was used to define regions or to delineate regional boundaries, and therefore, it would not be possible to reproduce his climate region map based on data analysis alone.

Each precipitation-rate region (or type) is associated with its own characteristic precipitation-rate frequency-of-occurrence distribution. In order of increasing frequency of high one-minute average precipitation rates, he identified the eight types as follows:

A = Polar Tundra
B = Polar Taiga
F = Subtropical Arid
C = Temperate Maritime
D = Temperate Continental

---

* Telephone discussion between R.K. Crane (Environmental Research and Technology Inc., Concord, MA) and R.E. Huschke on January 26, 1979.

G = Tropical Moderate

E = Subtropical Wet

H = Tropical Wet

Originally, the regional climate model was confined to the land masses. The model was then refined according to inputs from member nations of the International Radio Consultative Committee (CCIR), for whose use the model was developed. They provided inputs which extended the model to include the oceans. Crane's refinement of the original map in Reference 5 appears in Figure 1. Crane stated that currently there is no formal effort to further improve the model, e.g., to incorporate seasonal variations.* Variations in precipitation-rate distributions among locations within a given type were determined by Crane, to be approximately bounded by the distributions for the geographically adjacent types. Table 1 reproduces the rain-rate distributions given by Crane.

3.1 Rationale for Changes

If the Crane model were an accurate representation of precipitation-rate statistics over the open oceans (from which there are no precipitation rate data), it would be a useful tool for predicting outage probabilities, but only on an annual basis. However, we lose interseasonal variations by aggregating data around the calendar. The model (which includes the associated attenuation calculation methodology) would have to be considerably extended to permit us to calculate statistics of outage durations. The limitations appear especially severe at the lower attenuation (higher frequency-of-occurrence or longer duration) end of the precipitation-rate distributions.

Setting aside the latter problem (duration at low attenuation) for the moment, we began our analysis by examining the Crane model to assess its representativeness of ocean precipitation rates. The following questions needed answers:

---

* Private communication, January 26, 1979.

1. Do the climate types appear properly distributed over the oceans?
2. Do the seasonal variations in precipitation data justify significantly altering the model?
3. Is the Crane approximation for freezing height adequate?

The following answers are based on a brief examination of readily available data. In all cases the answers indicate a need for a deeper investigation, tempered by the awareness that the basic precipitation rate data simply do not exist over the oceans.

3.1.1 Ocean Distribution of Climate Regions

Three independent analyses of ocean precipitation and cloudiness were used as an initial check on the representativeness of Crane's climate region map over the oceans: (1) a global, monthly analysis of precipitation amounts[7], (2) a global, monthly analysis of precipitation frequency[8]; and (3) a monthly analysis of average cloud amount over the Pacific Basin[9].

The analysis of precipitation amounts[7] was available only in chart form, without text. Therefore, the quality and quantity of data that went into the analysis are not readily known. Precipitation amount is not generally measured on ships at sea. The data probably represent the 1930s through the mid-1940s. The author's reputation is such that the quality of his analysis and his judgment can be relied upon.

The precipitation frequency analysis,[8] used all available data from the early 1940s through the early 1960s. The frequencies are defined as the fraction of all "present weather" observations reporting precipitation. This could introduce a small bias toward inflated frequencies because, in the absence of significant weather phenomena, merchant vessels might neglect reporting "present weather". As an additional caveat, the authors state, "... [procedural and coding] difficulties have reached their peak in the analysis of precipitation data. Hence, percentage frequencies indicated should be interpreted with particular caution."[8]

The cloud amount analysis[9] comes from meteorological satellite data over the Pacific Basin, 1965-1973. It is the least uncertain and most objective of the three analyses; however, it is only an indirect and crude indication of precipitation amount and frequency.

The above comments illustrate the inherent difficulties in describing precipitation over the oceans; and this is further illustrated in Figures 19-22. In these figures, the three types of analysis are superposed, one set each for (Northern Hemisphere) winter, spring, summer and fall. One looks for areas of consistency and inconsistency among the three analyses and with the Crane map. In general, consistency predominates with regard to the major features of ocean climate. However, and with due regard for the fact that Figures 19-22 are seasonal representations, it would appear that the annual picture of Figure 1 should show (1) that more of the oceans are a subtropical arid (type F) climate, (2) that the polar tundra (type A) climate extends too far south into the North Atlantic, (3) that the Mediterranean should not be a continental (type D) climate, and (4), with less certainty, the tropical wet (type H) climate should appear over larger portions of the eastern tropical Pacific and eastern tropical Atlantic.

3.1.2 Seasonal Variation of Climate

Comparison of Figures 19-22 shows some significant seasonal variations in ocean climate:

1. Most major climatic features shift five to ten degrees in latitude toward the summer pole.
2. The subtropical arid areas tend to expand in the summer hemisphere and contract in the winter hemisphere.
3. "Wetness", in general, but especially in the subtropics and tropics, varies considerably from season to season.

To look in more detail at seasonal variations, thirteen specific locations of possible Navy communications interest were selected. We selected them with an eye to representing the complete

Average daily precipitation (——), precipitation frequency (- - -), average Pacific cloud cover (····)
Dec-Feb (Jan for cloud cover and precipitation frequency)

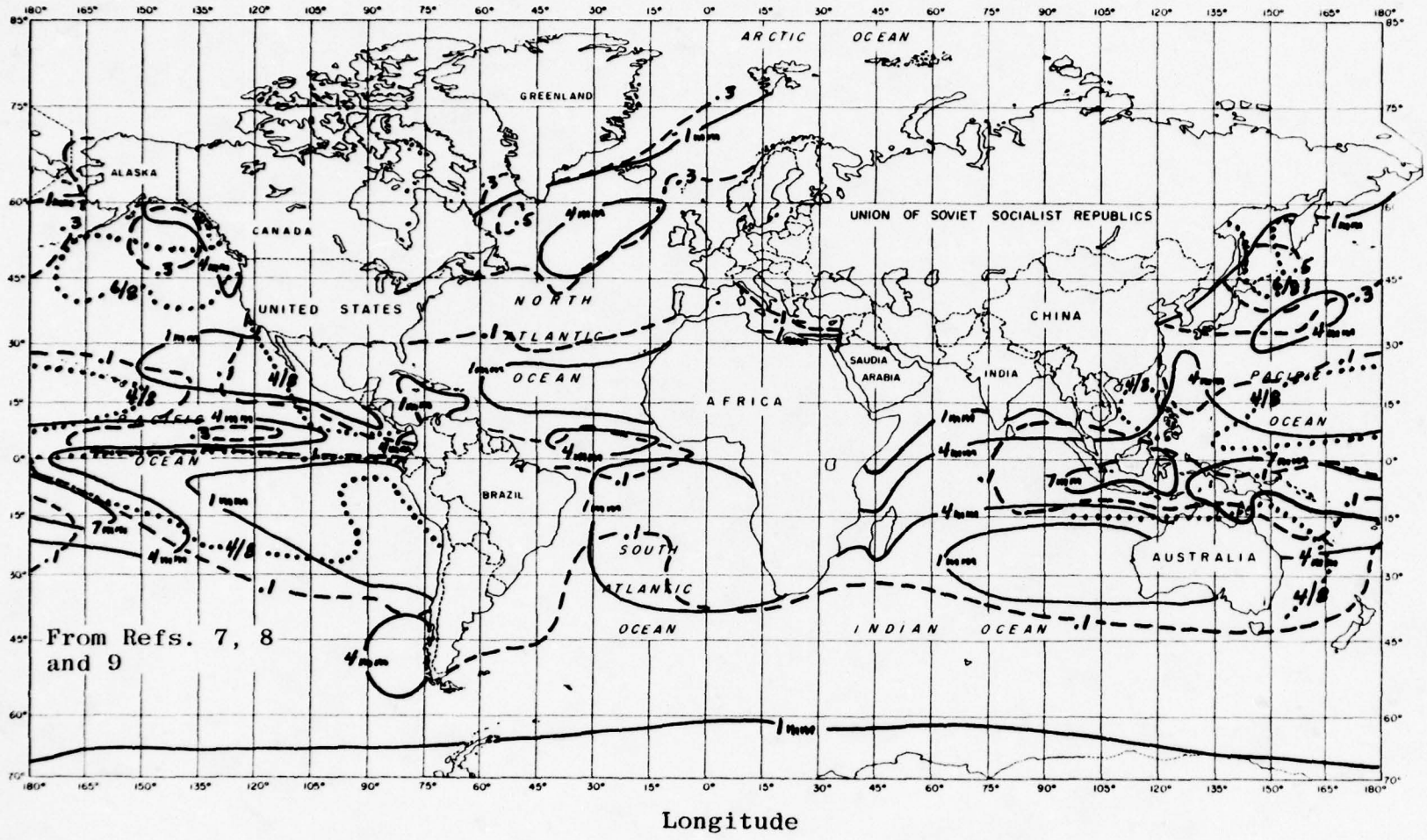

Fig. 19. Superposition of average daily precipitation, precipitation frequency and average cloud cover for Dec-Feb.

Average daily precipitation (——), precipitation frequency (- - -), average Pacific cloud cover (· · ·)
Mar-May (April for cloud cover and precipitation frequency)

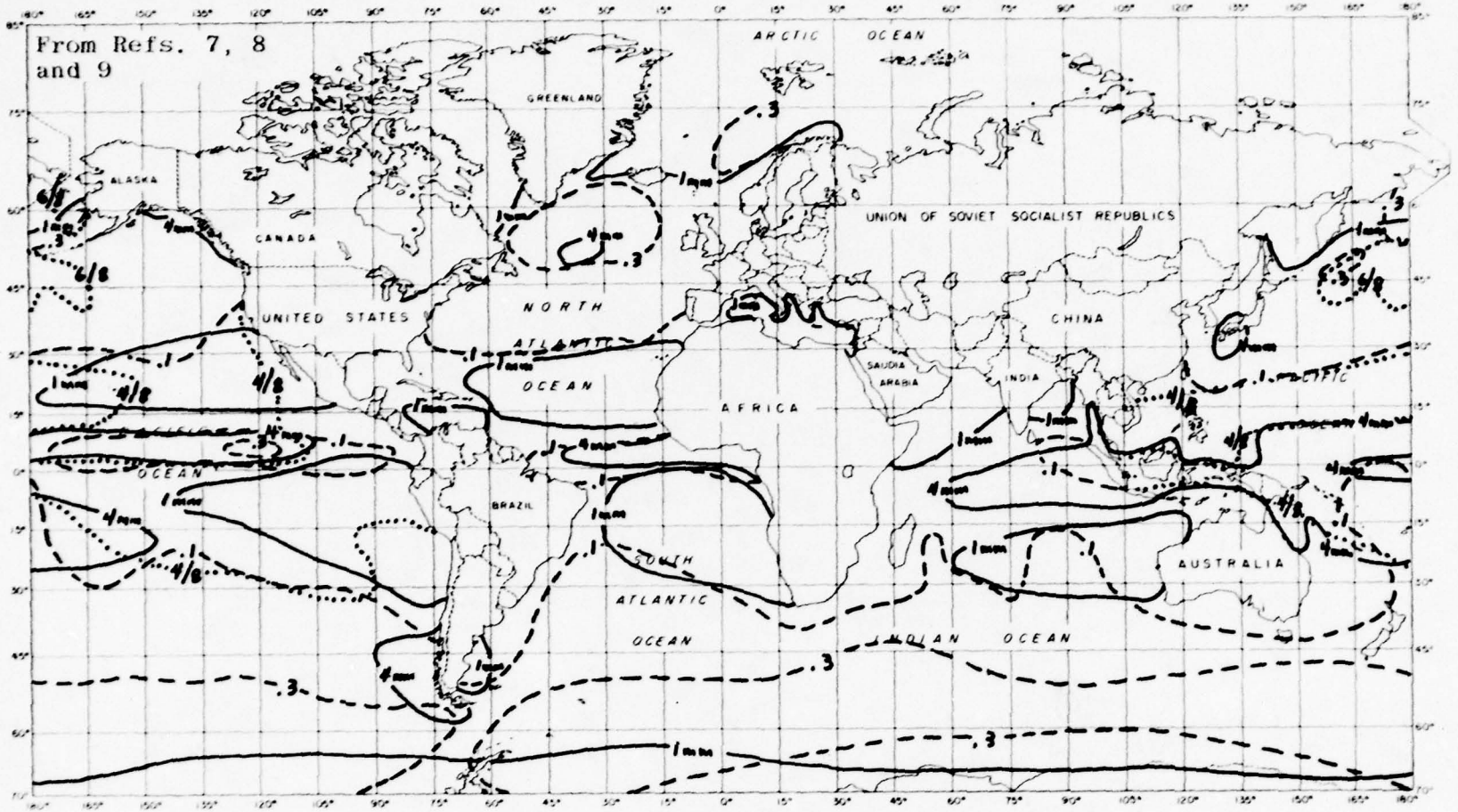

Fig. 20. Superposition of average daily precipitation, precipitation frequency and average cloud cover for Mar-May.

Average daily precipitation (——), precipitation frequency (- - -), average Pacific cloud cover (····)
Jun-Aug (Jul for cloud cover and precipitation frequency)

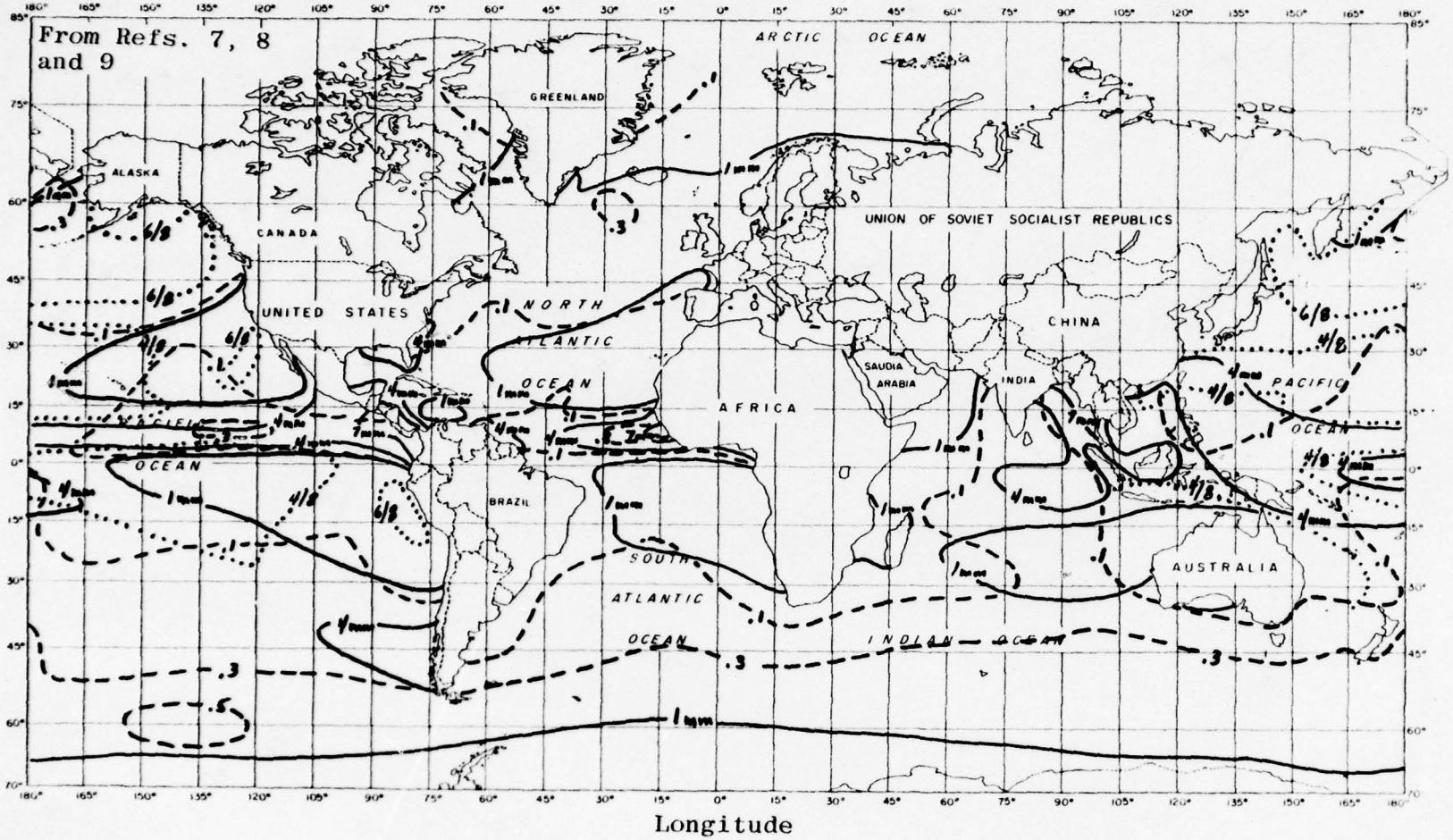

Fig. 21. Superposition of average daily precipitation, precipitation frequency and average cloud cover for Jun-Aug.

Average daily precipitation (——), precipitation frequency (- - -), average Pacific cloud cover (····)
Sep-Nov (Oct for cloud cover and precipitation frequency)

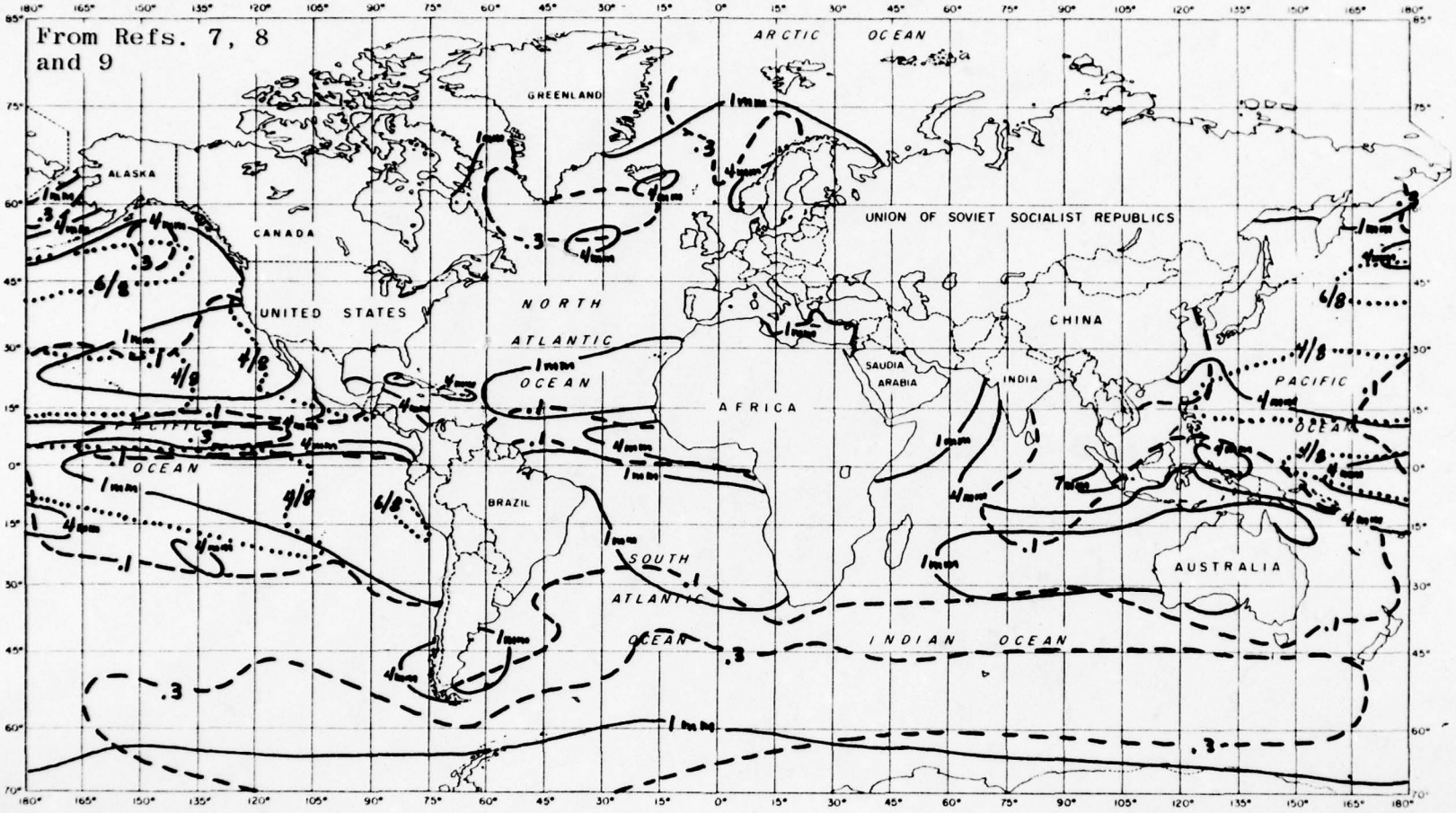

Fig. 22. Superposition of average daily precipitation, precipitation frequency and average cloud cover for Sep-Nov.

spectrum of rain-rate regions, and we estimated monthly and seasonal values of precipitation parameters using available sources. Seasonal (three-month) precipitation amounts were extracted from the Möller maps[7], monthly precipitation frequencies were extracted from the Crutcher and Davis maps[9], and estimates of monthly and annual "thunderstorm days" were extracted from maps and tables published by the World Meteorological Organization.[10] All are tabulated in Table 4; and the locations are mapped in Figure 23.

We previously discussed our confidence in the precipitation amount and precipitation frequency data. The "thunderstorm days" data, however, strained credibility. First, a "thunderstorm day" is defined as a day on which thunder is heard or lightning is observed: precipitation need not occur at the point of observation and many such observations can be made on one thunderstorm day. Confidence in shipborne observations of such phenomena has to be quite low. Second, Reference 10 provides four different ways of estimating annual thunderstorm days: monthly maps of thunderstorm-day isopleths that can be summed; seasonal maps that can be summed; an annual map; and tables that can be interpolated for any location. Table 5 summarizes the results of estimating annual thunderstorm days by all four methods. Assuming that table interpolation of annual values gives the most accurate estimates (one is not dependent on an analyst's judgment or an artist's ability), we see that summing the estimates from the monthly maps results in overestimating thunderstorm days by about a factor of two. Therefore, the thunderstorm days given in Table 4 are made consistent with the annual values obtained by table interpolation. We adjusted the monthly values in accordance with the relative frequencies obtained from the monthly maps.

In Table 4, we underlined precipitation amount for locations exhibiting a seasonal variation of precipitation (mm) of 2:1 or more. The seasonal variations revealed in Table 4 are most striking in the moist tropics (locations 7, 8 and 13, with location

Table 4. MONTHLY AND SEASONAL PRECIPITATION DATA FOR SELECTED OCEAN LOCATIONS

Location	Parameter	Dec	Jan	Feb	Mar	Apr	May	Jun	Jul	Aug	Sep	Oct	Nov
1. Mid Atlantic 40N 40N	Precipitation (mm)	←	300	→	←	250	→	←	175	→	←	200	→
	Precipitation Freq.	.21	.26	.25	.23	.20	.18	.14	.12	.11	.15	.18	.20
	Thunderstorm Days	2	1	2	2	1	0	1	1	2	1	1	1
2. North Atlantic 65N 0	Precipitation (mm)	←	200	→	←	100	→	←	100	→	←	200	→
	Precipitation Freq.	.36	.40	.38	.35	.30	.20	.20	.20	.30	.30	.31	.33
	Thunderstorm Days	0	0	0	0	0	0	0	1	0	0	1	0
3. Mediterranean 35N 20S	Precipitation (mm)	←	150	→	←	50	→	←	20	→	←	75	→
	Precipitation Freq.	.10	.10	<.10	<.10	<.10	<.10	<.10	<.10	<.10	<.10	.09	.09
	Thunderstorm Days	3	4	3	2	2	2	2	1	2	2	3	4
4. Persian Gulf 15N 60S	Precipitation (mm)	←	25	→	←	20	→	←	25	→	←	25	→
	Precipitation Freq.	<.10	<.10	<.10	<.10	<.10	<.10	.08	.08	<.10	<.10	<.10	<.10
	Thunderstorm Days	0	0	0	0	0	0	0	1	1	1	0	0
5. Indian Ocean 0N 75E	Precipitation (mm)	←	450	→	←	400	→	←	400	→	←	525	→
	Precipitation Freq.	.10	.10	.11	<.10	.09	.12	.12	.12	.12	.11	.09	.08
	Thunderstorm Days	1	1	2	1	2	2	1	1	1	1	1	2
6. W. Australia 20S 115E	Precipitation (mm)	←	75	→	←	50	→	←	50	→	←	20	→
	Precipitation Freq.	<.10	.08	<.10	<.10	<.10	<.10	<.10	<.10	<.10	<.10	<.10	<.10
	Thunderstorm Days	2	3	3	2	1	0	0	0	0	0	0	1
7. East Indies 5S 120E	Precipitation (mm)	←	600	→	←	500	→	←	200	→	←	150	→
	Precipitation Freq.	<.10	.12	.10	<.10	.10	.10	<.10	<.10	<.10	<.10	<.10	<.10
	Thunderstorm Days	5	8	4	4	5	2	1	1	1	2	3	5
8. Philippines 15N 120E	Precipitation (mm)	←	200	→	←	300	→	←	400	→	←	200	→
	Precipitation Freq.	.11	.08	.09	.08	.08	.08	.09	.11	.11	.10	.11	.09
	Thunderstorm Days	1	1	1	2	2	6	5	4	5	4	3	2
9. Sea of Japan 40N 135E	Precipitation (mm)	←	100	→	←	300	→	←	200	→	←	180	→
	Precipitation Freq	.40	.44	.35	.20	.19	.20	.21	.19	.17	.17	.20	.23
	Thunderstorm Days	0	0	0	0	0	1	1	2	2	1	1	0
10. Bering Sea 60N 175W	Precipitation (mm)	←	100	→	←	75	→	←	100	→	←	100	→
	Precipitation Freq.	.38	.25	.33	.31	.31	.30	.25	.31	.31	.30	.35	.35
	Thunderstorm Days	0	0	0	0	0	0	0	0	0	0	0	0
11. NE Pacific 45N 125W	Precipitation (mm)	←	400	→	←	200	→	←	150	→	←	400	→
	Precipitation Freq.	.17	.20	.17	.15	.13	.12	.10	.10	.04	.10	.17	.17
	Thunderstorm Days	0	0	0	0	0	1	1	1	1	0	0	0
12. Hawaii 20N 155W	Precipitation (mm)	←	125	→	←	80	→	←	75	→	←	100	→
	Precipitation Freq.	.09	.08	.10	.08	<.10	<.10	<.10	.10	.10	<.10	<.10	.09
	Thunderstorm Days	1	1	1	0	0	0	0	0	0	0	0	0
13. Panama 10N 80W	Precipitation (mm)	←	200	→	←	400	→	←	600	→	←	600	→
	Precipitation Freq.	.10	.10	.10	.10	.10	.10	.17	.20	.20	.18	.15	.10
	Thunderstorm Days	3	4	4	2	4	6	12	10	11	9	6	4

NOTE: Underlined values indicate ≥2:1 seasonal variation

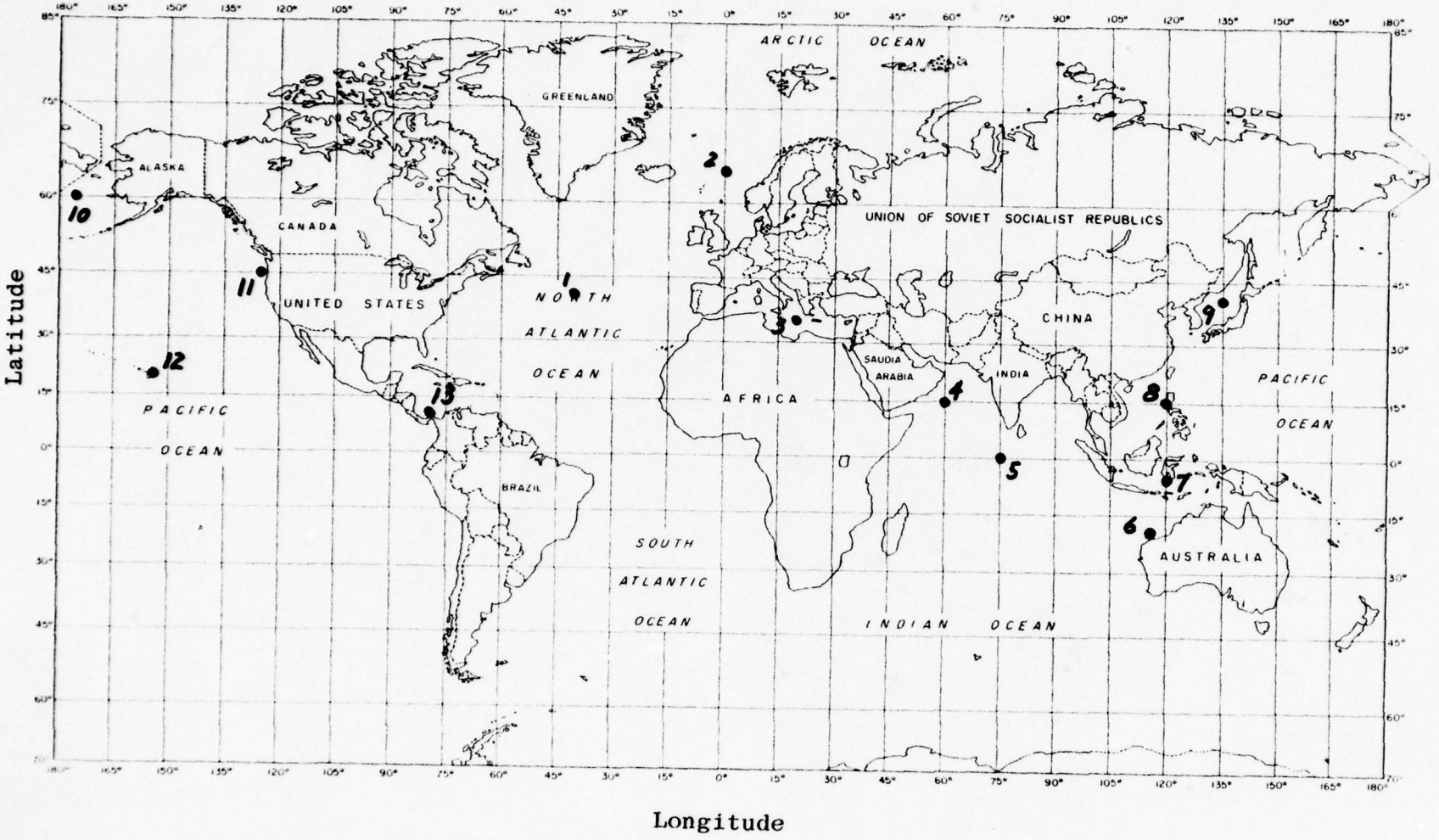

Fig. 23. Locations of the 13 points examined

Table 5. ANNUAL NUMBER OF THUNDERSTORM DAYS ESTIMATED BY FOUR DIFFERENT METHODS [a]

Location	Estimated Annual Thunderstorm Days			
	Monthly Maps	Quarterly Maps	Annual Maps	Table Interpolation
1. 40N 40W	25	20	17	15
2. 65N 0	2	2	1	2
3. 35N 20E	45	36	30	30
4. 15N 60E	30	15	5	3
5. 5S 120E	81	61	41	41
6. 15N 120E	72	58	30	36
7. 40N 135E	21	14	18	8
8. 60N 175W	3	1	1	0
9. 45N 125W	13	8	8	4
10. 20N 155W	24	10	5	3
11. 10N 80W	82	65	90	75
12. 20S 115E	39	22	20	12
13. 20S 75E	32	27	16	16

[a]From reference 10.

5 an exception) and, to a smaller extent, in the temperate region storm belts (locations 1, 2, 9 and 11) and the arid subtropical regions (locations 3 and 6). As a general rule, the three parameters vary consistently, the major exception being location 9 (Sea of Japan), where the highest frequencies of precipitation appear to coincide with the smallest amounts.

3.1.3 Variation In Mean Freezing Height

Crane[4] suggests a simple algorithm for freezing height as a function of latitude, saying that it approximates the average of the spring/fall and summer freezing height profiles averaged (zonally) around the globe. The Crane approximation appears as the long-dash profile in Figure 24. Two other sources provided data on the seasonal and spatial variations of freezing height, and the approximations from them are also plotted in Figure 24. The zonally averaged profiles for January and July are from the Handbook of Geophysics[11]. Crutcher and Meserve[12] provide maps of average upper air temperature in the Northern Hemisphere at selected constant pressure levels. From surface, 850 mb (~1.5 km) and 700 mb (~3 km) maps, crude longitudinal profiles of freezing height can be extracted. These are shown as the short-dash profiles grouped around the zonal averages in Figure 24. Since calculations of millimeter-wave precipitation attenuation are quite sensitive to the freezing height assumed, we conclude that mean freezing height must be treated as a variable, a function of location (longitude as well as latitude) and season (rather than the annual mean).

3.2 Proposed Seasonal, Oceanic Precipitation-Rate Climate Model

We begin with the premise that precipitation-rate frequency of occurrence statistics are properly related by Crane to gross climatic variables; it becomes our initial point of departure. Certain aspects of the time and space distributions of climate types have, however, been questioned. We propose the following seasonal oceanic precipitation-rate climate model as a preliminary solution to the problems raised.

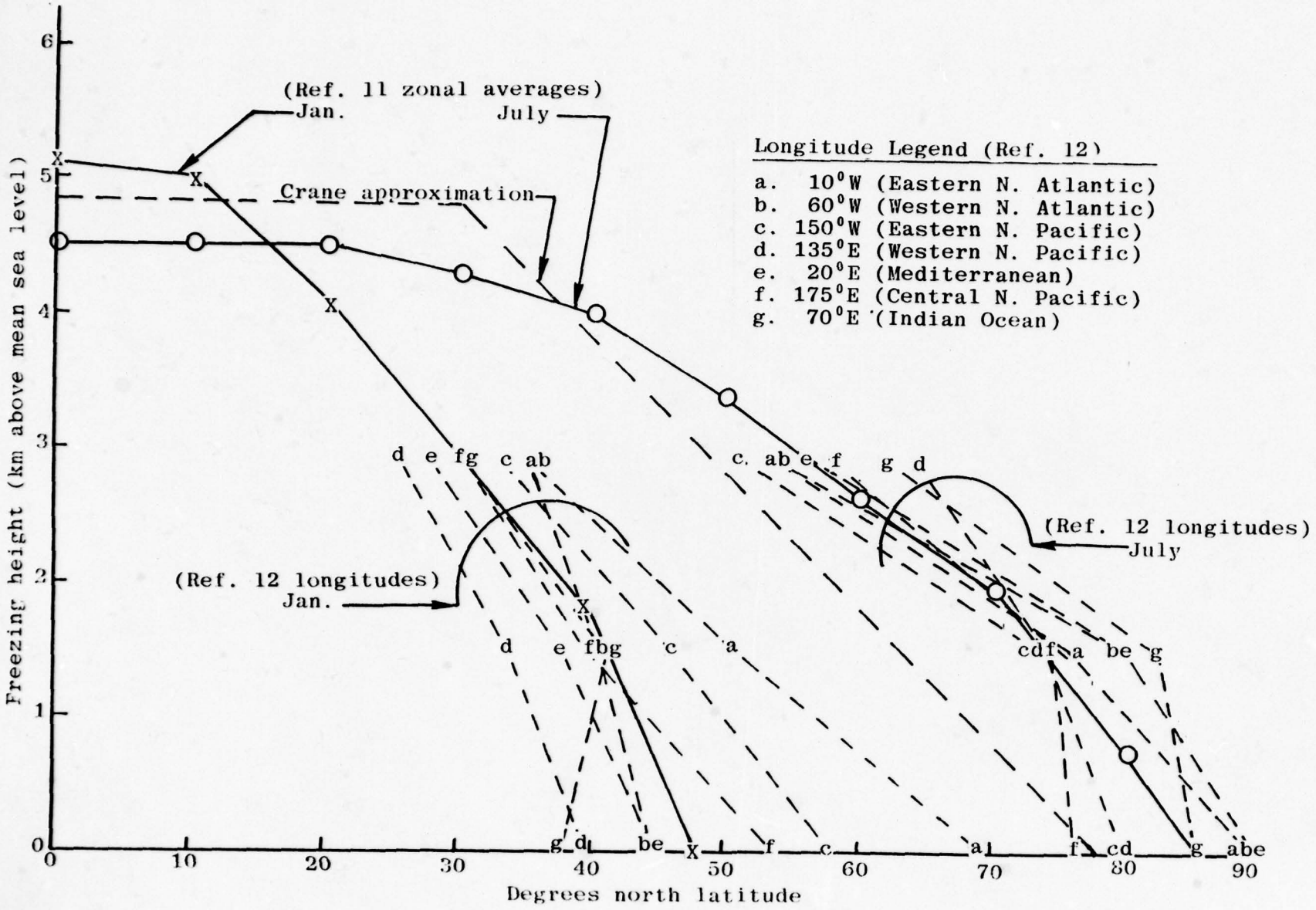

Fig. 24. Freezing height variation

3.2.1 Seasonal Maps of Oceanic Precipitation-Rate Regions

The first step is to provide separate precipitation-rate climate region maps for the four seasons. Monthly maps are not warranted by currently available data. Using the Crane map (Fig. 1) as a first approximation (and inferring from it the approximate regional bounding values of precipitation amount, frequency, etc.), the precipitation and cloud analyses of Figures 19-22 were scrutinized and used as guides in delineating four seasonal climate region distributions over the oceans. As in Crane's original work, the process remains highly judgmental. Precipitation amount was the primary criterion, then precipitation frequency.

Some modifications of climate types are introduced at this stage (denoted by the prime symbol in the following list of criteria and on the maps). The modifications affect the precipitation rate distributions assumed typical of those climate types, discussion of which follows in the next section of this report.

The basic guidelines used for delineating the ocean precipitation rate regions were as follows:

A', Polar Ice Cap - The Arctic Basin portion of Crane's type A (Polar Tundra) climate; over ice covered oceans and significantly poleward of the paths of most major extratropical cyclones; insignificant precipitation amount and very low frequency. Differs from Crane's type A in that it excludes the summertime precipitation regime found over continental tundra.

B', Polar Maritime - The maritime portions of Crane's type B (Polar Taiga) climate; the transition zone between the icecap and temperate maritime climates, located along the sea-ice fringe. Average precipitation about 1 mm/day; high frequencies of light, nonconvective precipitation is possible. Frequencies of high precipitation rates should be much less than indicated by Crane's distribution for type B, because the latter distribution includes a convective component found over continents much more frequently than over the polar oceans.

F, Subtropical Arid - Primarily the westward extensions of the subtropical continental deserts; poleward boundaries can be highly variable from year-to-year (e.g., off the California and Chile coasts); average precipitation about 1 mm/day or less and frequency about 0.1 or less, varying from convective at low latitudes to partially stratiform at higher latitudes.

C, Temperate Maritime - The major portions of the oceans, generally poleward and westward of the subtropical highs (F-type regions) and excluding the primary paths of extratropical storms; average daily precipitation ranges from 1 mm to 4 mm, and frequency from about 0.1 to greater than 0.5; stratiform (storm-related) precipitation predominates in poleward portions, convective in equatorward portions.

C' Maritime Cyclonic - A new precipitation rate region introduced to account for the high precipitation amounts (average greater than 3.5 mm/day) and high frequencies (0.25 to greater than 0.5) associated with the most frequent oceanic paths of extratropical cyclones. We assume it has a precipitation-rate frequency distribution midway between types C and G (i.e., near type D) at the high precipitation-rate end of the distribution, and approaching types B and C at the low precipitation-rate end.

D, Temperate Continental - Minor eastward extensions from the major continents into offshore waters; a mixture of stratiform and convective precipitation averaging 1.5 to 3.5 mm/day at frequencies of about 0.1 to 0.2.

G, Tropical Moderate - Includes essentially all of the tropical oceans except those portions that (seasonally) experience intense and frequent convective precipitation; precipitation amounts vary widely (perhaps too widely) from more than 1 mm/day to less than 6 mm/day at frequencies of less than 0.1 to about 0.3; precipitation is essentially all convective.

E, Subtropical Wet - A minor summertime region near the southeast coasts of North America and Asia, characterized by convective rainfall generally less intense than that found in type H (Tropical Wet); average precipitation amounts about 3.5 to 6 mm/day with frequency of about 0.1.

H, Tropical Wet - The most intensely convective portions of the intertropical convergence zone; the ocean regions of heaviest rainfall, enhanced (and perhaps the data are biased by) local land effects in the East Indies and Central America; precipitation averages greater than 5 mm/day with frequencies of about 0.1 to 0.4.

Figure 25 illustrates the oceanic climate-type boundaries in terms of precipitation amounts and frequencies. This way of depicting the climate types serves two purposes:

1. It clearly reveals the range of precipitation characteristics included within each region. (The convective fraction of precipitation, which strongly influences the precipitation rate distribution, is missing up to this point. The convective fraction is simply assumed to be high in the subtropical and tropical E, F, G and H climates, low in the polar A' and B' climates and mid-range in the temperate C, C', and D climates.) For example, large ranges of precipitation amount and frequency are covered by types C and G, which also cover major portions of the oceans, and there is a substantial overlap between them. This indicates the likelihood of a large variance among precipitation rate distributions within those regions, and points up a possible need for further model refinements (either a new approach or a method for correcting for local variation).

2. Figure 25 provides a check for logical consistency in mapping the climate regions geographically. In addition to the obvious rule that polar climate types should not be adjacent to tropical and subtropical types, no two climate types should touch that do not touch or overlap in figure 25.

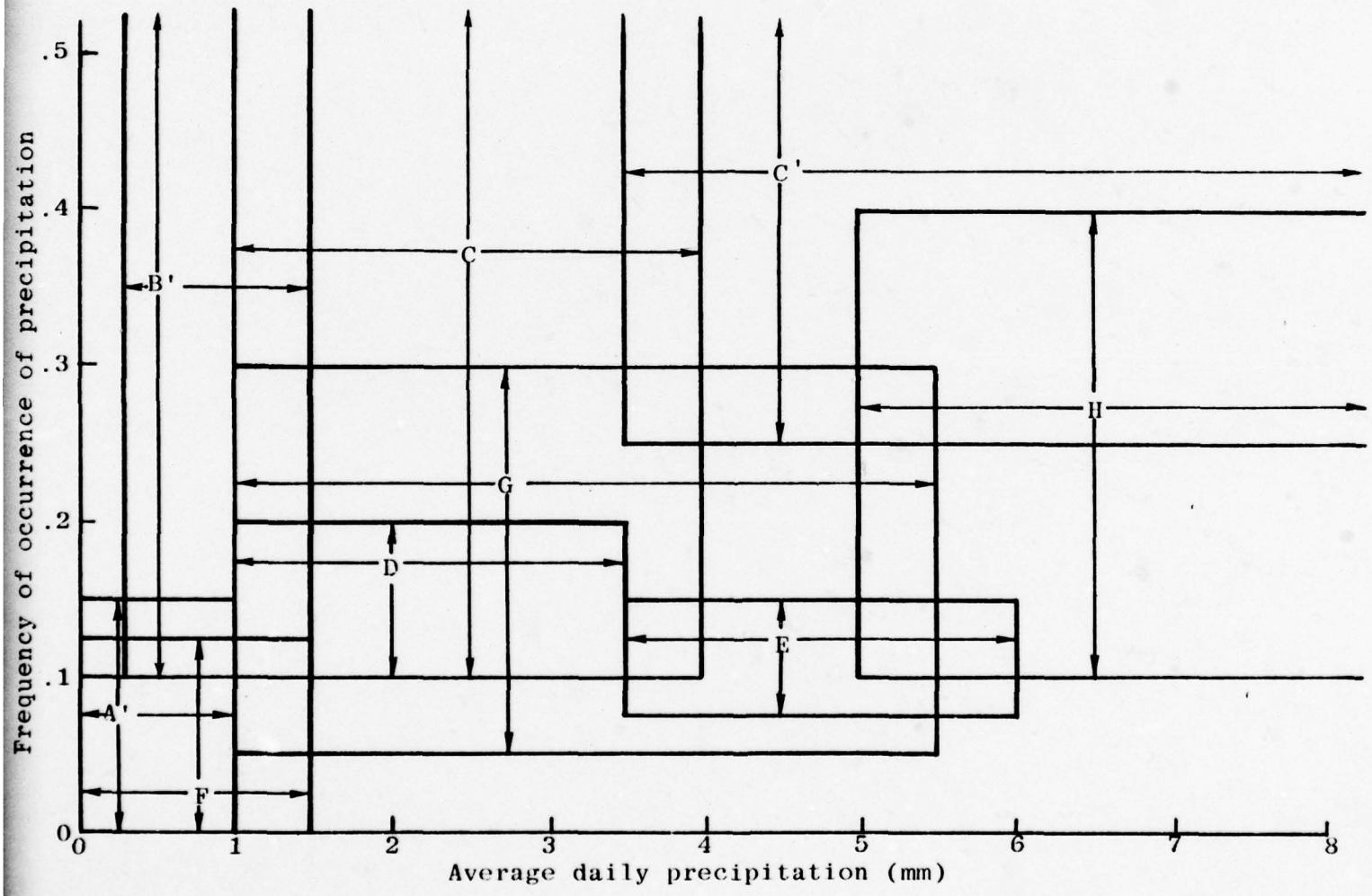

Fig. 25. Precipitation amount and frequency bounds for the oceanic climate regions

The proposed seasonal oceanic precipitation-rate climate region maps are shown in Figures 26-29.

3.2.2 Seasonal Maps of Mean Freezing Height

Along with the maps for the oceanic precipitation-rate regions a correspondingly detailed set of seasonal mean freezing height approximations must be used to calculate attenuation. Crutcher and Meserve[12] also prepared seasonal maps of freezing heights worldwide. Figures 30-33 are simply redrawn versions of their charts with an estimate of the 4.5 km freezing height added.

In many parts of the world, there may well be a correlation between freezing height and the occurrence of precipitation as rain. Although such a correlation would affect attenuation calculations, the data to quantify it are not easily acquired. Thus we do not address this potential problem further in this study.

3.3 Modified Precipitation-Rate Distributions

The precipitation-rate distributions assigned by Crane to the climate types (see Table 1) have the following qualities:

1. They reflect around-the-calendar average amount, frequency, and convective fraction of precipitation. Therefore, for locations where the precipitation varies significantly through the course of the year, the precipitation rate distributions reflect a temporal mixture of precipitation regimes.

2. The distributions are, of necessity, all based on land station data. Within the same climate type, the nature of the precipitation, and thus the distribution, can be significantly different between continental and oceanic locations.

3. The high frequency of occurrence low precipitation-rate tails of Crane's distributions are uncertain because the measurement of low precipitation rates is an uncertain, low confidence process. For example, meteorologists make no attempt to distinguish between liquid and solid precipitation in these measurements; but, because

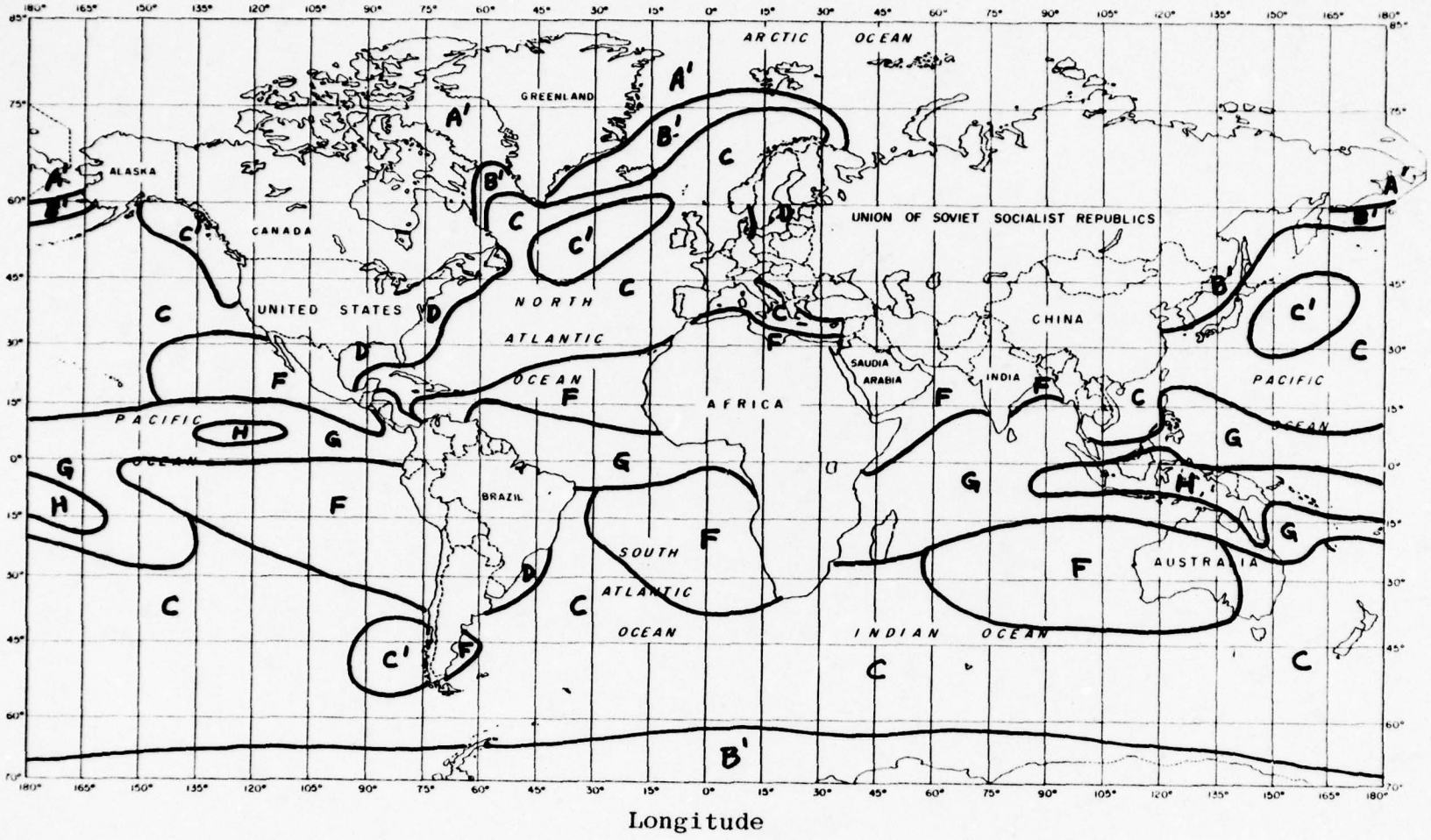

Fig. 26. Oceanic climate regions for December through February

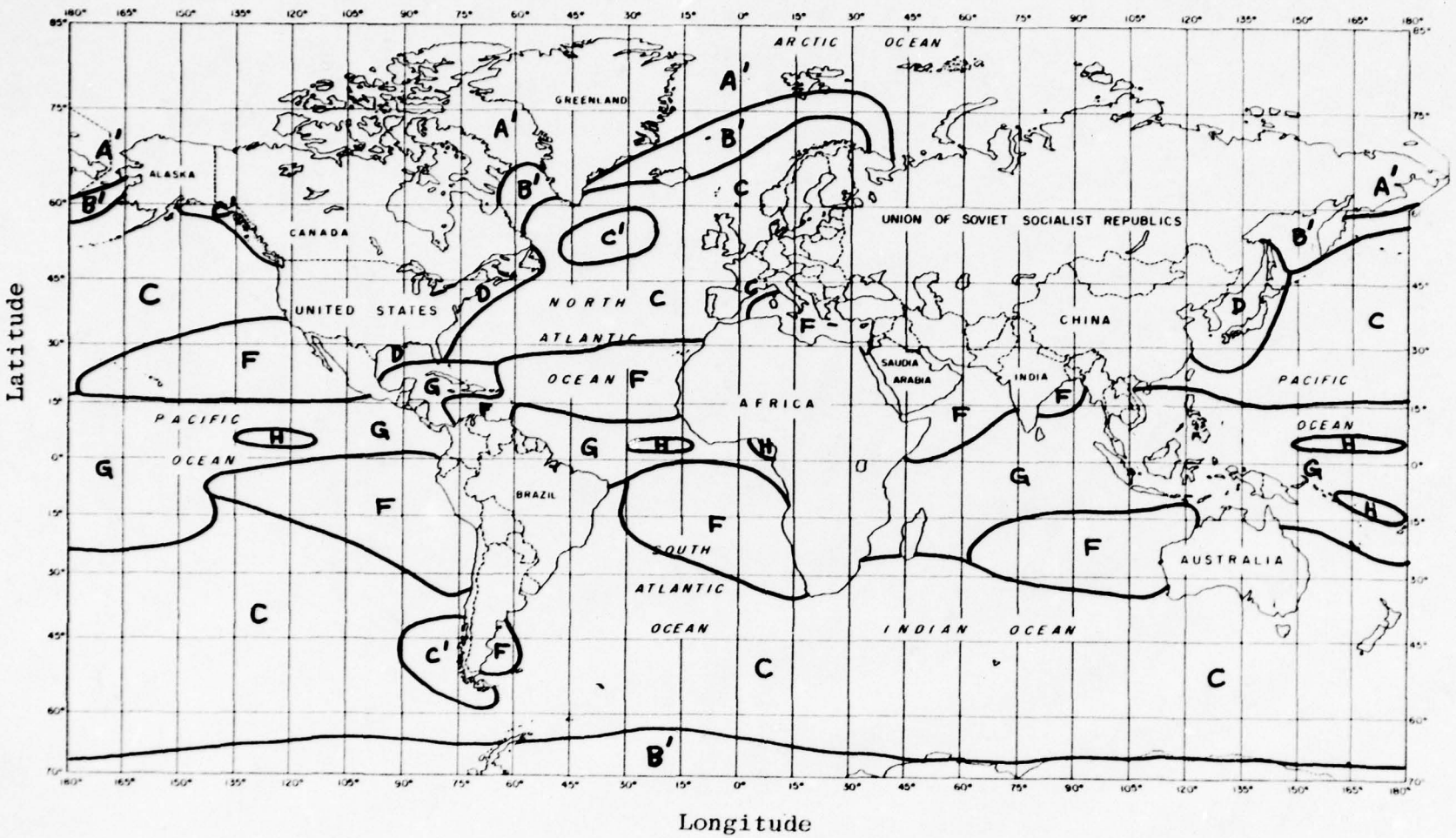

Fig. 27. Oceanic climate regions for March through May

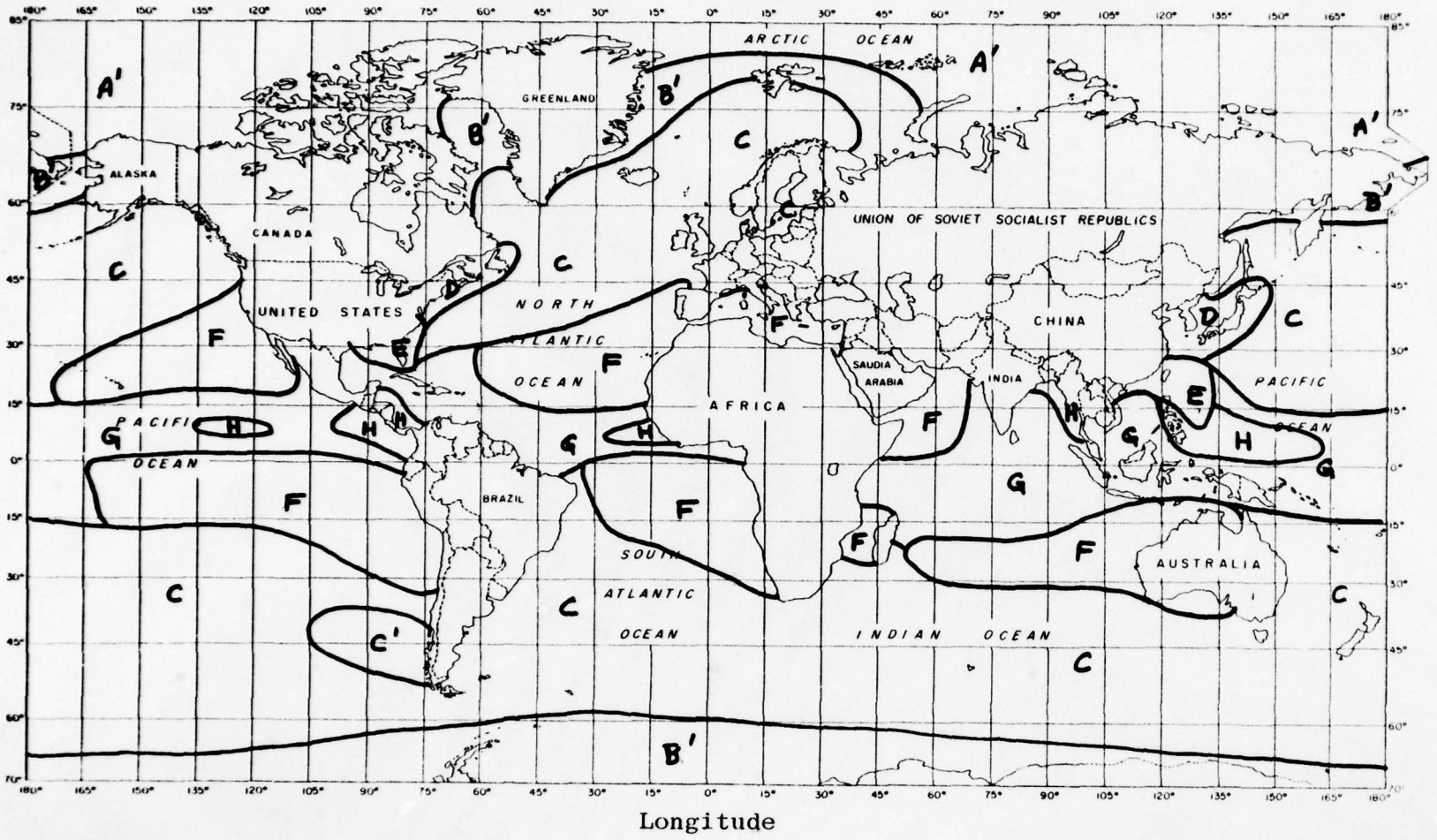

Fig. 28. Oceanic climate regions for June through August

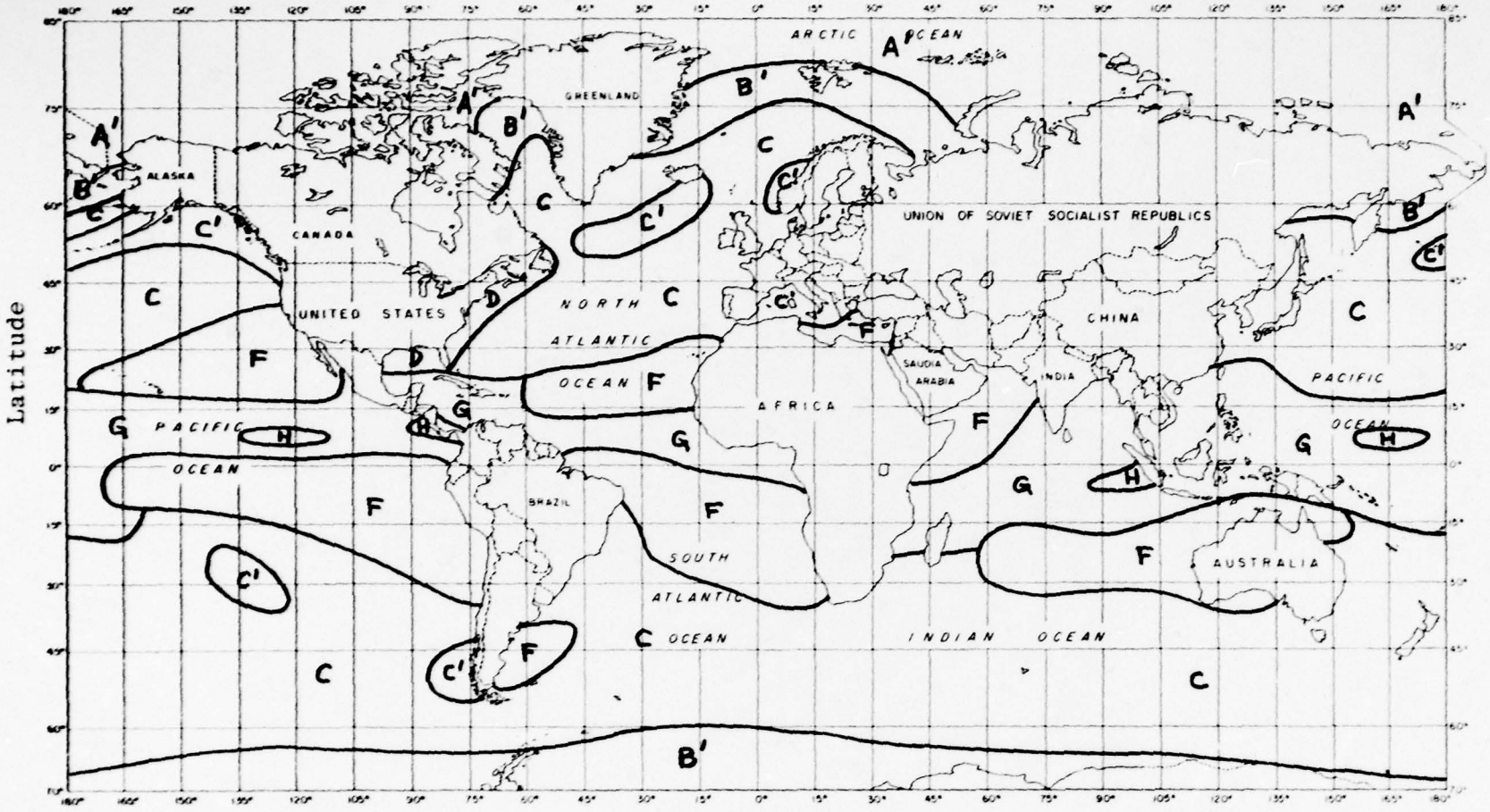

Fig. 29. Oceanic climate regions for September through November

From Ref. 12

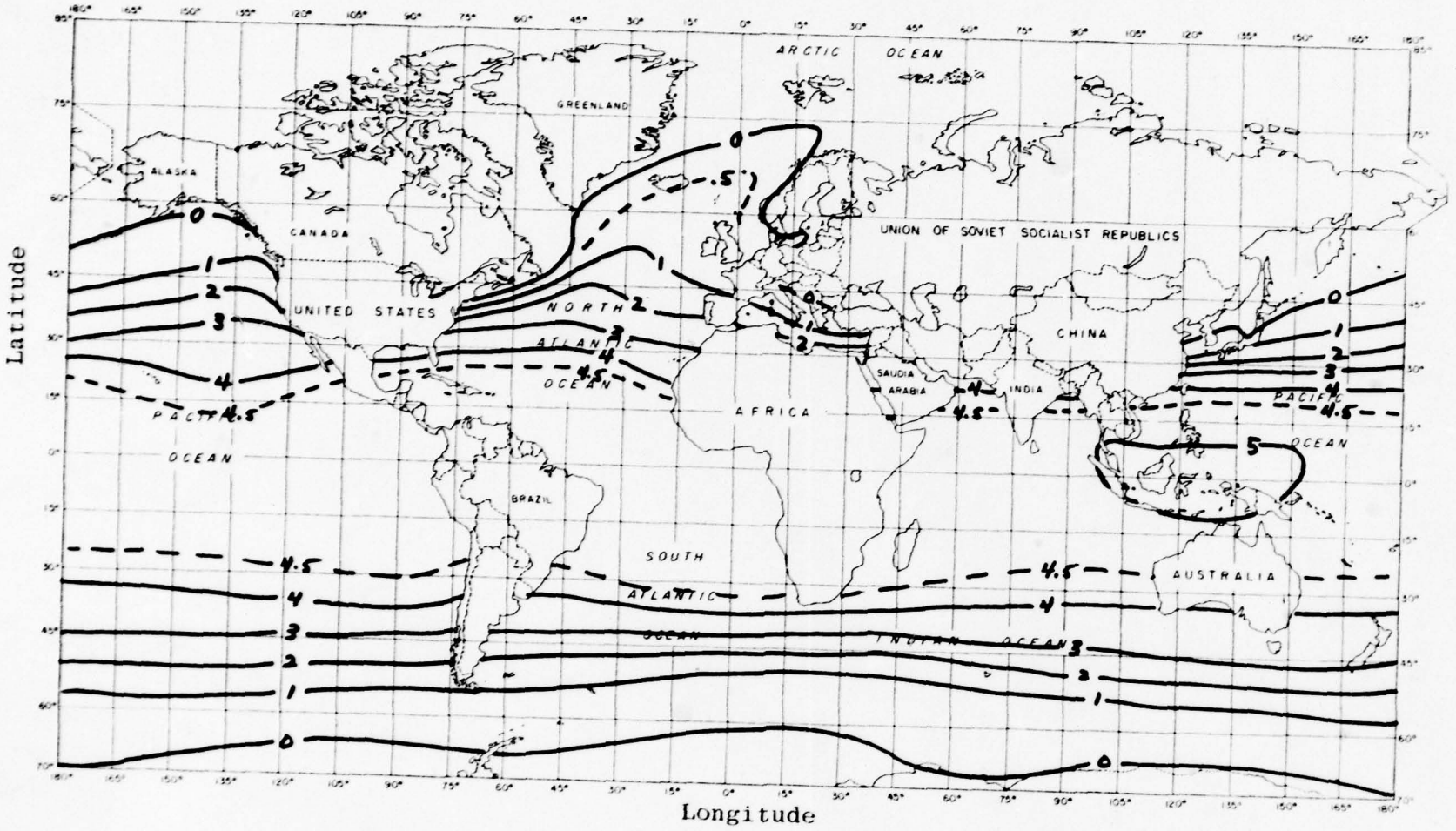

Fig. 30. Average freezing height (km) for December through February

From Ref. 12

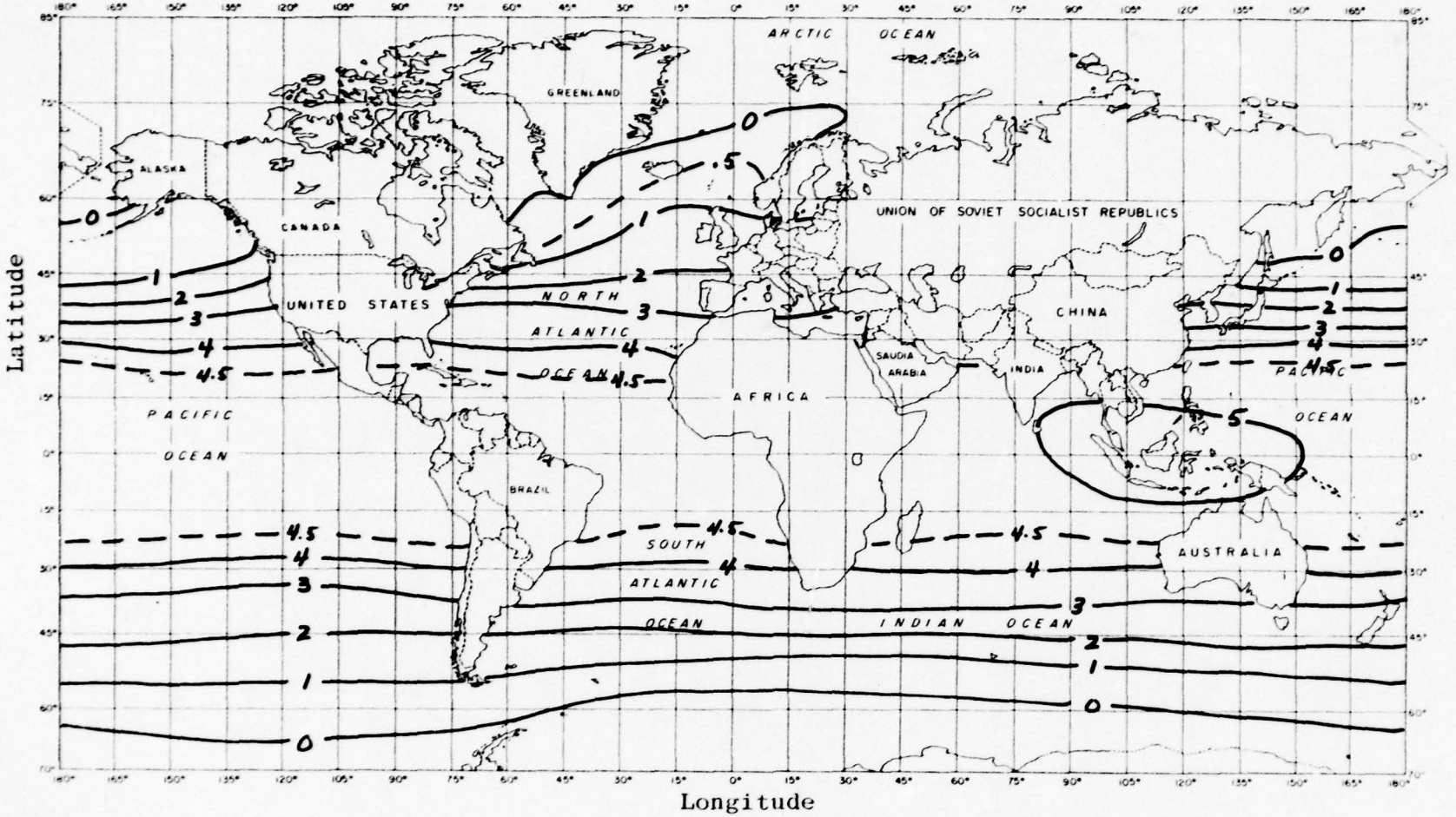

Fig. 31. Average freezing height (km) for March through May

From Ref. 12

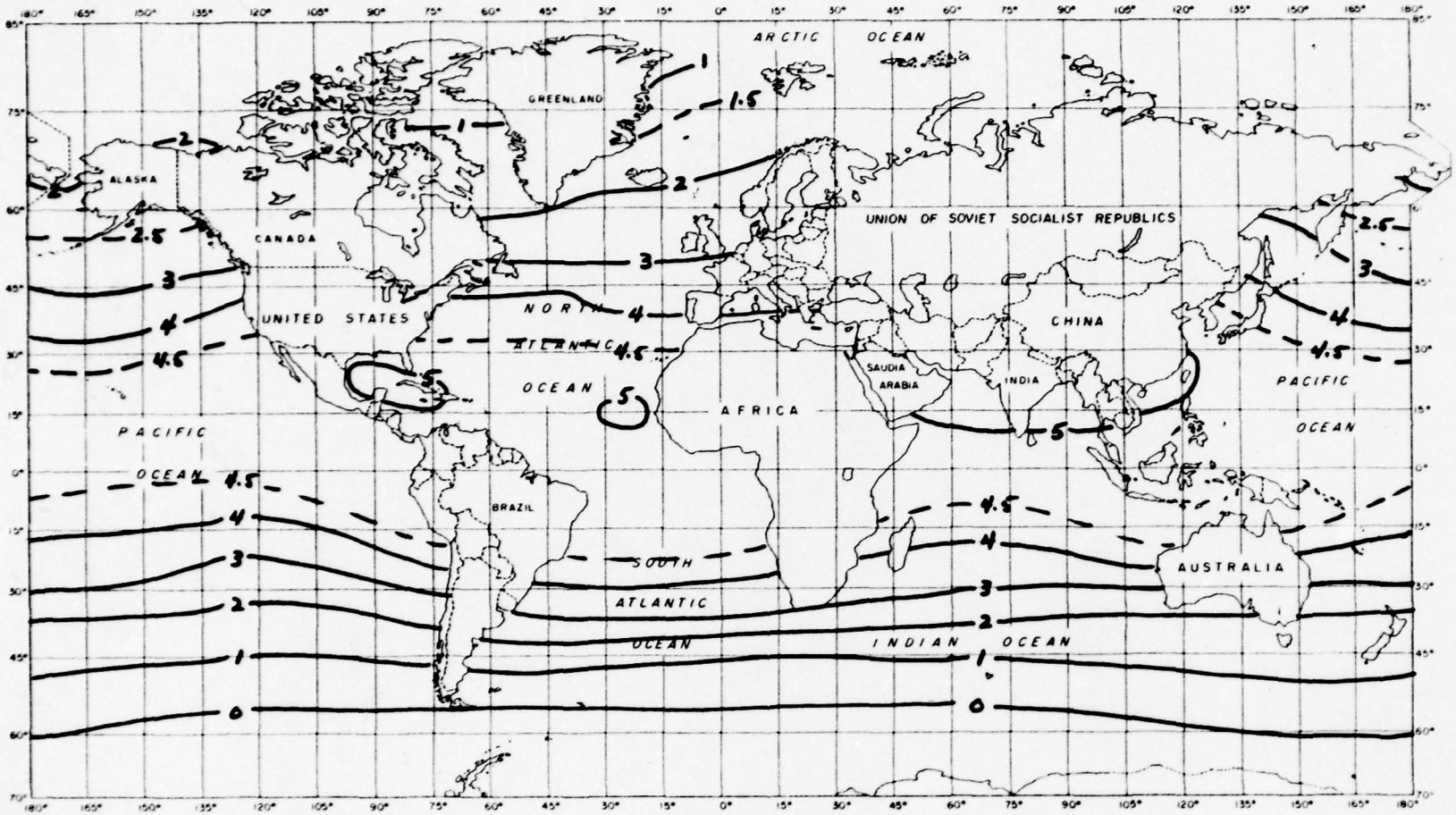

Fig. 32. Average freezing height (km) for June through August

From Ref. 12

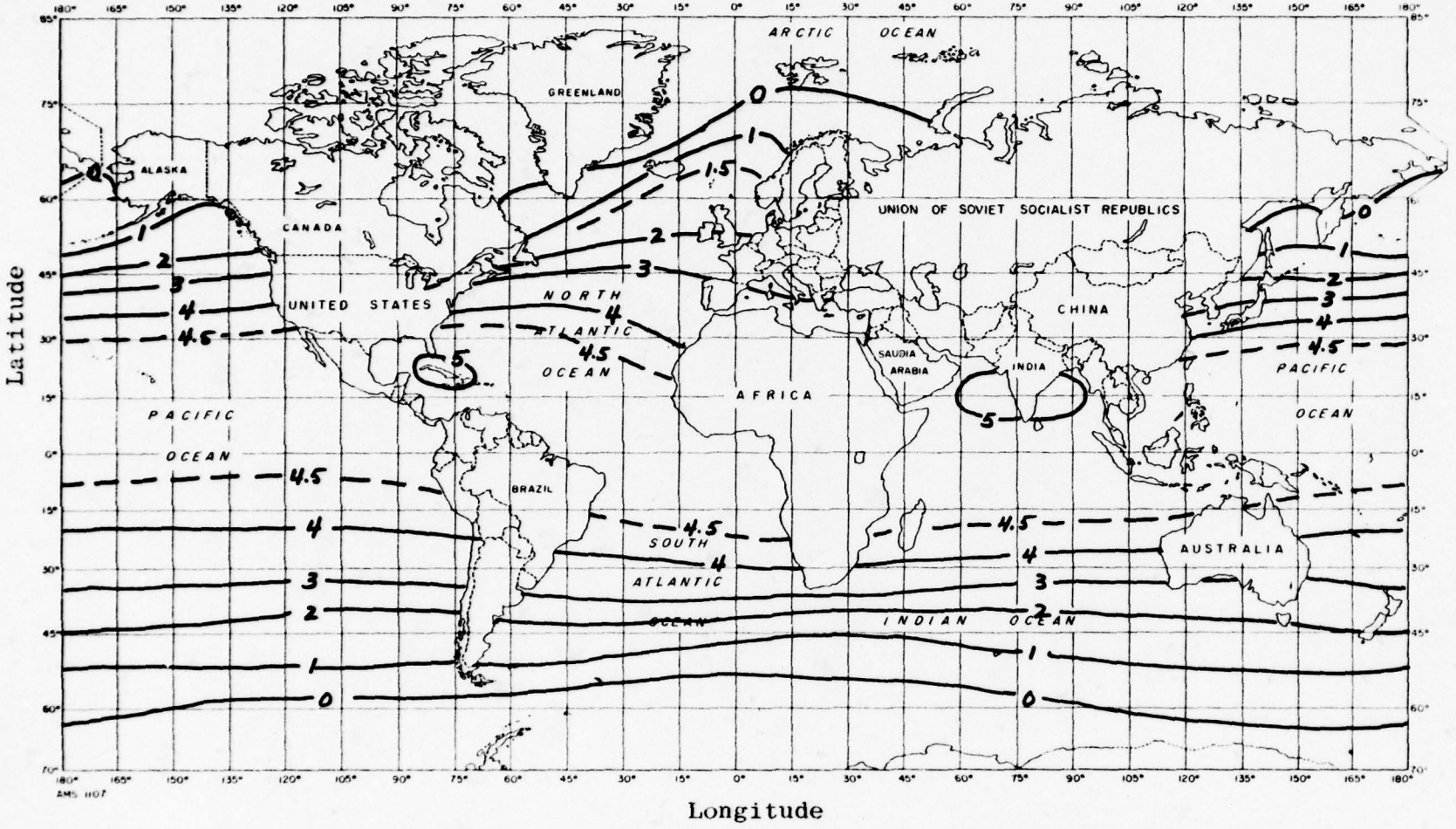

Fig. 33. Average freezing height (km) for September through November

of instrumentation problems, precipitation rates of snow are frequently omitted by default -- and snow invariably falls at a very low equivalent "rain rate". This occurs because the amount of snow precipitation is defined as the equivalent liquid water content of the snow.

To reduce the broadening of precipitation-rate distributions caused by spatially and temporally aggregating different precipitation regimes, we propose a seasonal oceanic model of climate types. Consistency would require that we calculate a new and narrower set of distributions for the "purer" seasonal oceanic climate types. To do so would require a substantial effort clearly beyond the scope of the present study. Instead, we propose some extensions and revisions of Crane's distributions as an interim measure.

In modifying the distributions, the first objective is to correct the most obvious and largest inconsistencies between the annual, land-oriented Crane model and the seasonal ocean model. We integrate the area under the precipitation rate distributions to see if the resulting total precipitation is consistent with the annualized precipitation amounts typical of the ocean precipitation rate regions. To do this, however, we should extend the distributions to the lowest observable precipitation rates.

To extend the distributions, we first assume that 0.1 mm/hr approximates the lowest precipitation rate recorded in weather records.* It follows from that assumption that the frequency at which 0.1 mm/hr is equaled or exceeded is approximated by the overall precipitation frequency as observed at any given location. Characteristic subjectively weighted values of overall precipitation frequency are estimated for all climate types from the guidelines used in delineating the ocean precipitation-rate regions (summarized in Figure 25). The estimated characteristic values for precipitation

---

*This approximation warrants further study. Light snow, especially, is probably often observed at much lower rates than 0.1 mm/hr of equivalent liquid water content. The eye can detect the falling of very sparsely distributed snow flakes.

frequency and average daily precipitation are given in Table 6.

3.3.1 Procedure For Modifying the Distributions

A few scattered changes were first made to Crane's tabulated values for the eight rain-rate distributions (Table 1). There are two fairly obvious discontinuities, possibly typographical errors. The value at 0.1 percent for A is changed from 6.5 to 5.8 and the value at 0.2 percent for C is changed from 6.8 to 4.8. In addition, several small changes were introduced--shifts of 1 or sometimes 2 in the least significant figure, roughly balanced between up and down. We did not make these changes to dispute Crane's data, but rather (a) to reflect his and our point of view that given sufficient world-wide data the curves would probably be smooth, monotonic and unimodal (see Crane's plot, our Figure 2); and (b) to facilitate consistent smoothing of the subsequent attenuation curves.

We suggest a change in the F curve. This precipitation-rate region is quite dry; but when it does rain, it is usually convective. Thus the general shape of the curve seems plausible from physical considerations. However, we find no obvious basis for the slight bulge at 1 mm/hr and 1 percent in Table 1. Of much greater importance, the integrated precipitation (discussed in the following section) comes out too high. To correct this, we arbitrarily drew a simpler (i.e., without the inflection of Figure 3) and lower curve for the F region. This constitutes a significant change (see Figure 34).

The major modification to the distribution curves was their extension to an assumed lowest rate of observable precipitation. Per previous discussion (and the footnote regarding observable snowfall rates), we tentatively tagged this minimum rate at 0.1 mm/hr, except for the polar A' and B' climates where we assumed 0.05 mm/hr, as shown in Figure 34. For most of the cumulative distribution curves, extension to the minimum precipitation rate required only a smooth extrapolation from the 2 percent values (where Crane's data end) to the overall precipitation frequencies of occurrence (Table 6) plotted at a 0.1 mm/hr precipitation rate. Three exceptions to this general procedure follow:

Table 6. REGIONAL CHARACTERISTIC VALUES OF PRECIPITATION FREQUENCY AND AVERAGE DAILY PRECIPITATION

Region	Characteristic Values	
	Precipitation Frequency	Average Precip. (mm/day)
A'	0.10	0.5
B'	0.25	1.0
C	0.30	2.5
C'	0.35	4.5
D	0.15	2.25
E	0.10	4.25
F	0.08	0.75
G	0.20	3.25
H	0.20	6.5

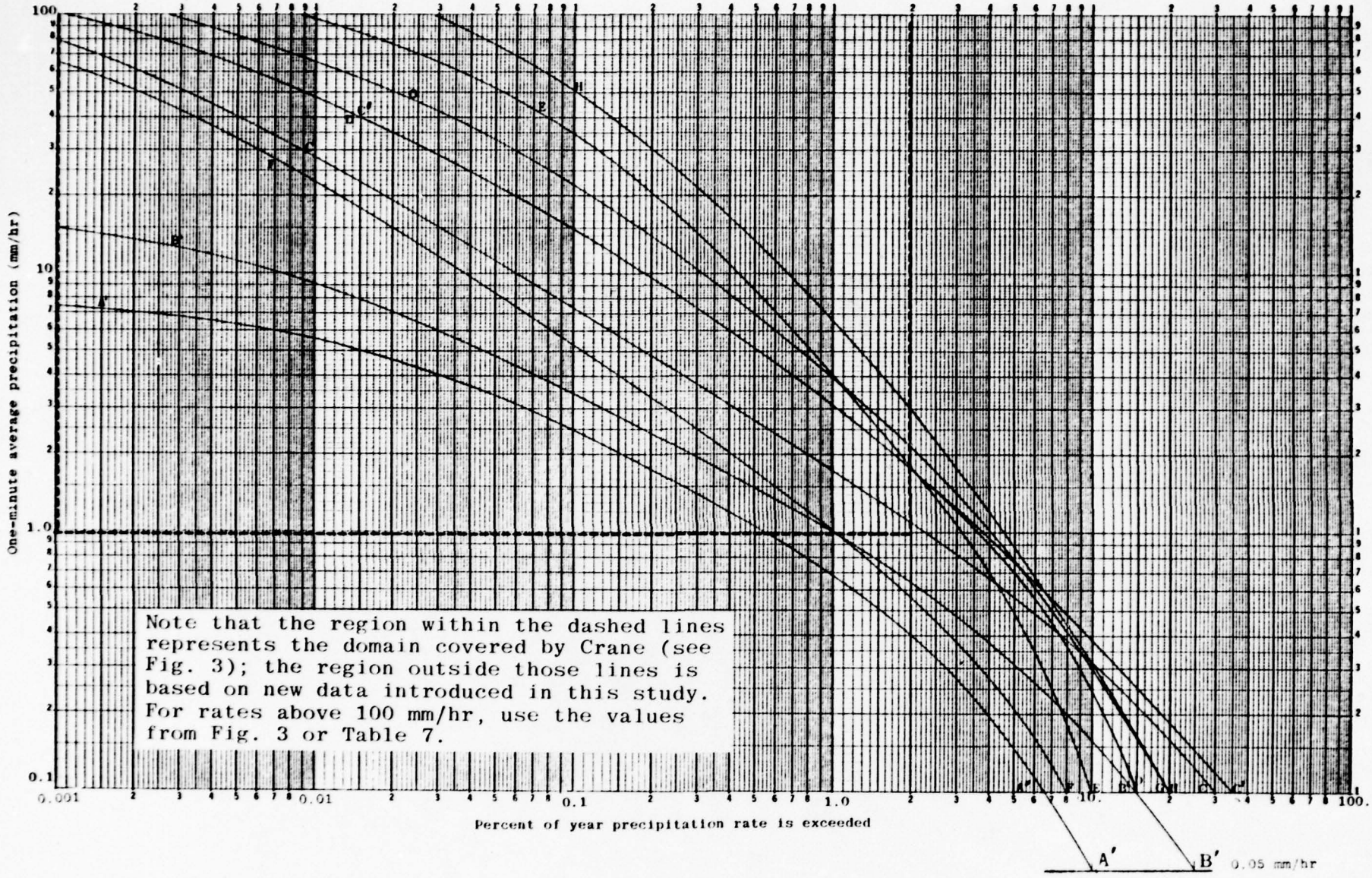

Fig. 34. Cumulative distributions of one-minute surface precipitation, proposed model

1. By the stated criteria for the new C' (Maritime Cyclonic) climate type, the precipitation rate distribution is similar to type D at high precipitation rates, but the total precipitation amount and frequency of occurrence are greater. The proposed C' distribution curve reflects these criteria.

2. Examination of basic precipitation data for continental locations within Crane's type B (Polar Taiga) climate zone reveals a significantly higher amount and frequency of precipitation in the summer half-year than would be expected (at any time of year) over the maritime, ice fringe extensions (type B') of that climate zone. That continental summertime precipitation also has a large convective component that would not be found in B' regions. Therefore, we suggest a precipitation-rate distribution for B' that is much lower than that for B at high precipitation rates. Further, since much precipitation in the B' regions is snow, the assumed minimum observed precipitation rate is tentatively taken as 0.05 mm/hr.

3. We suggest an A' distribution that differs from Crane's A distribution in the same qualitative manner that B' differs from B. The arguments for the changes are the same as for the B' curve; they differ only in degree (smaller precipitation amounts and frequencies are involved).

The set of the oceanic precipitation-rate distributions, including the new tentatively proposed ones, is plotted in Figure 34. Values above 100 mm/hr are unchanged from Figure 3. Table 7 presents numerical values to facilitate computer calculations.

3.3.2 Consistency of Modified Distributions with Climate Type Criteria

It is possible to make a rough check on the consistency of the precipitation-rate distributions (Fig. 34) with the precipitation criteria (Fig. 25) by comparing the integral under the distributions with the typical annual precipitation amounts in the precipitation-

Table 7. CUMULATIVE PRECIPITATION-RATE DISTRIBUTIONS FOR A PROPOSED OCEANIC CLIMATE MODEL (SEE FIGURE 34).

P, Percent of Year	Value of Precipitation Rate (mm/hr) that is Exceeded P Percent of the Time								
	A'	B'	C	C'	D	E	F	G	H
0.001	7.5	15.0	80	102	102	168	66	129	251
0.002	7.1	13.7	62	86	86	144	51	109	220
0.005	6.4	11.2	40	64	64	117	33	83	178
0.01	5.6	9.1	28	48	48	96	22.5	67	147
0.02	4.6	7.1	19	35	35	77	15.0	51	115
0.05	3.4	4.8	11	22	22	52	8.5	33	77
0.1	2.5	3.4	7.3	15	15	35	5.3	22	51
0.2	1.75	2.4	4.8	9.8	9.8	20.5	3.3	14	30
0.5	1.05	1.5	2.7	5.2	5.2	8.7	1.7	7.0	13.5
1.0	0.68	1.0	1.75	3.1	3.1	4.1	1.0	4.0	6.6
2.0	0.40	0.64	1.10	1.8	1.8	1.8	0.56	2.2	3.0
5.0	0.145	0.31	0.56	0.77	0.70	0.49	0.21	0.78	0.88
10.0	0.05	0.16	0.33	0.38	0.24	0.10	0.00	0.30	0.31
20.0	0.00	0.07	0.16	0.19	0.00	0.00	0.00	0.10	0.10

rate regions. The integration cannot be precise because (a) there is no analytic formulation for these empirical curves, and (b) the great range of the variables precludes plotting them on linear graph paper and using conventional planimetric techniques. However, we can approximate this process using simple numerical methods. One can easily visualize the process used.

Firstly, Figure 34 gives cumulative or exceedance probabilities, and these must be converted into probability density functions. For example, the probability that the precipitation rate exceeds 5 mm/hr in Region A' is read as 0.015 percent (or about 1.32 hrs in a year). Similarly, the probability that the rain rate exceeds 2.5 mm/hr is 0.100 percent. Thus, the probability that the rain rate lies between 2.5 and 5 mm/hr is the difference or 0.085 percent. By taking differences in this manner, each of the curves of Figure 34 can be replotted as a histogram approximating the probability density distribution over the whole range of precipitation rates.

Secondly, the total area under any such histogram, integrated over all precipitation rates and multiplied by the number of hours in a year, equals the annual precipitation in millimeters for that particular region. We can carry out straightforward numerical integration by multiplying the value of the histogram (the differential probability for a given precipitation rate interval) by the midpoint precipitation rate, and then summing these products over all intervals. We have done this, assuming all precipitation at rates less than 0.1 mm/hr (or 0.05 in the polar regions) vanishingly small, i.e., this assumes that lower rates contribute nothing to the integral we calculate.

There is one further complication. The above procedure is, of course, most accurate if the curves are broken up into a large number of small intervals, where the criterion for "small" is that the actual curve can be approximated by a straight line segment. It would appear from Figure 34 that some dozen intervals each covering a range of about 2:1 in precipitation rate would be adequate, until we recall that Figure 34 is a log-log plot and

that the actual integration must be linear. There are two alternatives: to use perhaps 100 intervals of about 1.1:1 each, or to use the 2:1 intervals and calculate a correction factor on the selection of the "midpoint". We have chosen the second procedure, even though the correction factor depends on both the size of the interval and the slope on the log-log plot of the original curve. Without giving all of the details--since the purpose of this whole integration is merely to provide a rough check on the precipitation rate distributions -- suffice it to say that rules were established (by carrying out several representative cases in detail) for estimating these correction factors. These factors were applied to every interval while calculating the rainfall integrals. The final results are shown in Table 8, where the integral under the curves of Figure 34 is compared with the total precipitation obtained by multiplying the right-hand column in Table 6 by 365. The two approaches are consistent to 30 percent or better in all cases.

Table 8. COMPARISON OF INTEGRATED PRECIPITATION RATE WITH CHARACTERISTIC ANNUAL PRECIPITATION FOR EACH CLIMATIC REGION

Climatic Region	Integral of Precipitation-Rate Distribution[a] (mm)	Characteristic Annual Precipitation[b] (mm)
A'	200	200
B'	500	375
C	850	900
C'	1400	1650
D	1050	825
E	1600	1550
F	350	275
G	1500	1200
H	2300	2375

[a]Rounded to nearest 50 mm.

[b]Rounded to nearest 25 mm. This is an estimate of the weighted average for each region.

4.0 APPLICATION OF PROPOSED OCEANIC MODEL TO 13 SELECTED LOCATIONS

The previous Section has provided a precipitation-rate climate model of the ocean areas suitable for calculating attenuation of millimeter waves over a wide variety of earth-satellite paths. To make such calculations as meaningful as possible, thirteen locations around the world have been selected for specific study. These locations are plotted in Figure 23 and defined by latitude and longitude in Table 4. These same points were used for the detailed analysis of precipitation-rate regions in section 3. In most instances, the importance of the chosen areas is obvious. Points 6 and 11 were included because they are the sites of important Navy communications installations. Points 5 and 7 were added for the extreme weather conditions they represent.

4.1 Inclusion Of The Local Precipitation-Rate Correction Factor, k

By comparing Figure 23 with Figures 26-29, the precipitation-rate region assignments by season can be read directly for each of the 13 locations; the corresponding mean seasonal freezing height can be read or interpolated from Figures 30-33. Thus using Eq. (1) on page 10 and the computer program described in Section 2.2, values of slant path attenuation can be calculated. One further refinement has been attempted. By taking the total seasonal precipitation for each location listed in Table 4, dividing by 90 to convert it to a daily average, and forming the ratio of this number to the characteristic precipitation (mm/day) assumed for each of the nine standard ocean precipitation-rate types listed in Table 6 (page 60), a correction factor k is generated. This k factor is applied to each of the precipitation rates given in Table 7 before inserting them into the formula for attenuation. The formula thus becomes modified as follows:

$$A(P) = L(\theta)\ \alpha(f,R_p)\ \gamma(D)\ \left[kR_p(P)\right]^{\beta(f,R_p)-\delta(D)} \qquad \text{Eq. (2)}$$

The precipitation-rate climate type, the correction factor k, and the mean freezing height for each of the thirteen chosen locations are given in Table 9 by season.

Rather than running attenuation calculations for all 52 cases, we examined each location and selected the best and worst seasons. In most cases, we found this selection obvious by keeping in mind that both $\overline{FH}$ (which determines path length) and the precipitation rate correction factor k (ignoring the exponent which is not far from unity) are primary determinants of the total attenuation. For location #1 in the Mid Atlantic, the interplay of these two effects was too close to call, and all four seasons were run. The seasons chosen are indicated in Table 9 with a solid underline for the worst (highest attenuation) cases and a broken underline for the best (least attenuation) cases. In many instances the effect of freezing height dominates; consequently, the best and worst attenuations do not coincide with one's intuitive notions about "good" and "bad" weather. The Sea of Japan and the Bering Sea constitute extreme cases where the "best" season is winter, with zero attenuation because the mean freezing height is on the surface; but of course the weather can be miserable.

For each of the 29 cases underlined in Table 9, attenuation calculations were run for six frequencies (7.5, 8.2, 21, 40, 44 and 45 GHz) and for six elevation angles (10, 20, 30, 45, 60 and 90°). We use the 20°C values of Table 2 for the coefficients α and β for regions F, G and H; otherwise we use the 0°C values of Table 2.

4.2 Seasonal Extremes Of Attenuation -- Results

As before, representative results have been plotted to display the range of variation and to summarize the large amount of information. First, three graphs for each of the thirteen locations show the exceedance probabilities vs. attenuation. These graphs, Figures 35-73, cover three frequencies (7.5, 21 and 44 GHz) and three elevation angles (10, 20 and 30°). In each case both the worst and best seasons are shown, thus indicating the range of attenuation values that can be expected.

Table 9. SEASONAL PRECIPITATION RATE, CLIMATE TYPE, k, AND $\overline{FH}$ FOR THIRTEEN SELECTED LOCATIONS[a]

No.	Location	Lat., Long.	Dec-Feb		Mar-May		Jun-Aug		Sep-Nov	
			Region k	$\overline{FH}$ (km)	Region k	$\overline{FH}$ (km)	Region k	$\overline{FH}$ (km)	Region k	$\overline{FH}$ (km)
1	Mid Atlantic	40 N, 40 W	C x 1.2	2.5	C x 1.0	2.7	C x 0.7	4.2	C x 0.8	3.8
2	North Atlantic	65 N, 0 W	C x 0.8	0.5	C x 0.4	0.7	C x 0.4	2.0	C x 0.8	1.6
3	Mediterranean	35 N, 20 E	C x 0.6	1.5	F x 0.7	3.0	F x 0.3	4.2	F x 1.0	3.3
4	Persian Gulf	15 N, 60 E	F x 0.3	4.5	F x 0.3	4.7	F x 0.3	5.0	F x 0.3	5.0
5	Indian Ocean	0 N, 75 E	G x 1.4	4.8	G x 1.2	4.8	G x 1.2	4.7	G x 1.6	4.8
6	W. Australia	20 S, 115 E	F x 1.0	4.5	F x 0.7	4.5	F x 0.7	4.5	F x 0.3	4.5
7	East Indies	5 S, 120 E	H x 0.9	5.0	G x 1.5	5.0	G x 0.6	4.9	G x 0.6	4.8
8	Philippines	15 N, 120 E	G x 0.6	4.7	G x 0.9	4.9	H x 0.6	4.9	G x 0.6	4.8
9	Sea of Japan	40 N, 135 E	B'x 1.0	0.0	D x 1.3	1.5	D x 0.9	4.4	C x 0.7	2.5
10	Bering Sea	60 N, 175 W	B'x 1.0	0.0	B'x 0.8	0.0	B'x 1.0	2.2	B'x 1.0	0.2
11	NE Pacific	45 N, 125 W	C'x 0.9	1.0	C x 0.8	1.8	C x 0.6	3.3	C'x 0.9	3.0
12	Hawaii	20 N, 155 W	C x 0.5	1.2	F x 1.1	4.5	F x 1.0	4.6	F x 1.3	4.6
13	Panama	20 S, 115 W	G x 0.6	4.7	G x 1.2	4.7	H x 1.0	4.8	H x 1.0	4.8

[a]Solid underline indicates worst season; broken underline indicates best season.

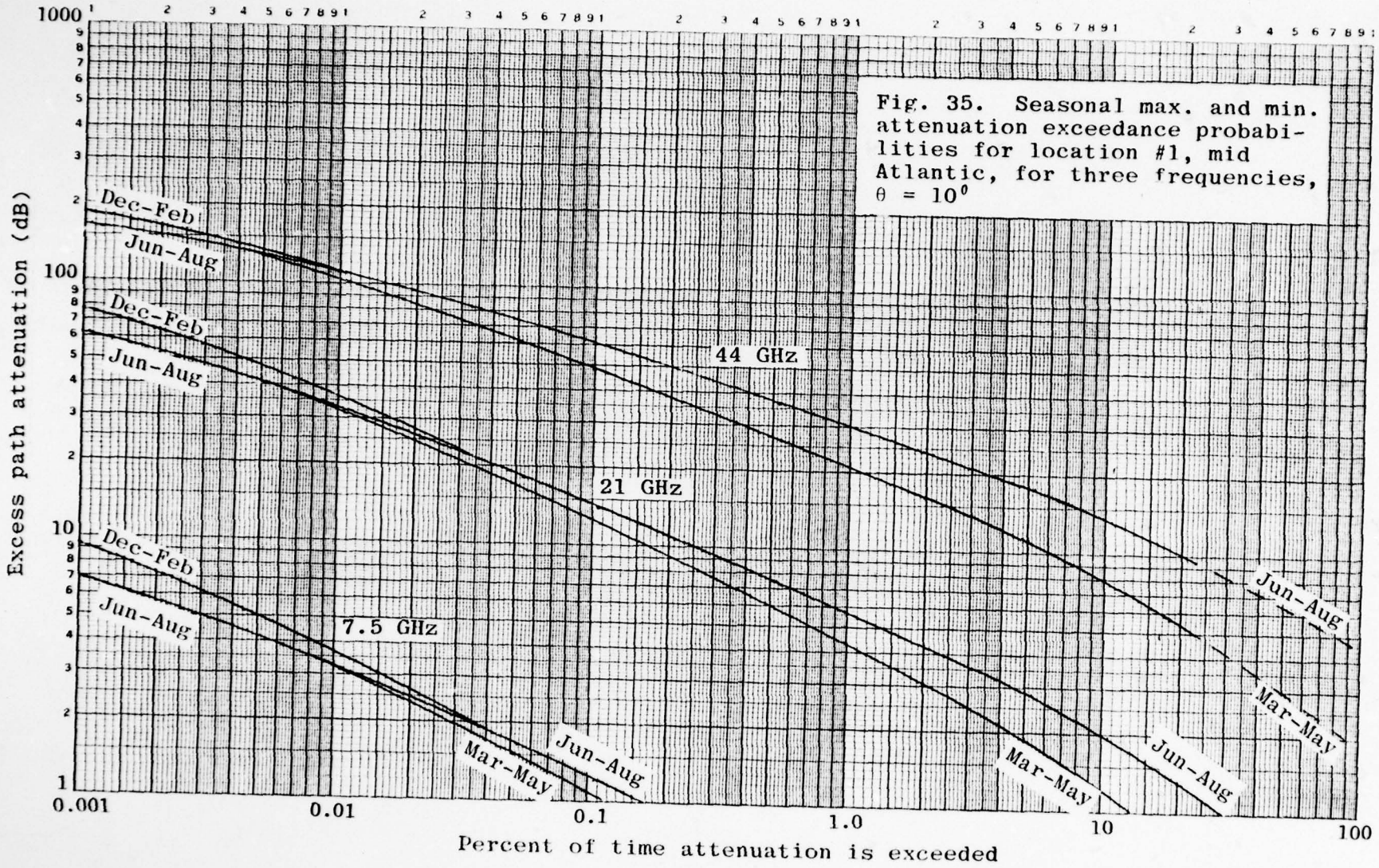

Fig. 35. Seasonal max. and min. attenuation exceedance probabilities for location #1, mid Atlantic, for three frequencies, $\theta = 10^0$

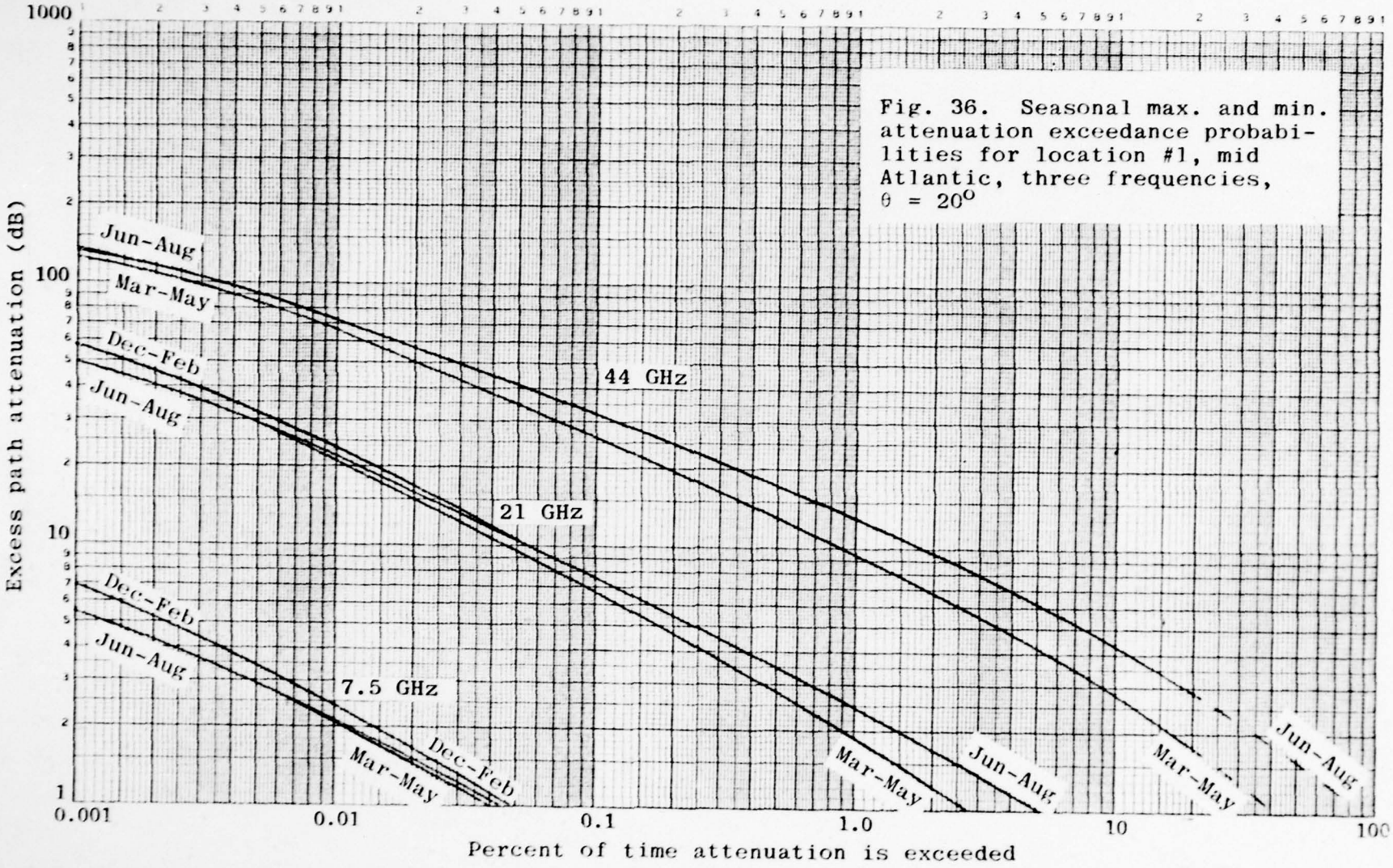

Fig. 36. Seasonal max. and min. attenuation exceedance probabilities for location #1, mid Atlantic, three frequencies, $\theta = 20^{o}$

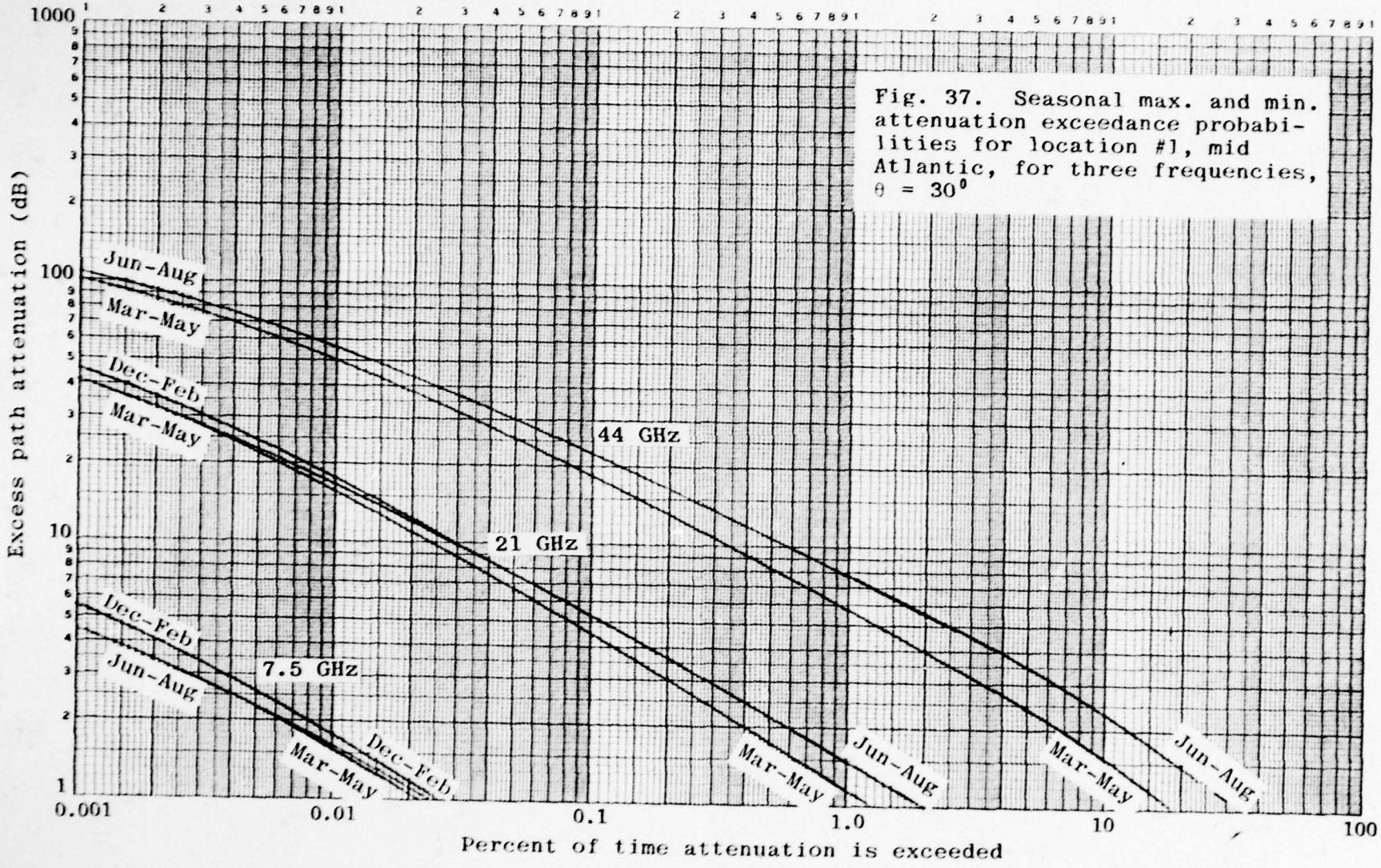

Fig. 37. Seasonal max. and min. attenuation exceedance probabilities for location #1, mid Atlantic, for three frequencies, $\theta = 30^0$

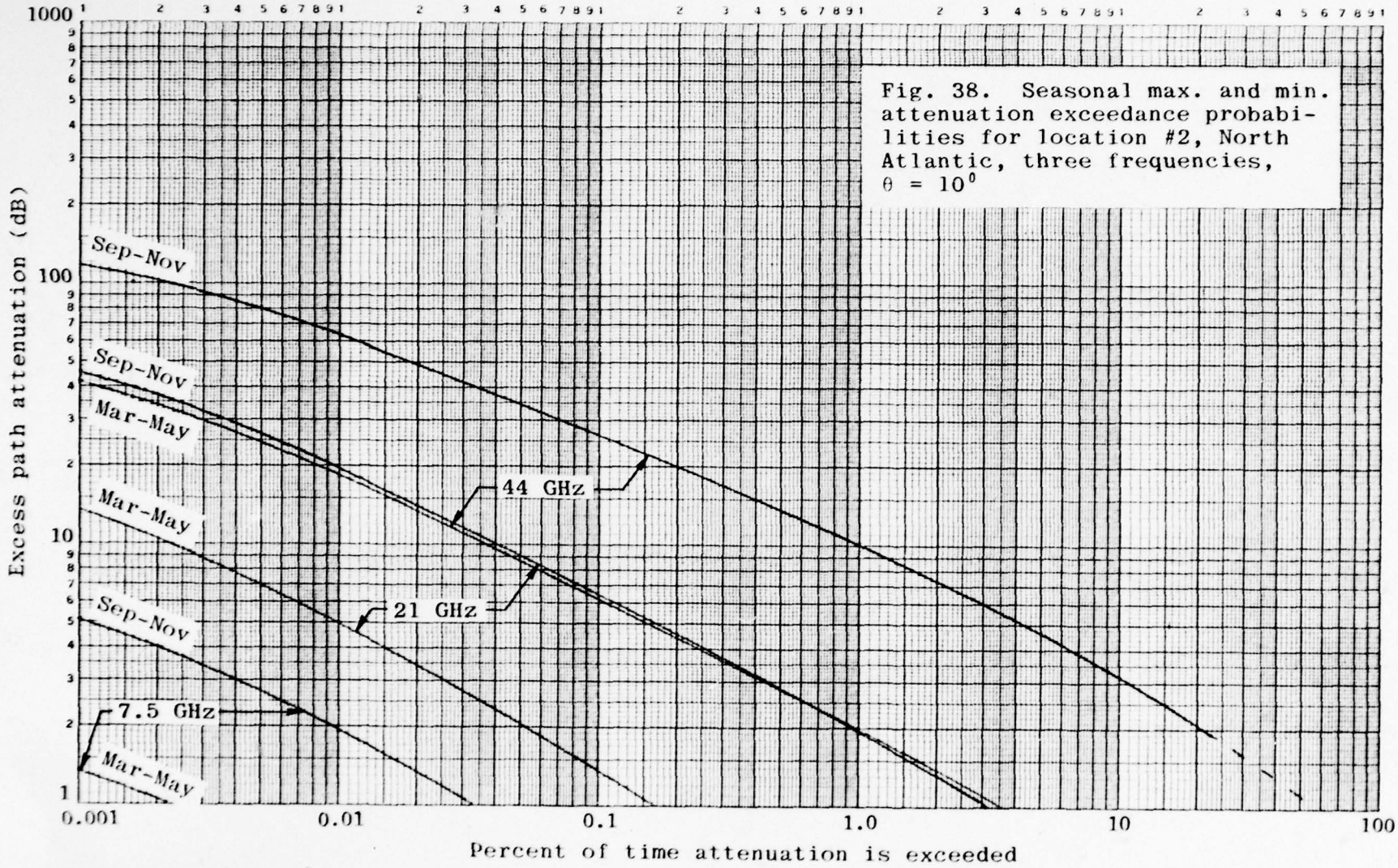

Fig. 38. Seasonal max. and min. attenuation exceedance probabilities for location #2, North Atlantic, three frequencies, $\theta = 10^0$

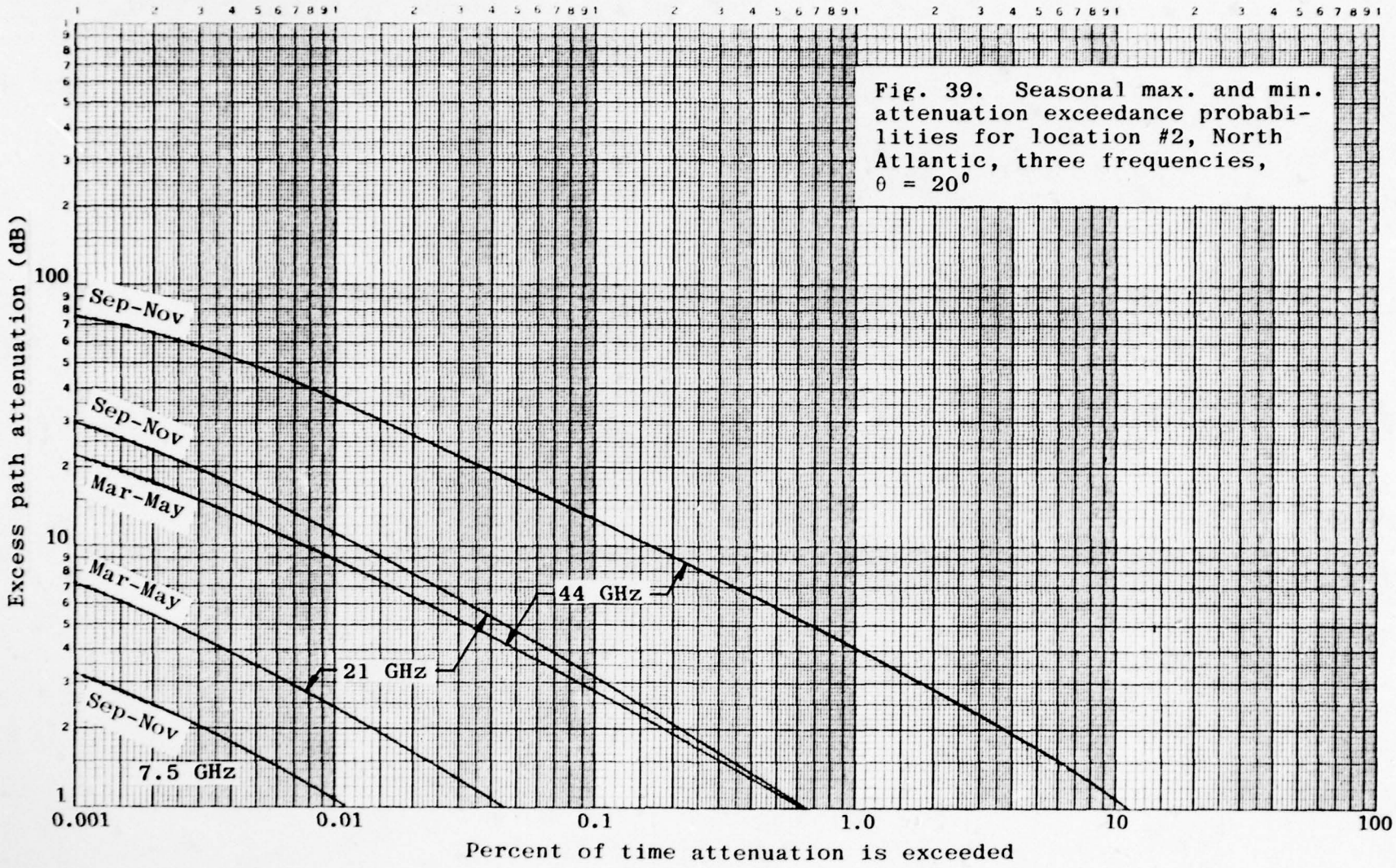

Fig. 39. Seasonal max. and min. attenuation exceedance probabilities for location #2, North Atlantic, three frequencies, $\theta = 20^0$

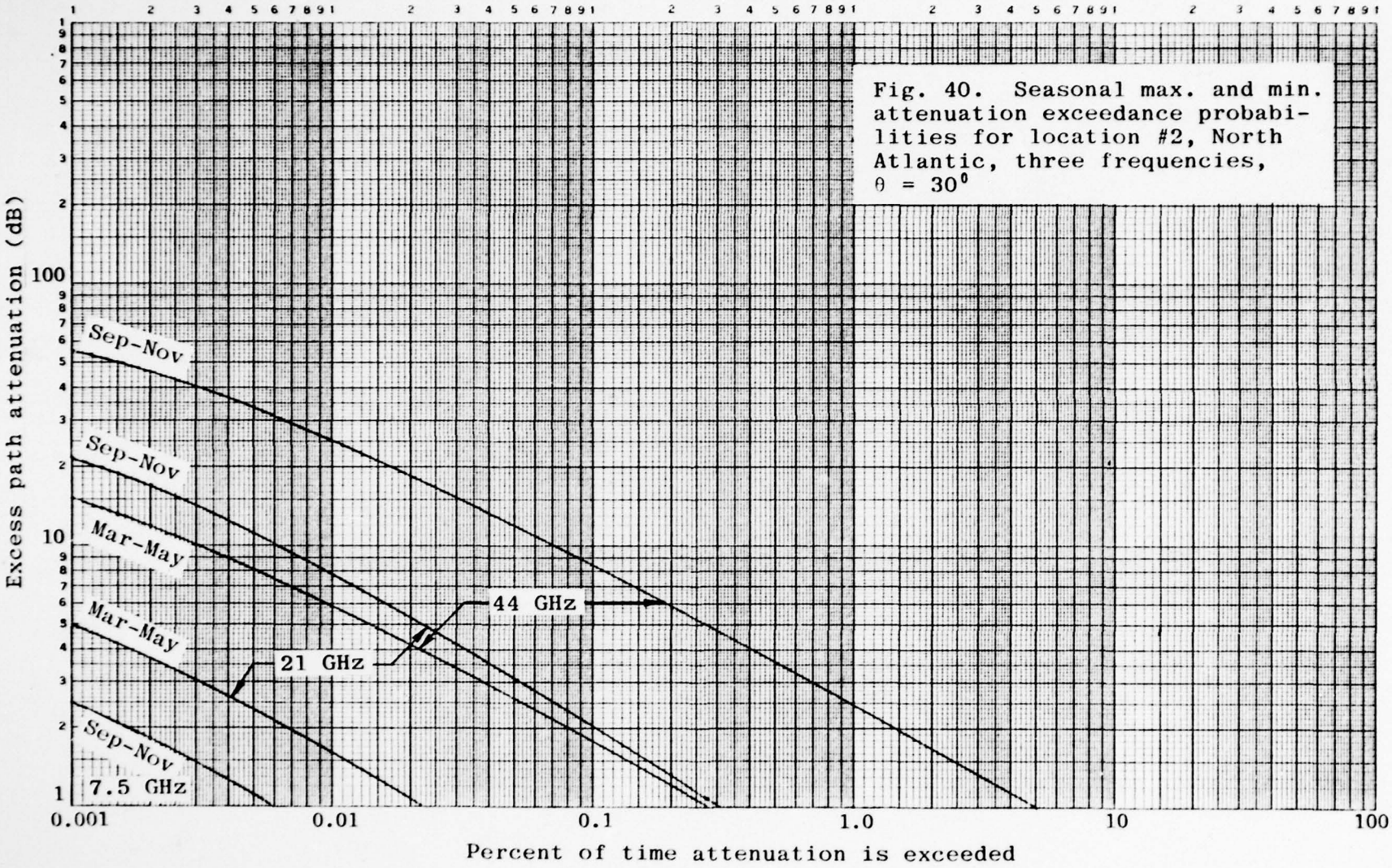

Fig. 40. Seasonal max. and min. attenuation exceedance probabilities for location #2, North Atlantic, three frequencies, $\theta = 30^0$

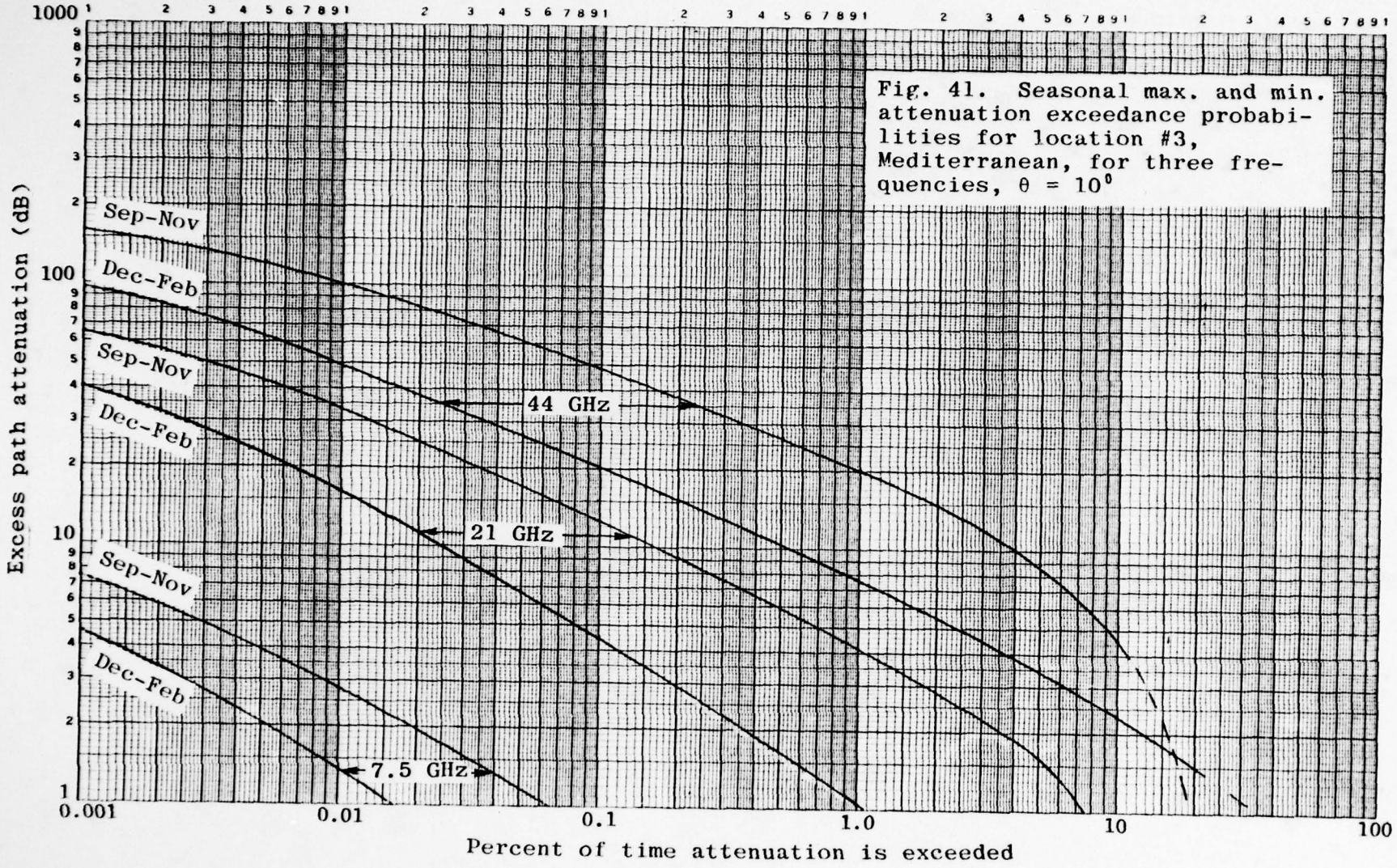

Fig. 41. Seasonal max. and min. attenuation exceedance probabilities for location #3, Mediterranean, for three frequencies, $\theta = 10^0$

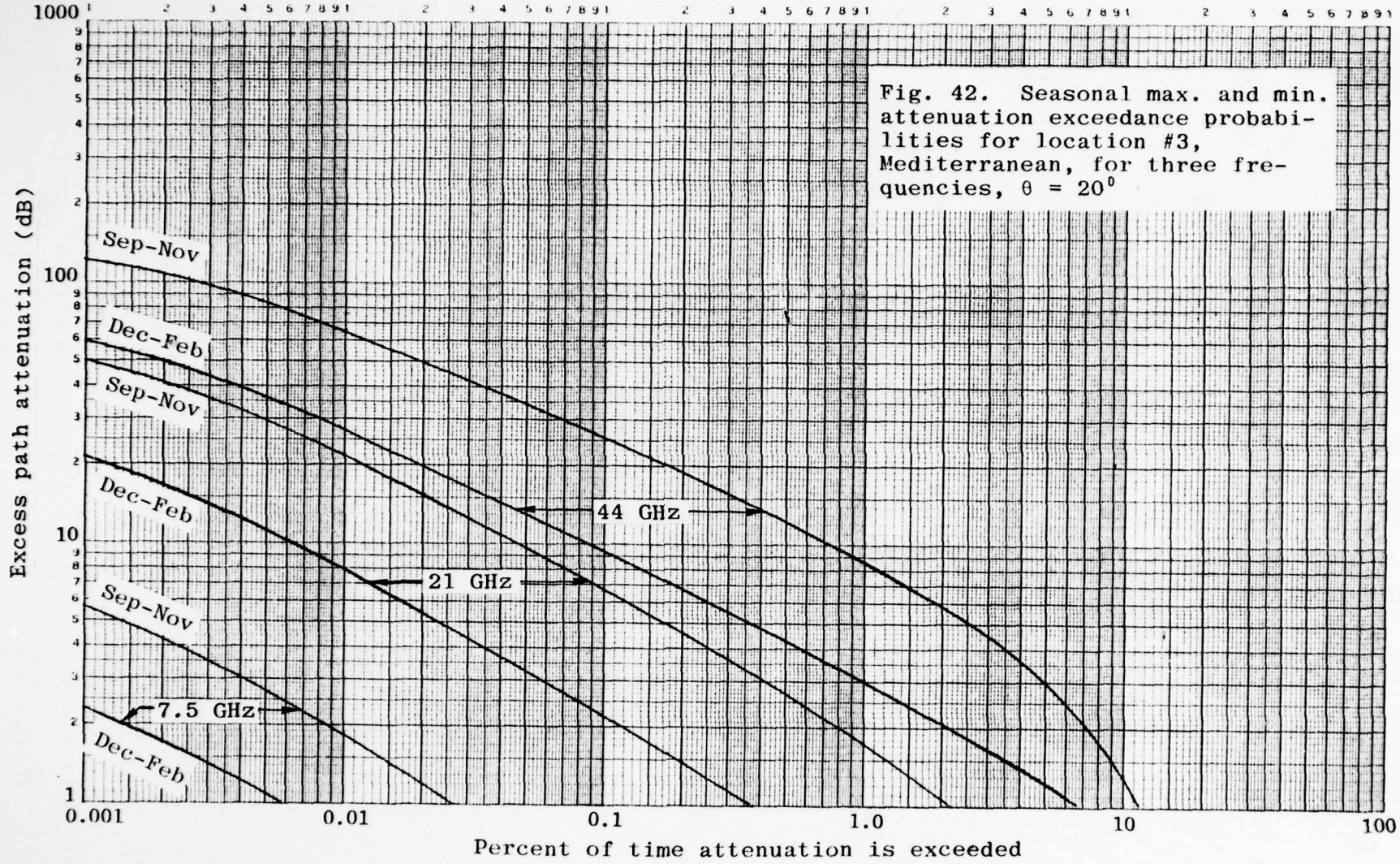

Fig. 42. Seasonal max. and min. attenuation exceedance probabilities for location #3, Mediterranean, for three frequencies, $\theta = 20^0$

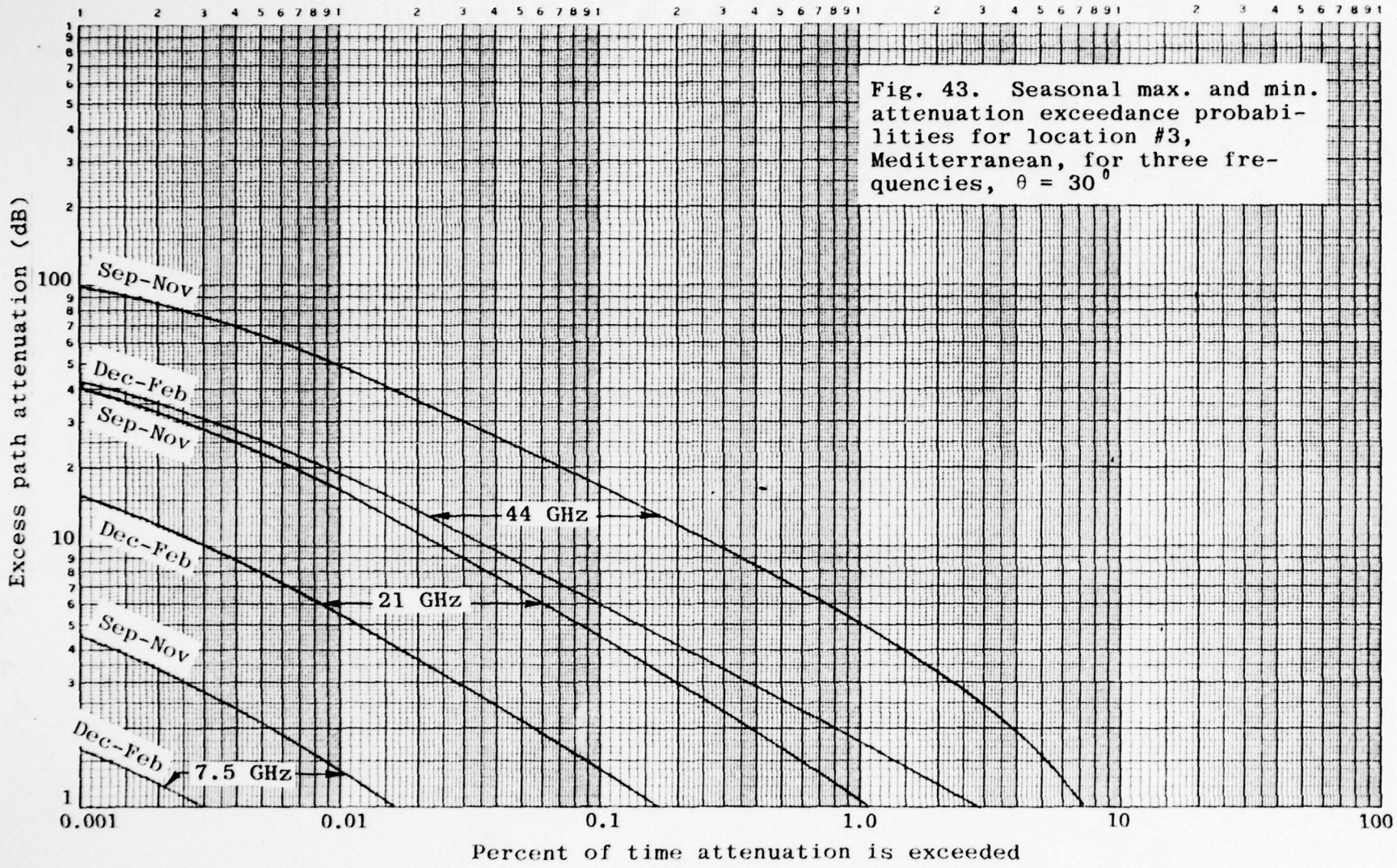

Fig. 43. Seasonal max. and min. attenuation exceedance probabilities for location #3, Mediterranean, for three frequencies, $\theta = 30^0$

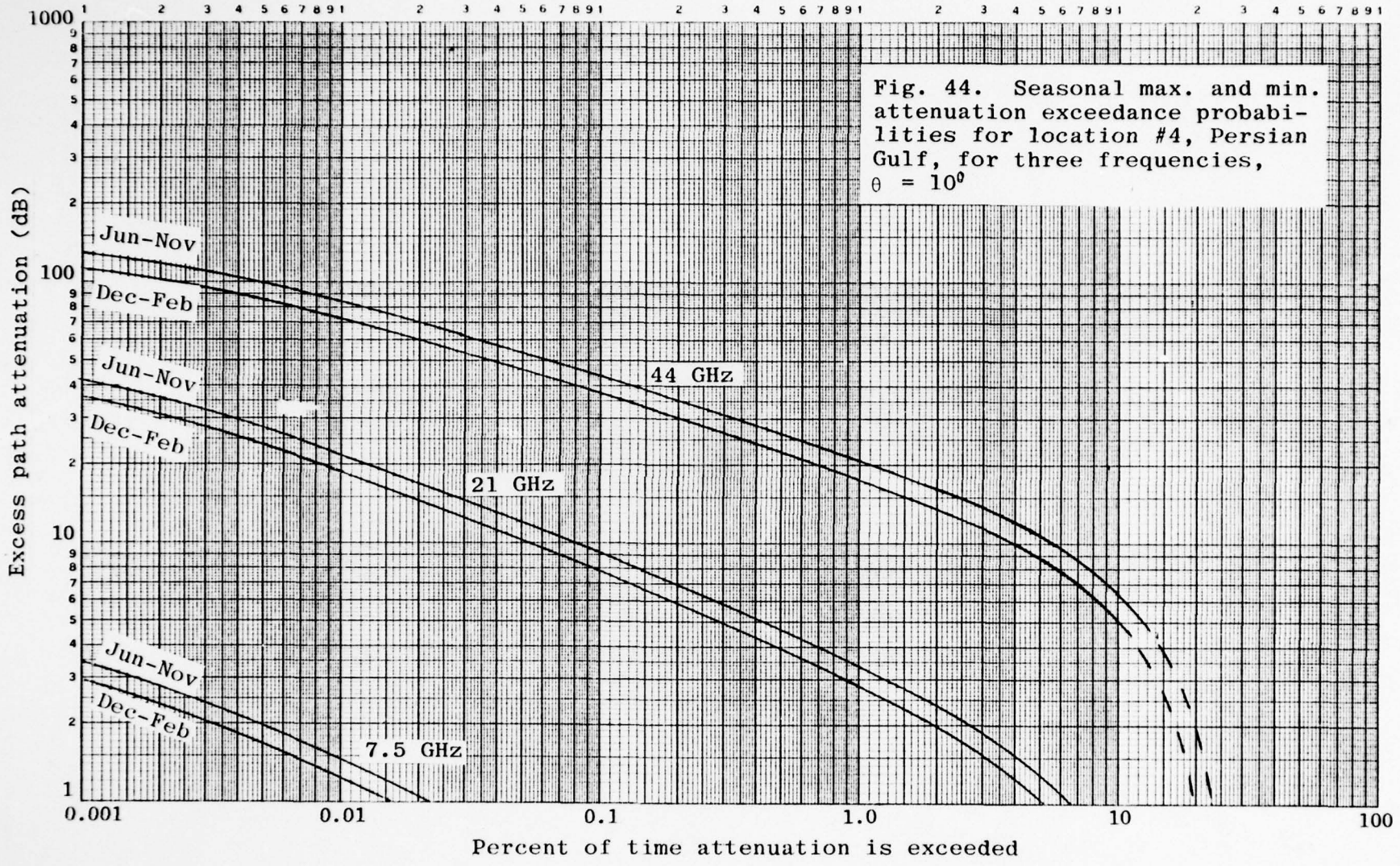

Fig. 44. Seasonal max. and min. attenuation exceedance probabilities for location #4, Persian Gulf, for three frequencies, $\theta = 10^0$

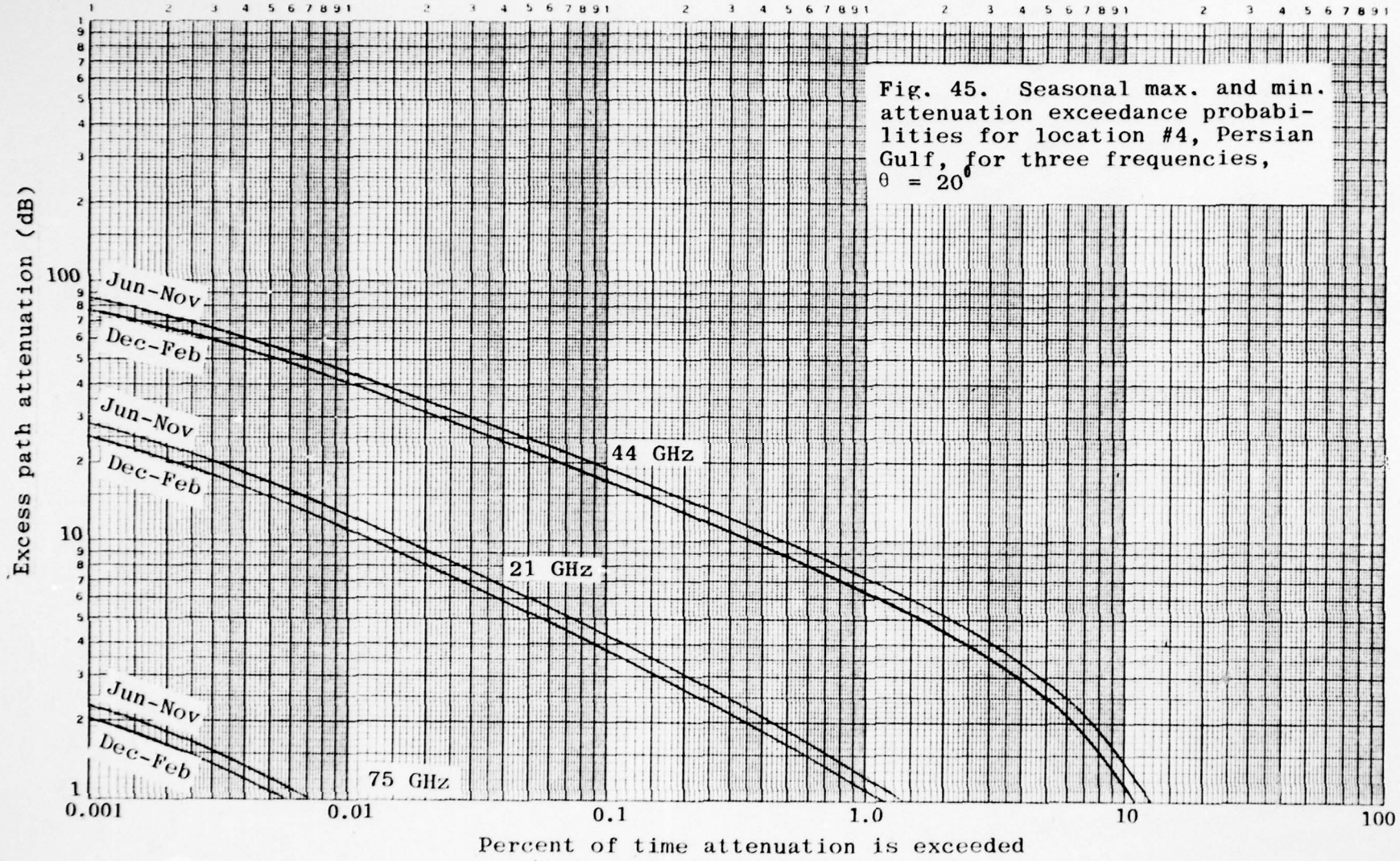

Fig. 45. Seasonal max. and min. attenuation exceedance probabilities for location #4, Persian Gulf, for three frequencies, $\theta = 20^{\circ}$

AD-A075 390 SCIENCE APPLICATIONS INC EL SEGUNDO CALIF F/G 4/2
RAIN ATTENUATION OVER EARTH-SATELLITE PATHS.(U)
MAY 79 N E FELDMAN N00039-79-C-0136
UNCLASSIFIED SAI-171-80-573-LA NL

2 OF 2
AD A075390

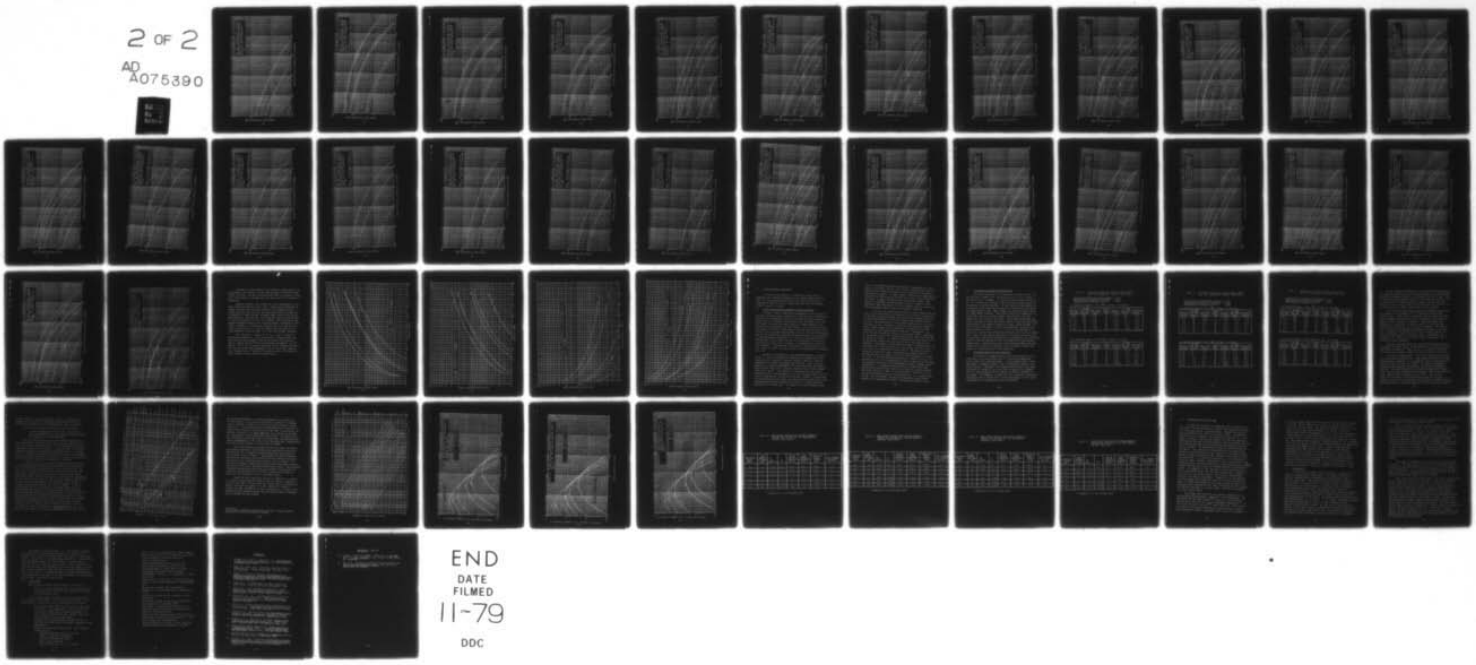

END
DATE FILMED
11-79
DDC

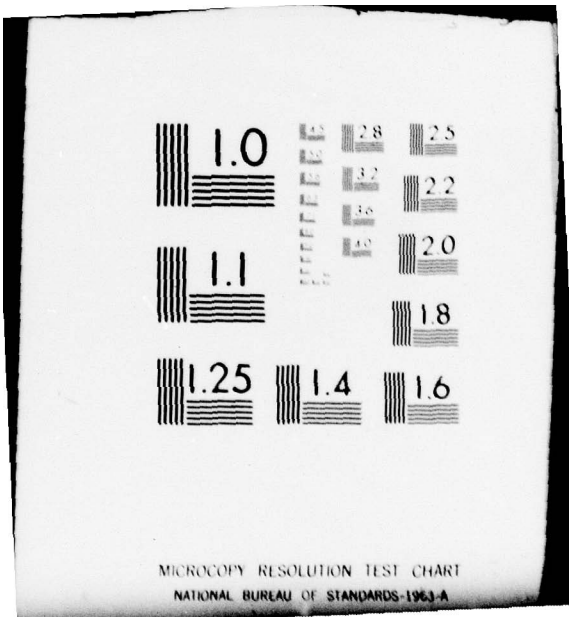
1.0
1.1
1.25
1.4
1.6
2.8
3.2
3.6
4.0
2.5
2.2
2.0
1.8
MICROCOPY RESOLUTION TEST CHART
NATIONAL BUREAU OF STANDARDS-1963-A

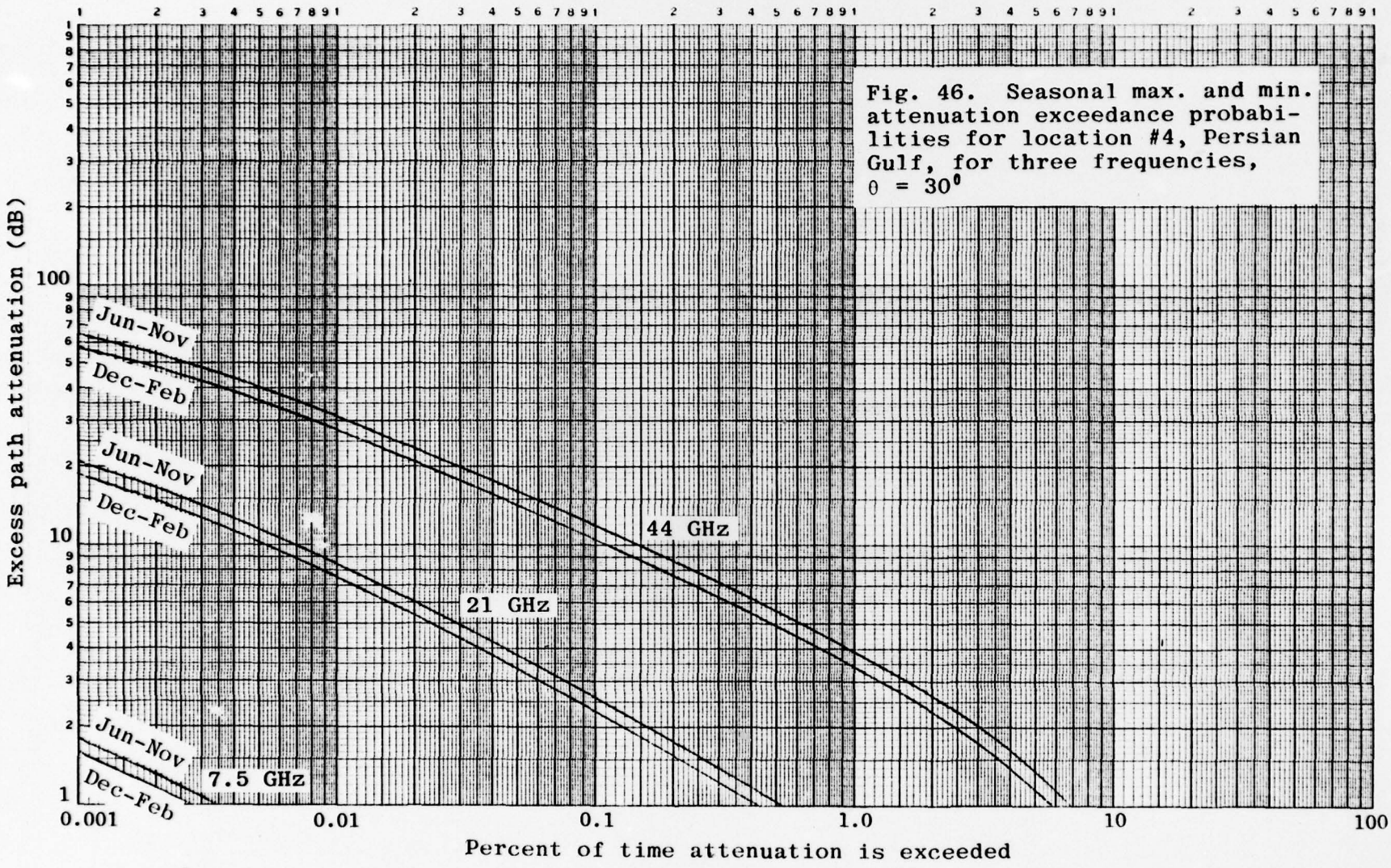

Fig. 46. Seasonal max. and min. attenuation exceedance probabilities for location #4, Persian Gulf, for three frequencies, $\theta = 30^0$

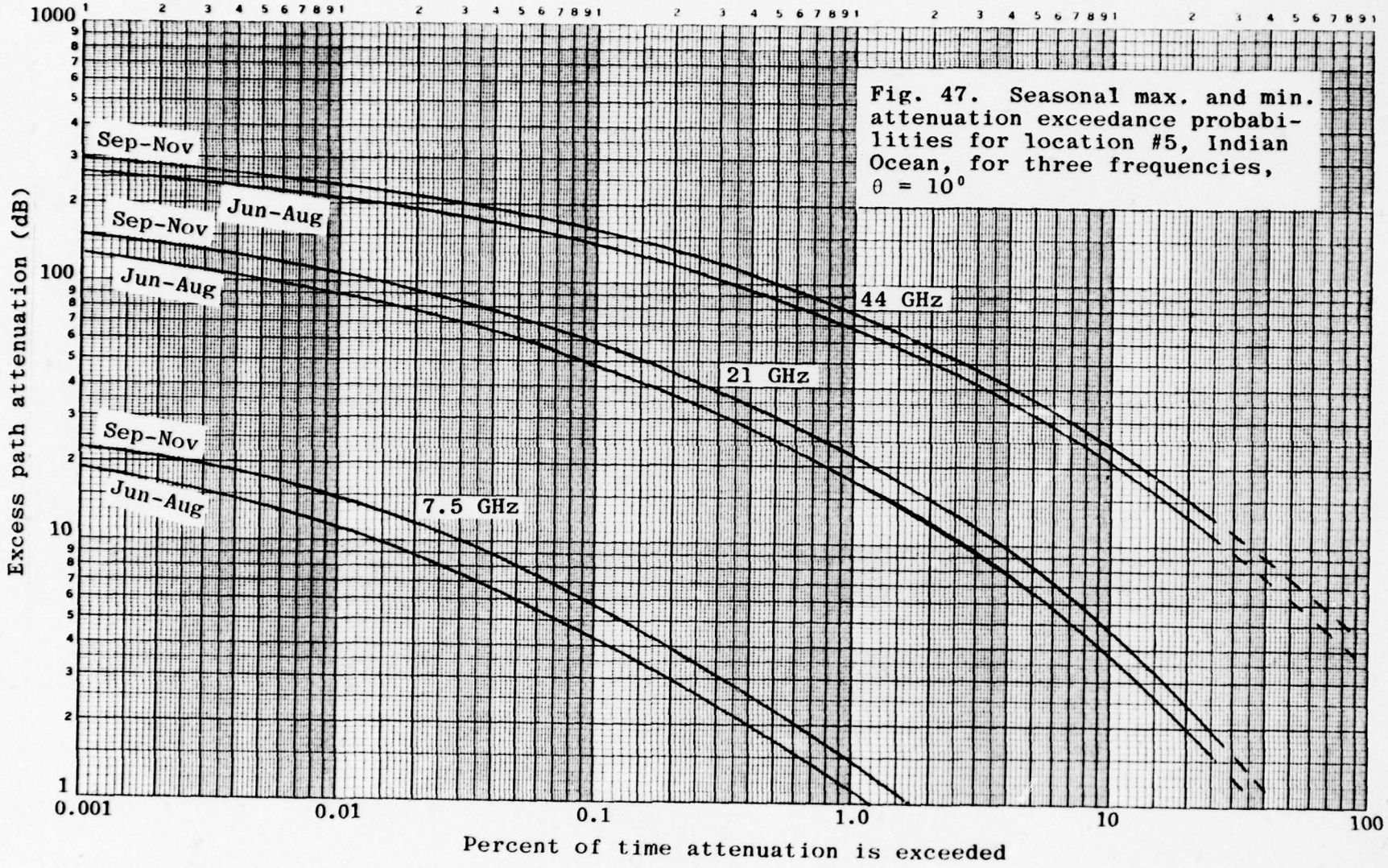

Fig. 47. Seasonal max. and min. attenuation exceedance probabilities for location #5, Indian Ocean, for three frequencies, $\theta = 10^0$

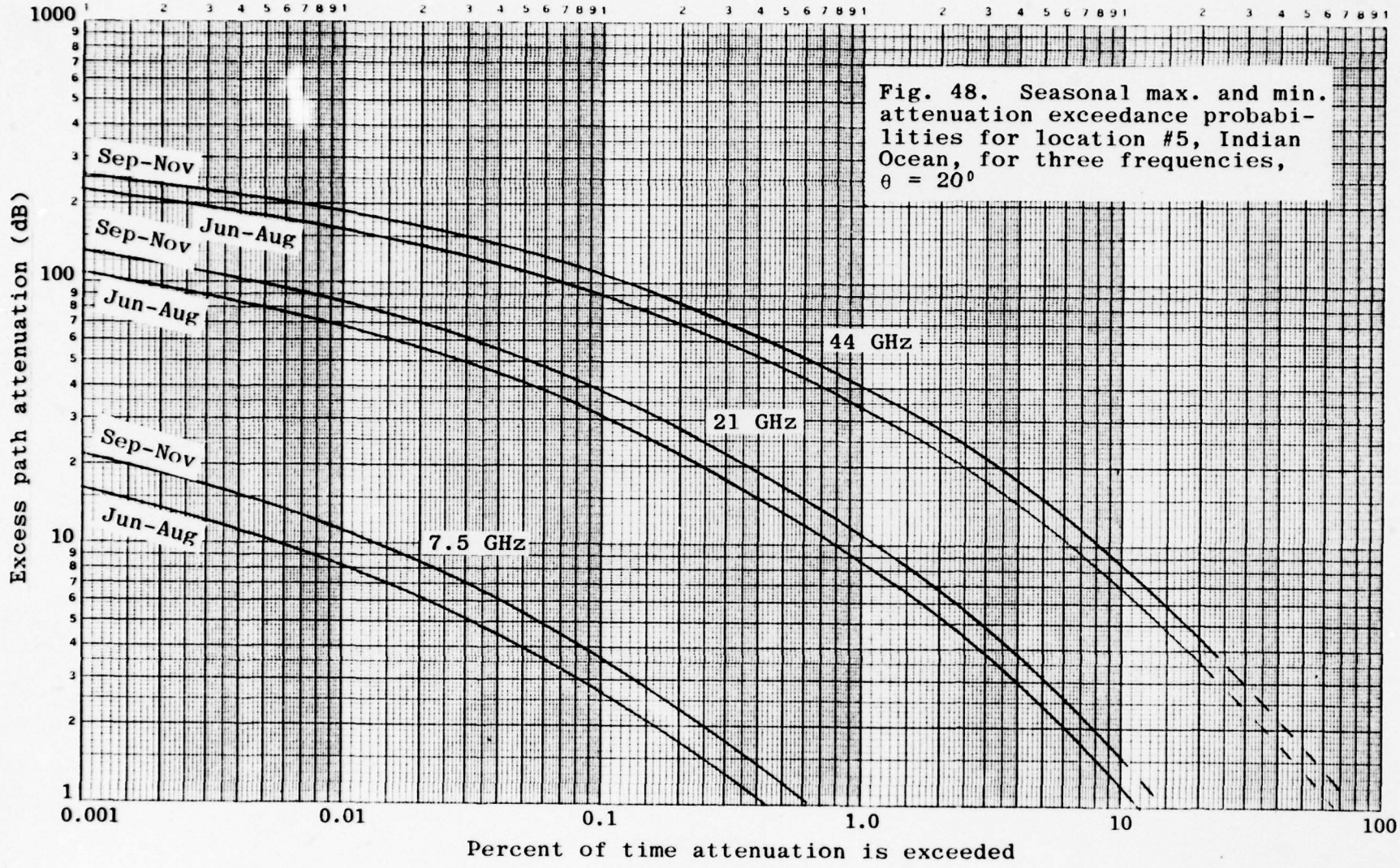

Fig. 48. Seasonal max. and min. attenuation exceedance probabilities for location #5, Indian Ocean, for three frequencies, $\theta = 20^0$

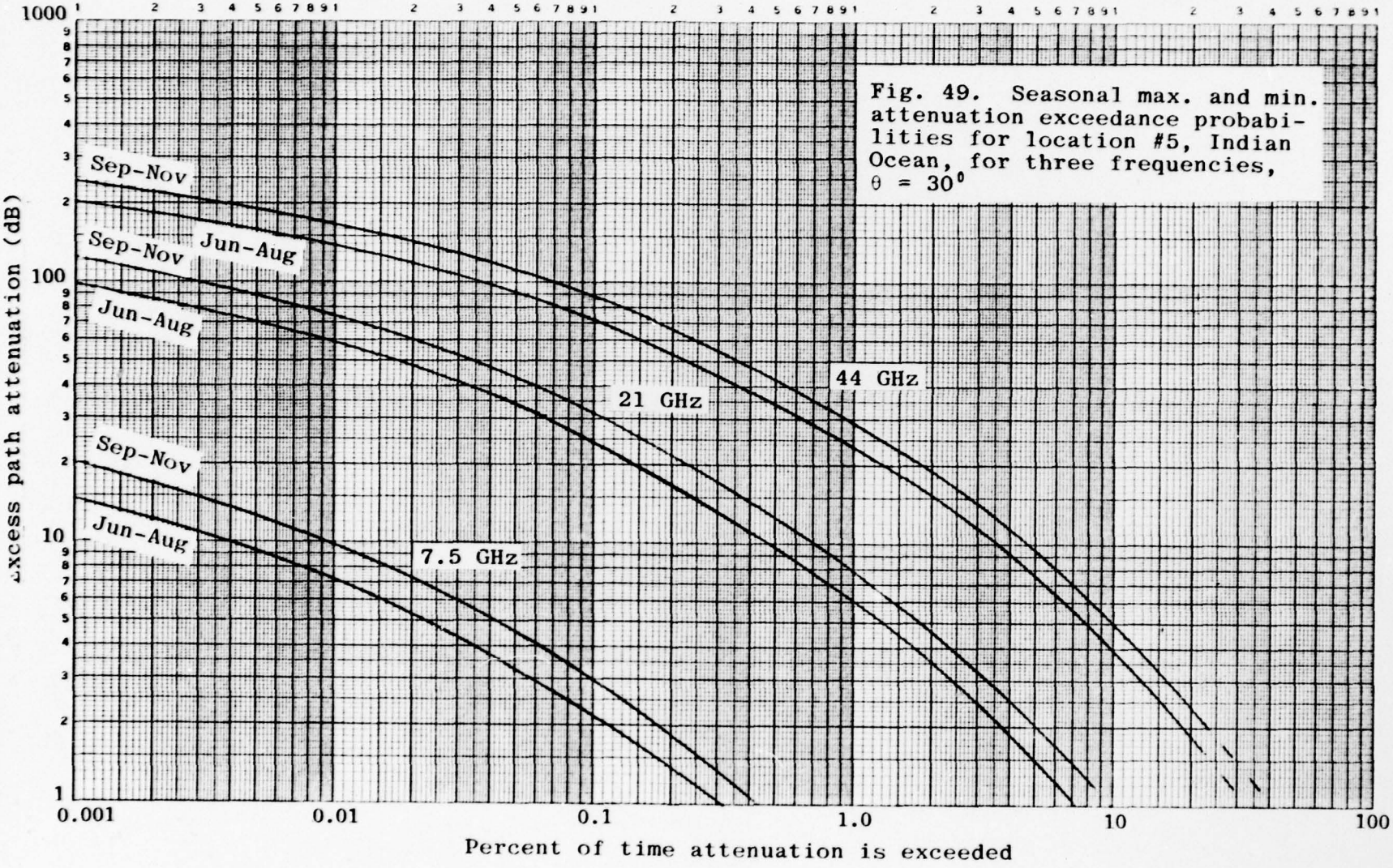

Fig. 49. Seasonal max. and min. attenuation exceedance probabilities for location #5, Indian Ocean, for three frequencies, $\theta = 30^0$

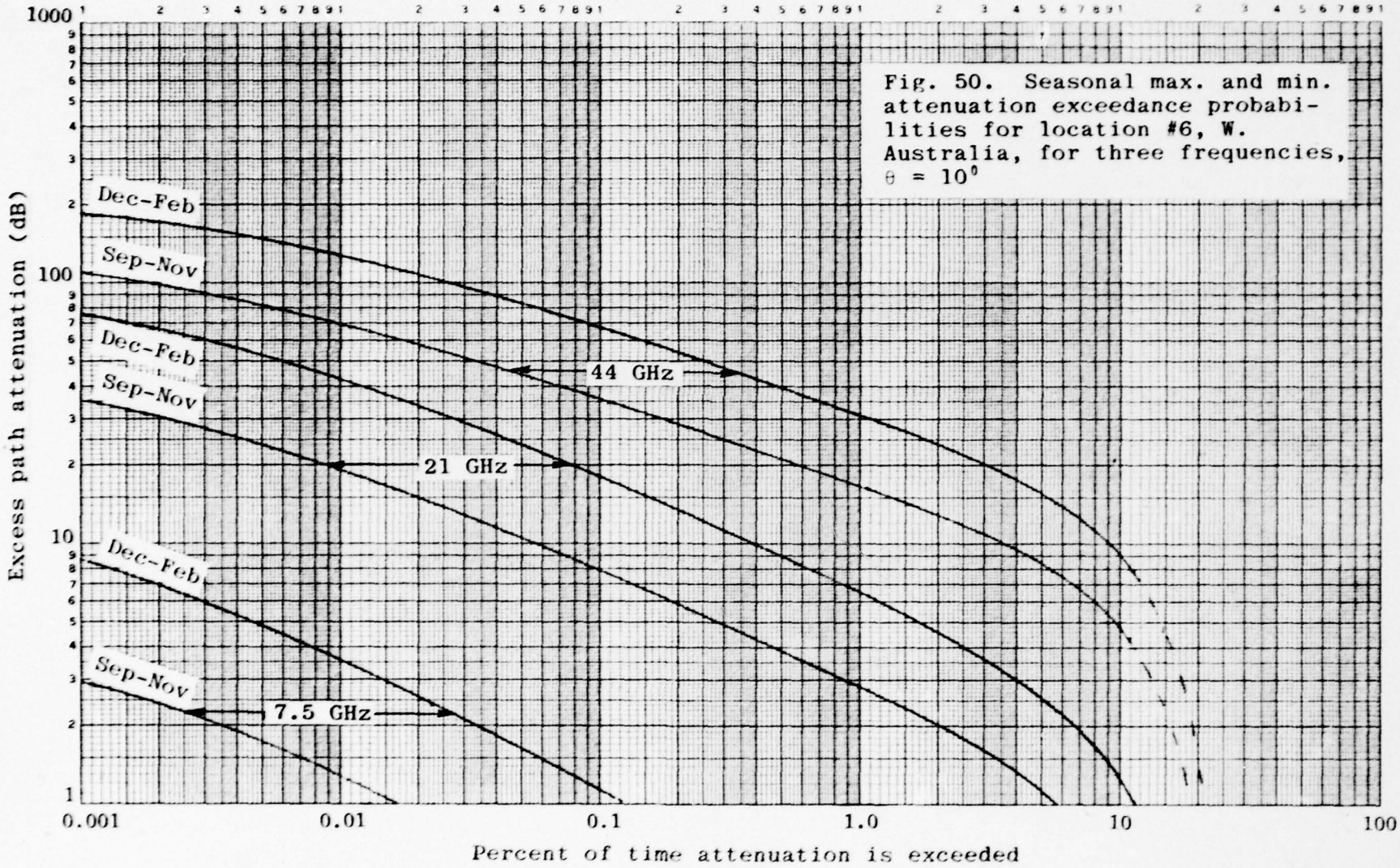

Fig. 50. Seasonal max. and min. attenuation exceedance probabilities for location #6, W. Australia, for three frequencies, $\theta = 10^0$

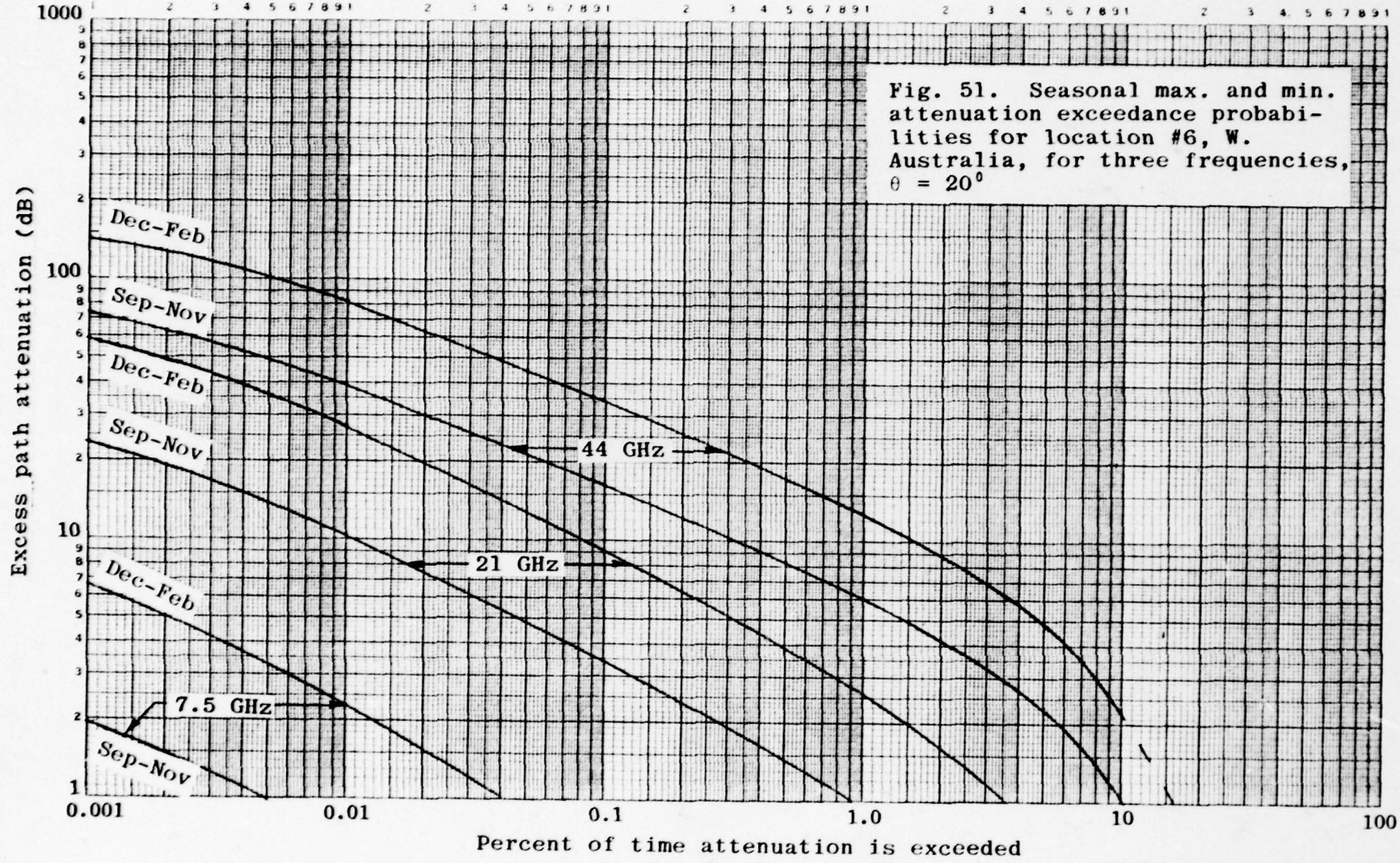

Fig. 51. Seasonal max. and min. attenuation exceedance probabilities for location #6, W. Australia, for three frequencies, $\theta = 20^0$

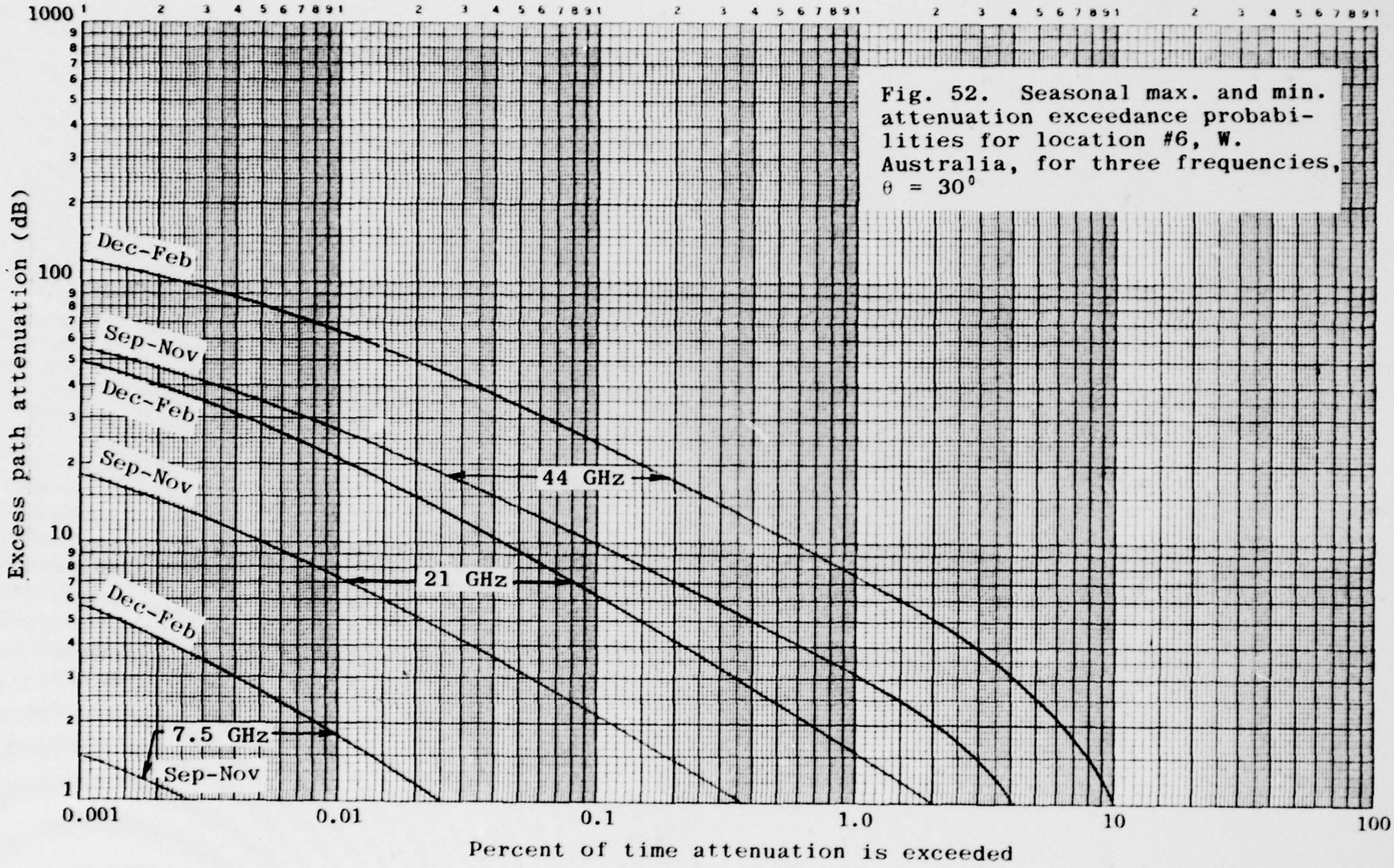

Fig. 52. Seasonal max. and min. attenuation exceedance probabilities for location #6, W. Australia, for three frequencies, $\theta = 30^0$

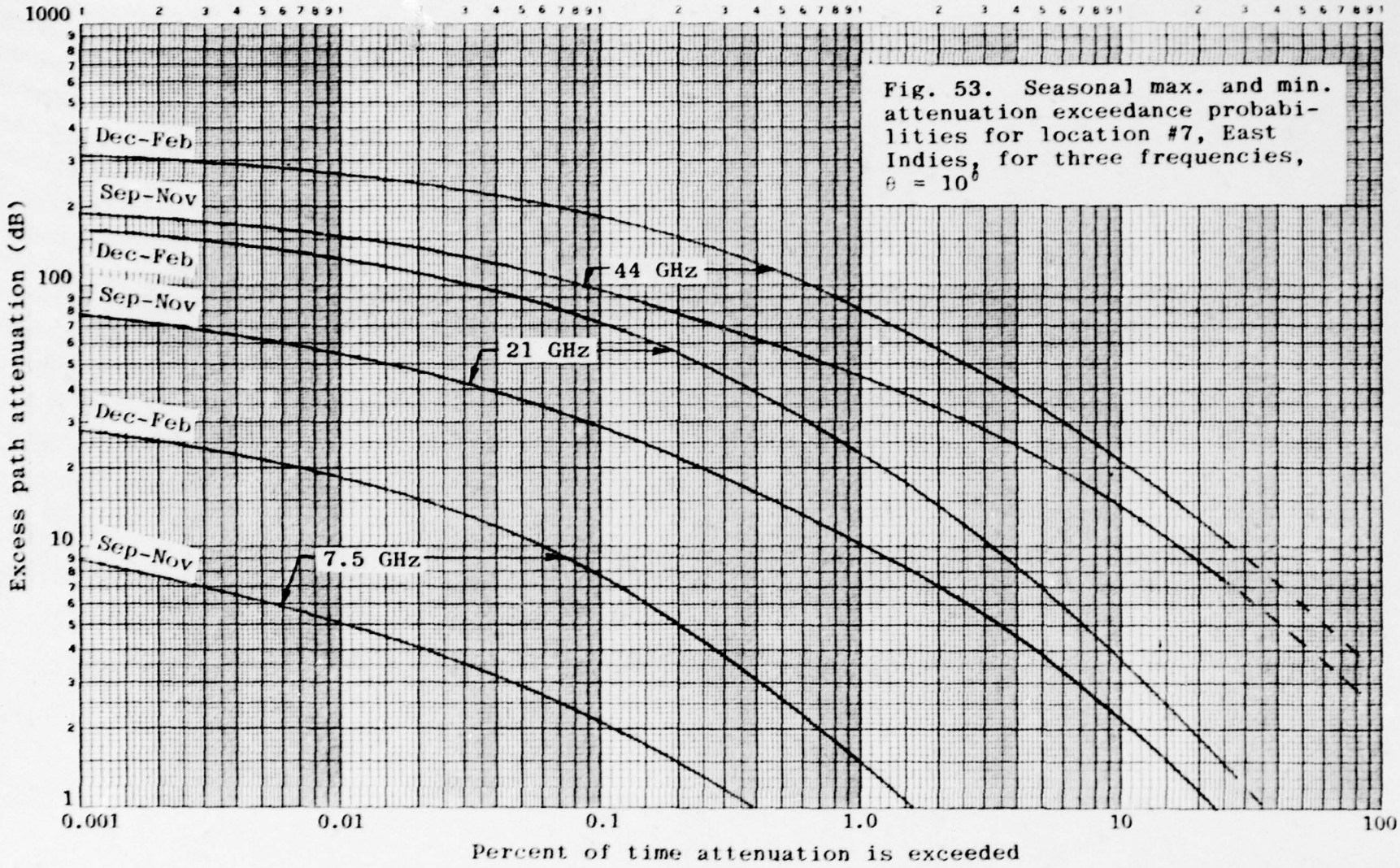

Fig. 53. Seasonal max. and min. attenuation exceedance probabilities for location #7, East Indies, for three frequencies, $\theta = 10^{\circ}$

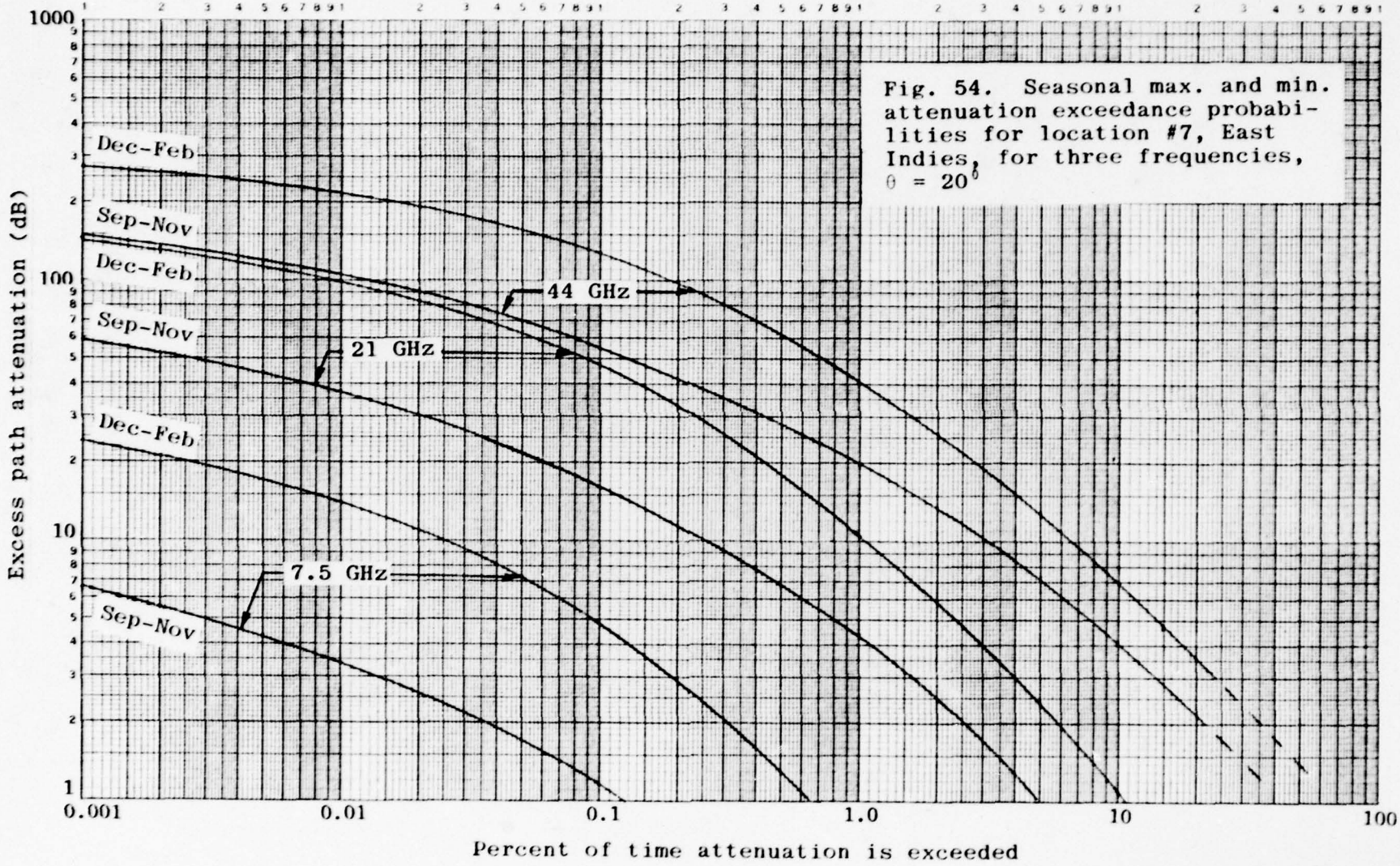

Fig. 54. Seasonal max. and min. attenuation exceedance probabilities for location #7, East Indies, for three frequencies, $\theta = 20^{\circ}$

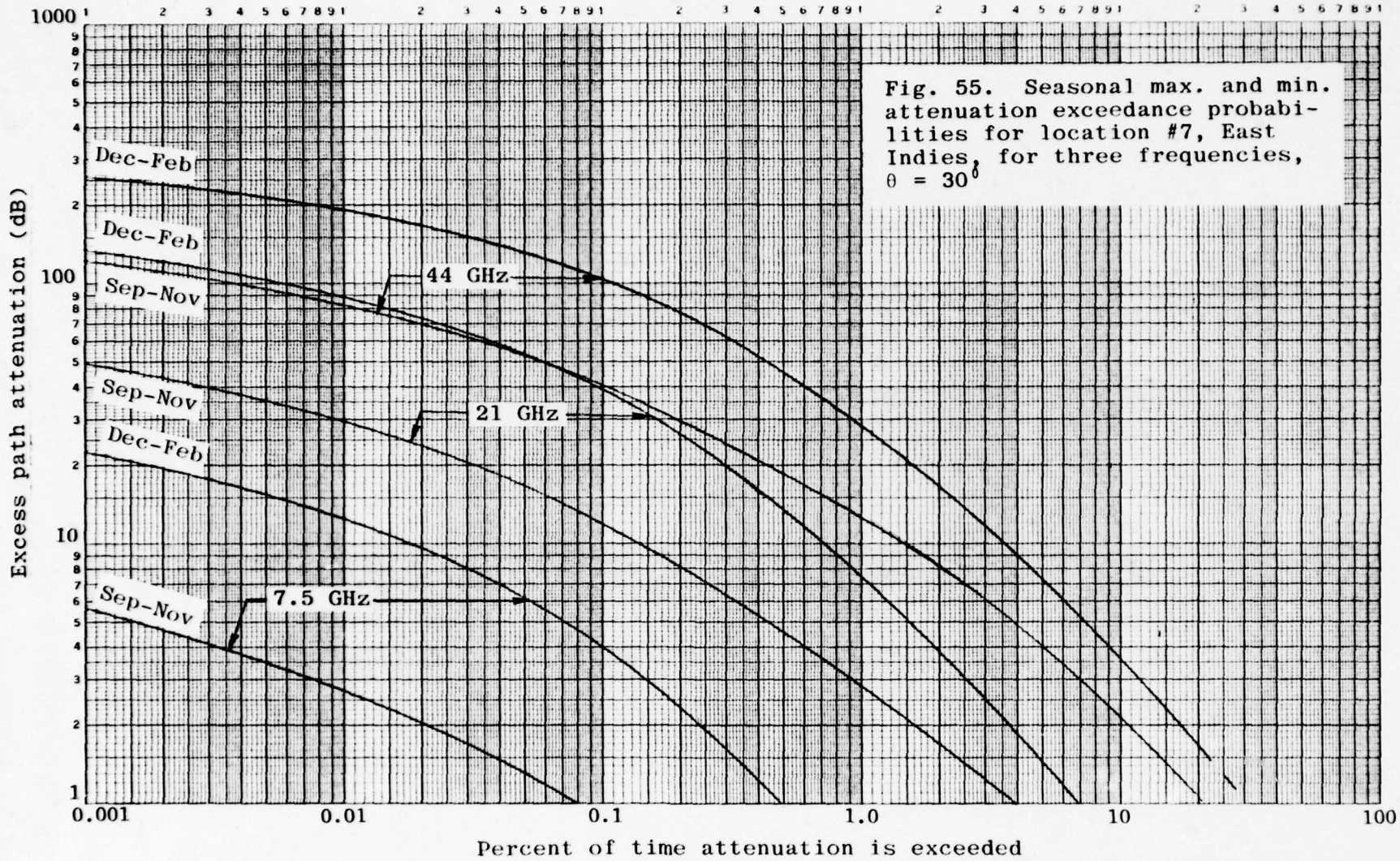

Fig. 55. Seasonal max. and min. attenuation exceedance probabilities for location #7, East Indies, for three frequencies, $\theta = 30^{\circ}$

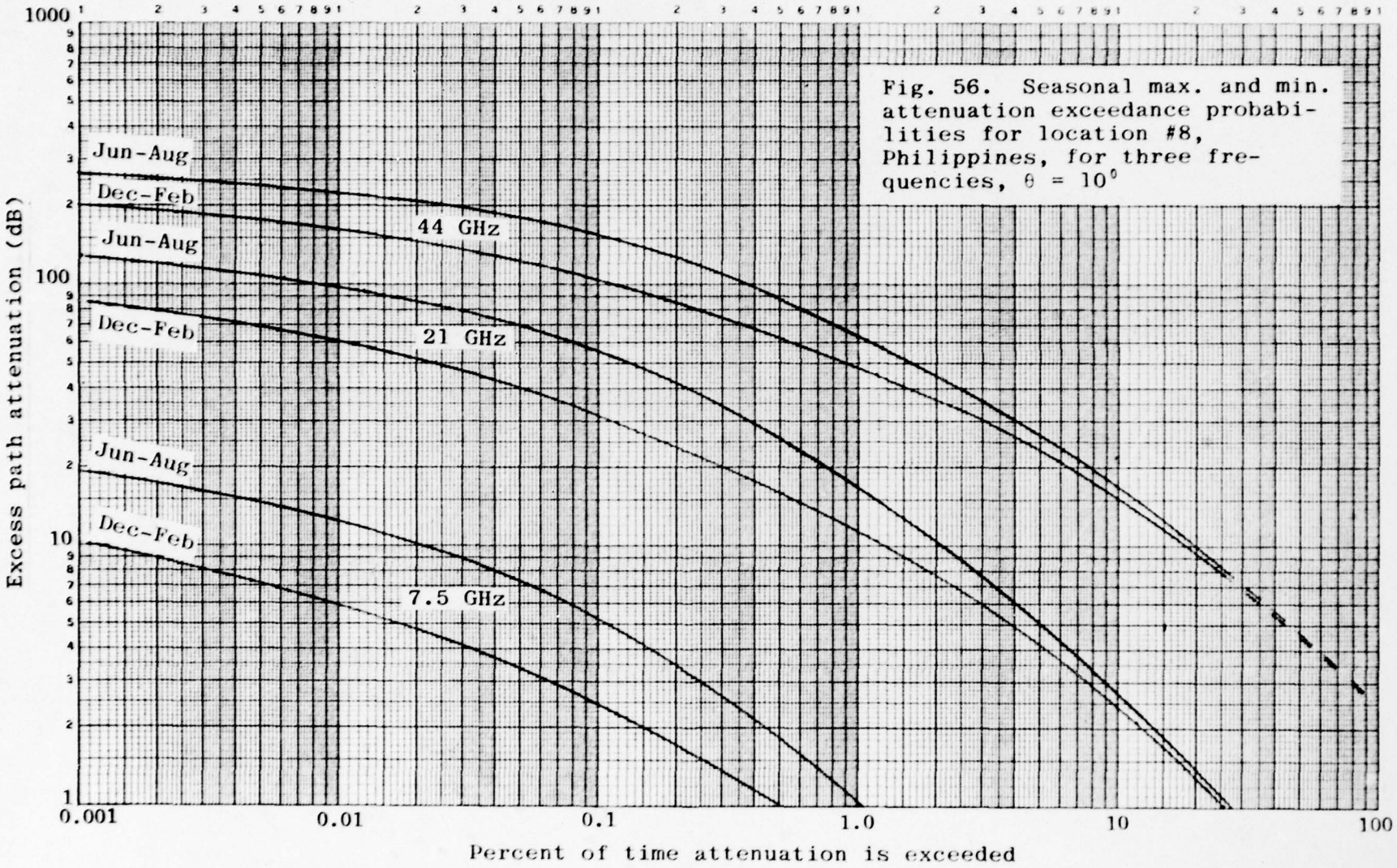

Fig. 56. Seasonal max. and min. attenuation exceedance probabilities for location #8, Philippines, for three frequencies, $\theta = 10^0$

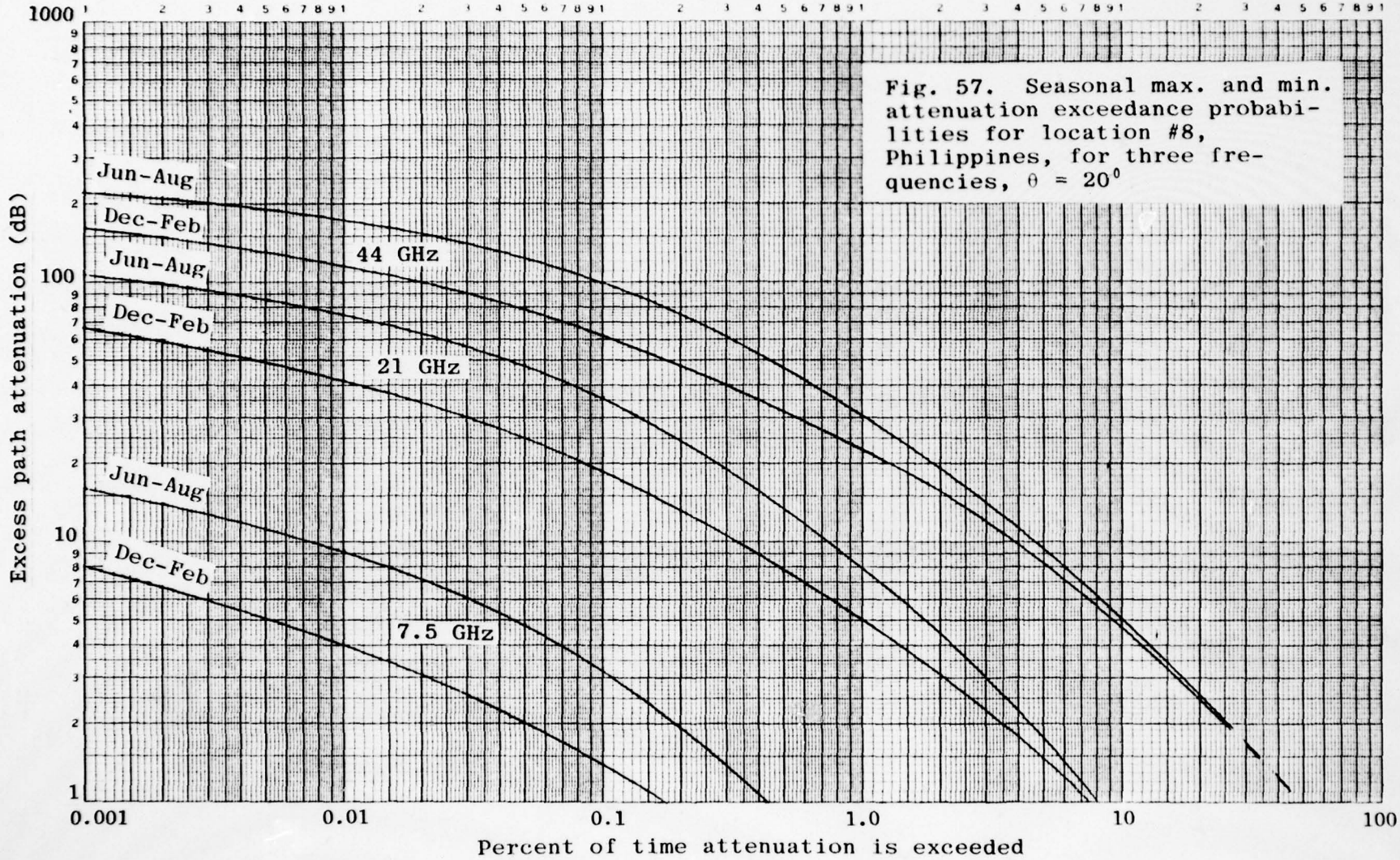

Fig. 57. Seasonal max. and min. attenuation exceedance probabilities for location #8, Philippines, for three frequencies, $\theta = 20^0$

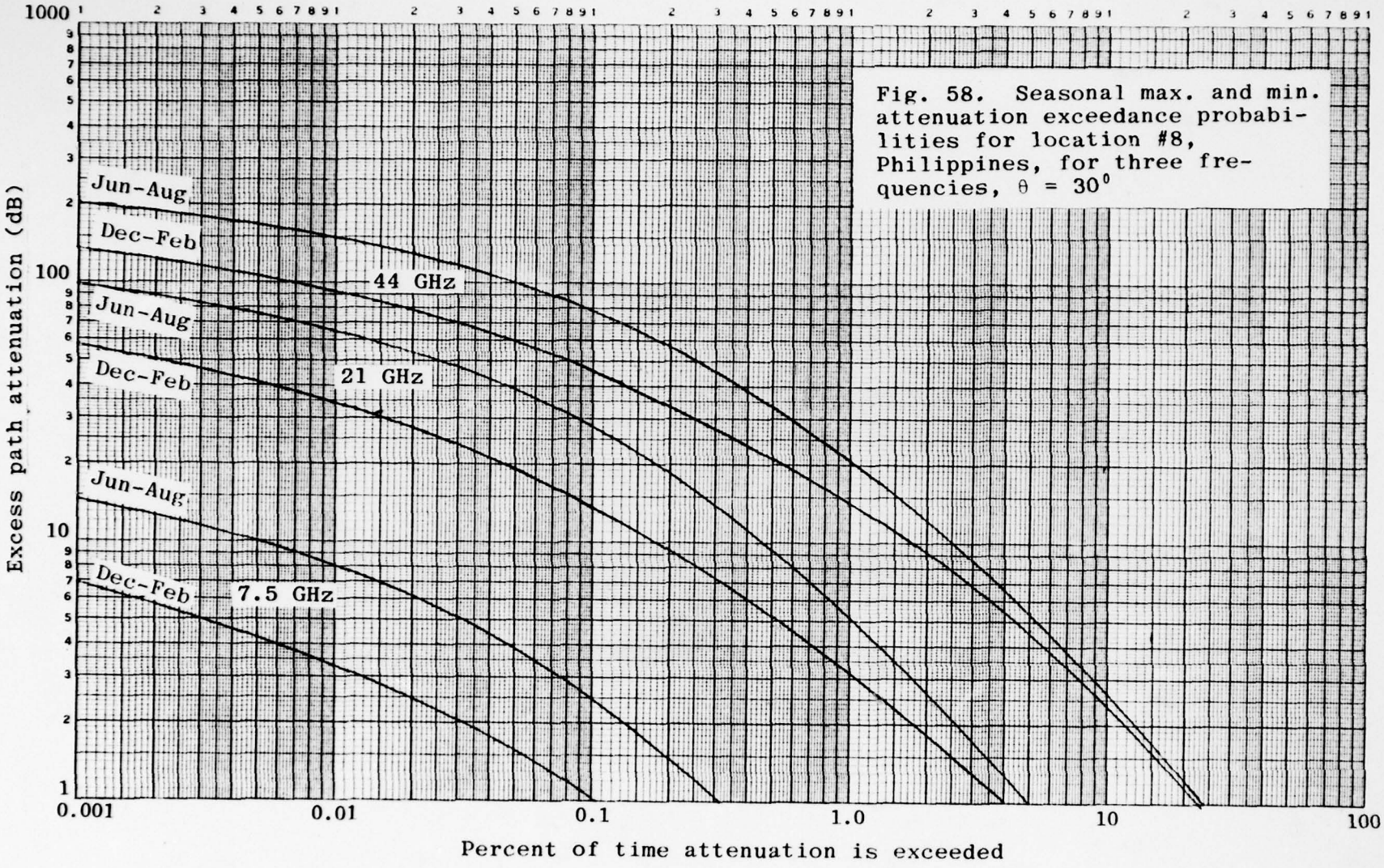

Fig. 58. Seasonal max. and min. attenuation exceedance probabilities for location #8, Philippines, for three frequencies, $\theta = 30^0$

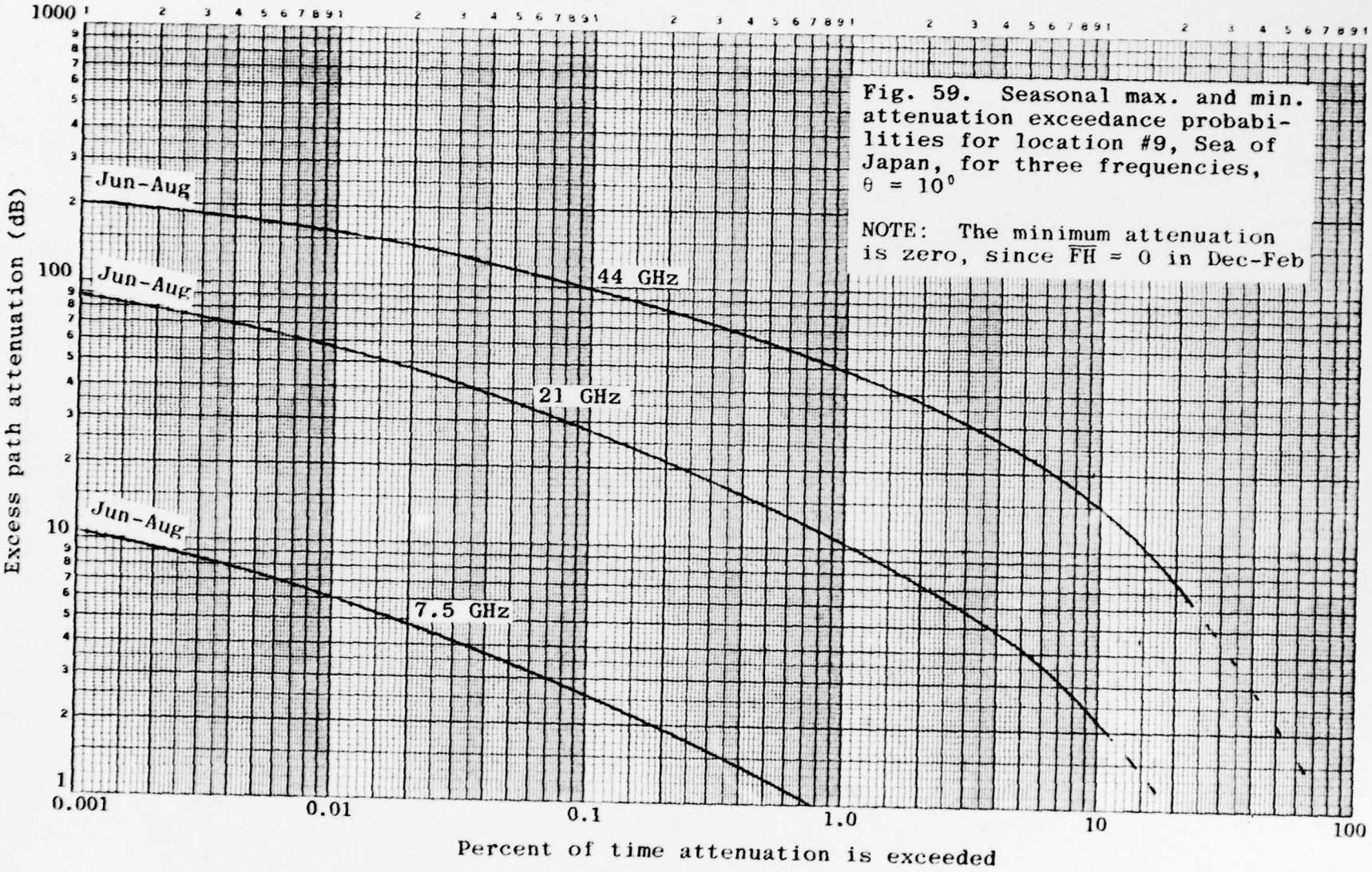

Fig. 59. Seasonal max. and min. attenuation exceedance probabilities for location #9, Sea of Japan, for three frequencies, $\theta = 10^0$

NOTE: The minimum attenuation is zero, since $\overline{FH} = 0$ in Dec-Feb

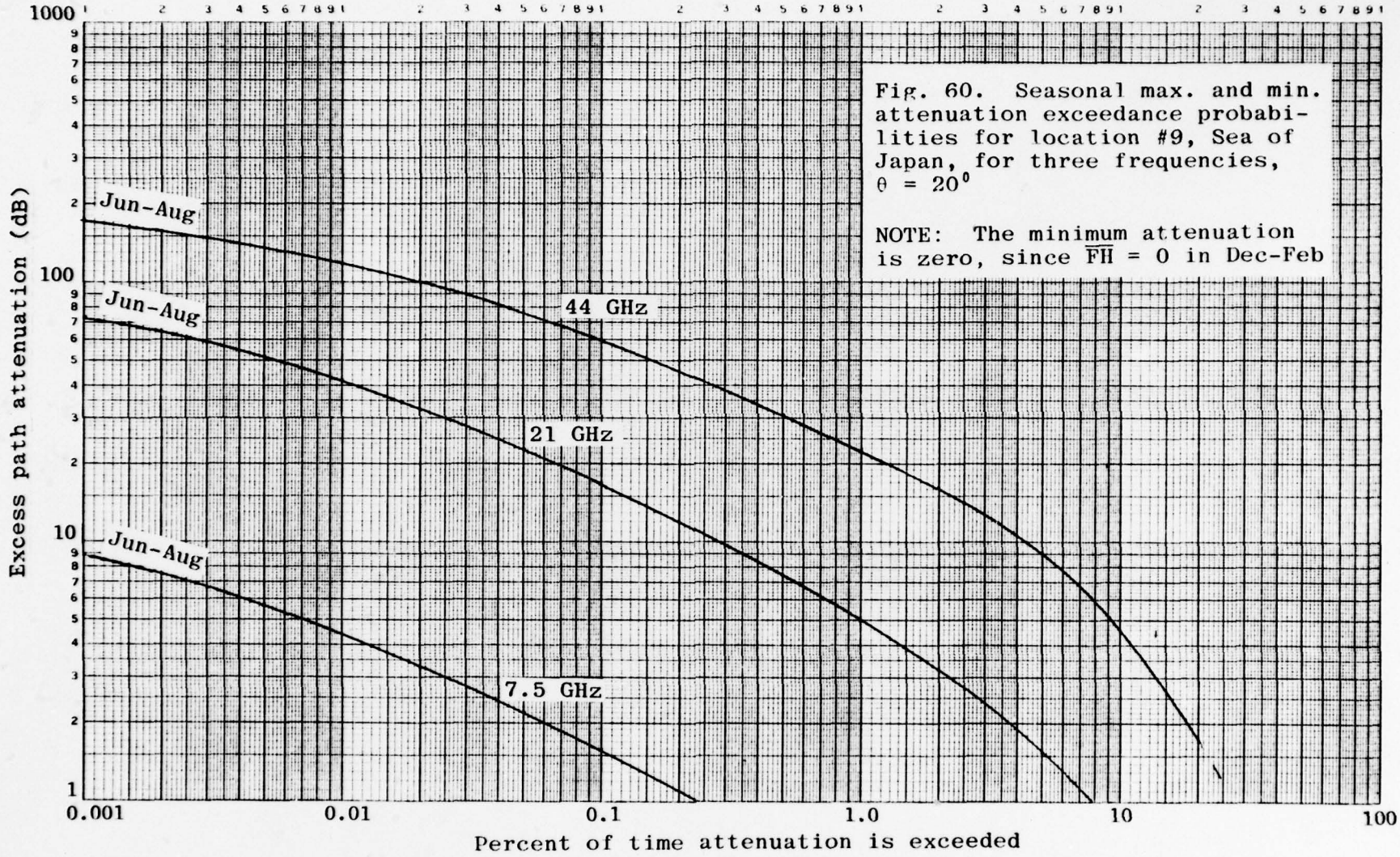

Fig. 60. Seasonal max. and min. attenuation exceedance probabilities for location #9, Sea of Japan, for three frequencies, $\theta = 20^0$

NOTE: The minimum attenuation is zero, since $\overline{FH} = 0$ in Dec-Feb

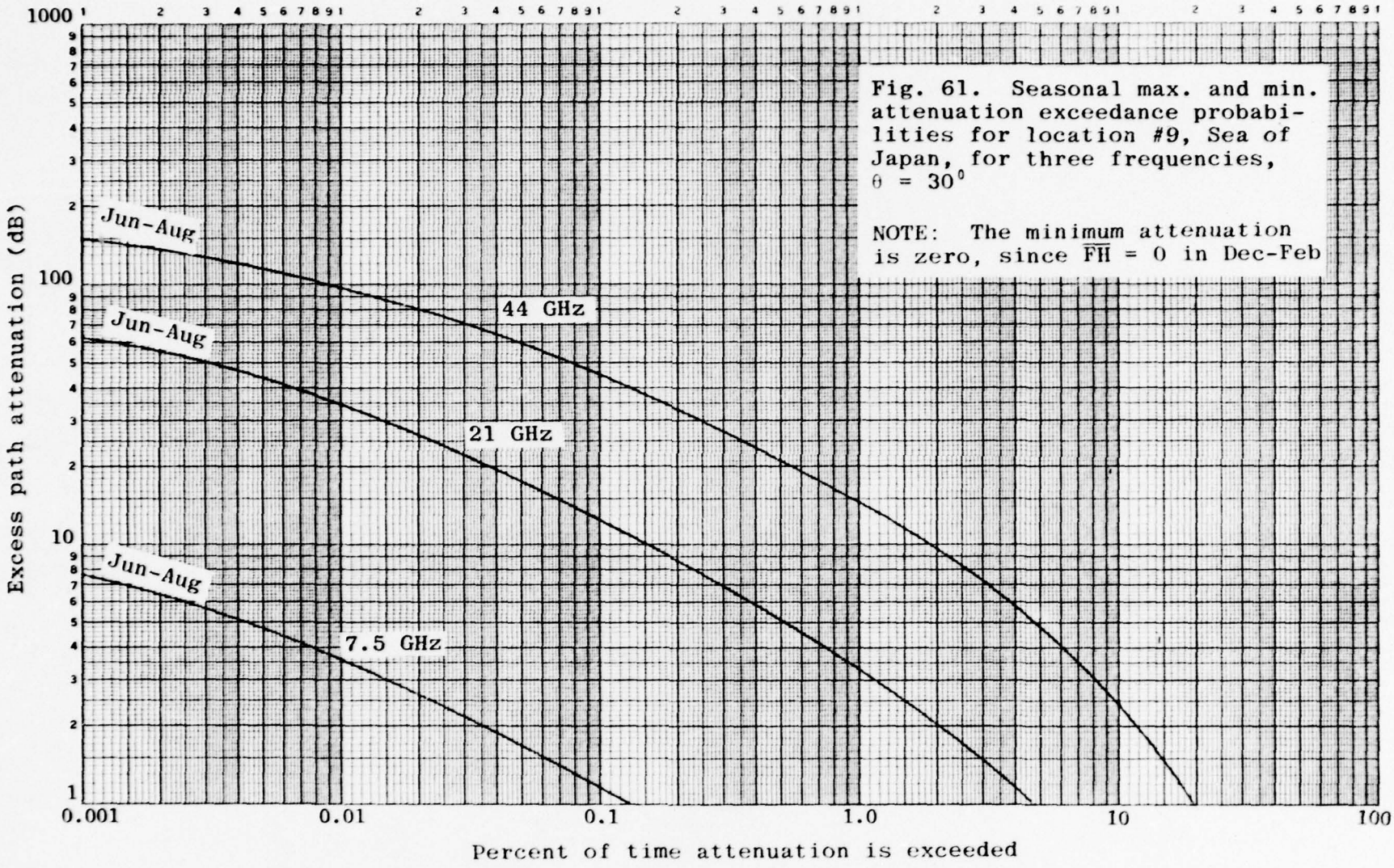

Fig. 61. Seasonal max. and min. attenuation exceedance probabilities for location #9, Sea of Japan, for three frequencies, $\theta = 30^0$

NOTE: The minimum attenuation is zero, since $\overline{FH} = 0$ in Dec-Feb

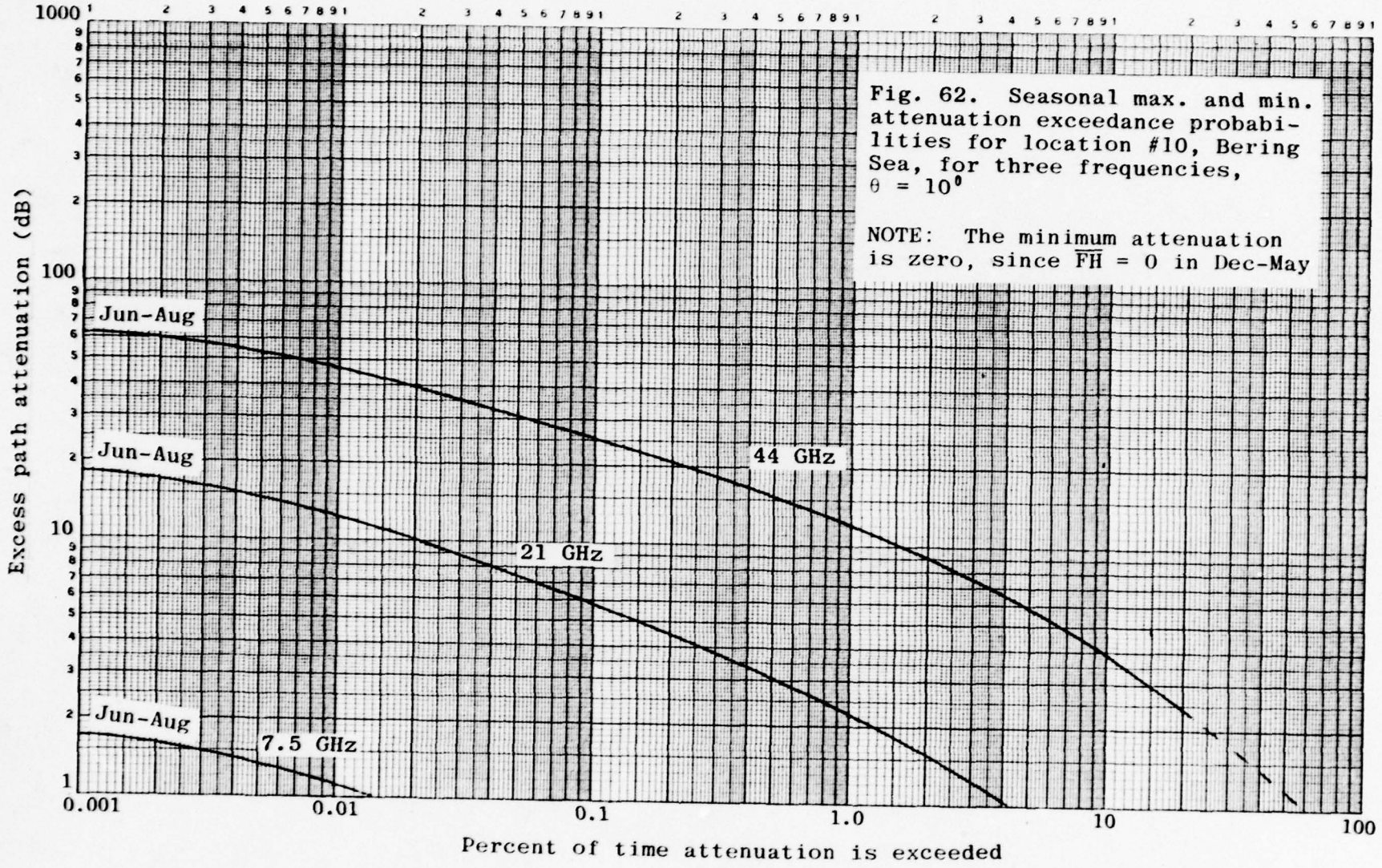

Fig. 62. Seasonal max. and min. attenuation exceedance probabilities for location #10, Bering Sea, for three frequencies, $\theta = 10^0$

NOTE: The minimum attenuation is zero, since $\overline{FH} = 0$ in Dec-May

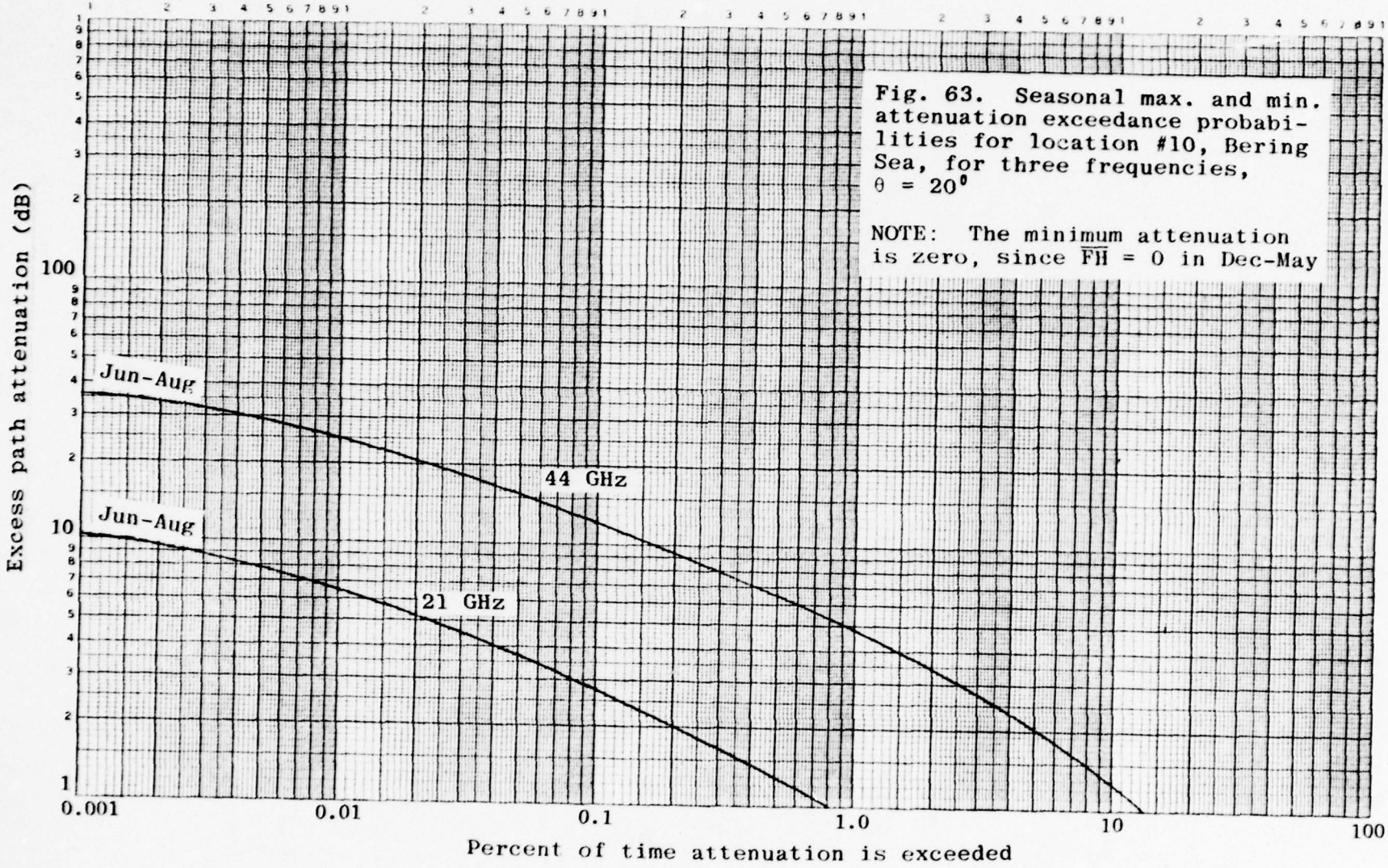

Fig. 63. Seasonal max. and min. attenuation exceedance probabilities for location #10, Bering Sea, for three frequencies, $\theta = 20^0$

NOTE: The minimum attenuation is zero, since $\overline{FH} = 0$ in Dec-May

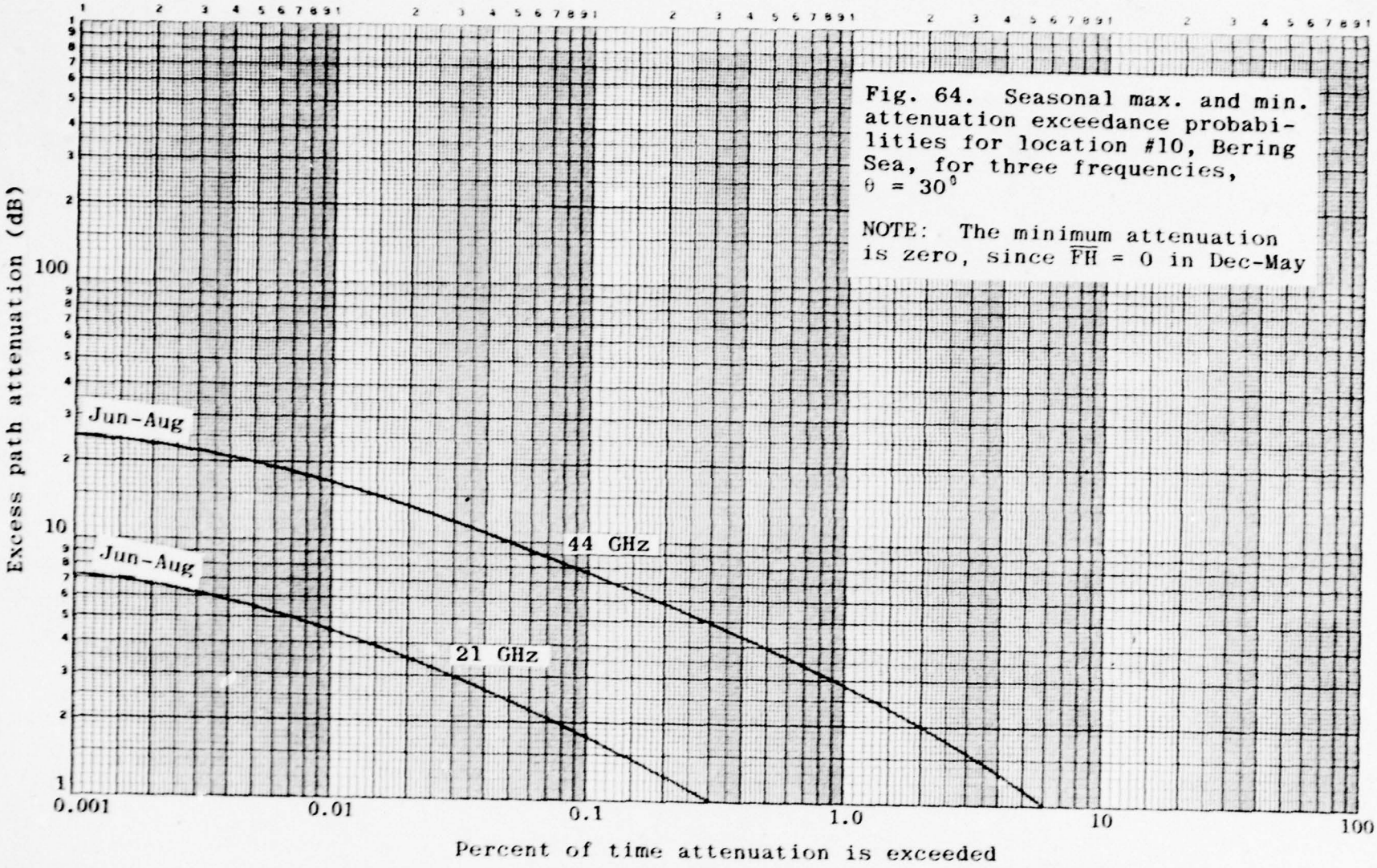

Fig. 64. Seasonal max. and min. attenuation exceedance probabilities for location #10, Bering Sea, for three frequencies, $\theta = 30^0$

NOTE: The minimum attenuation is zero, since $\overline{FH} = 0$ in Dec-May

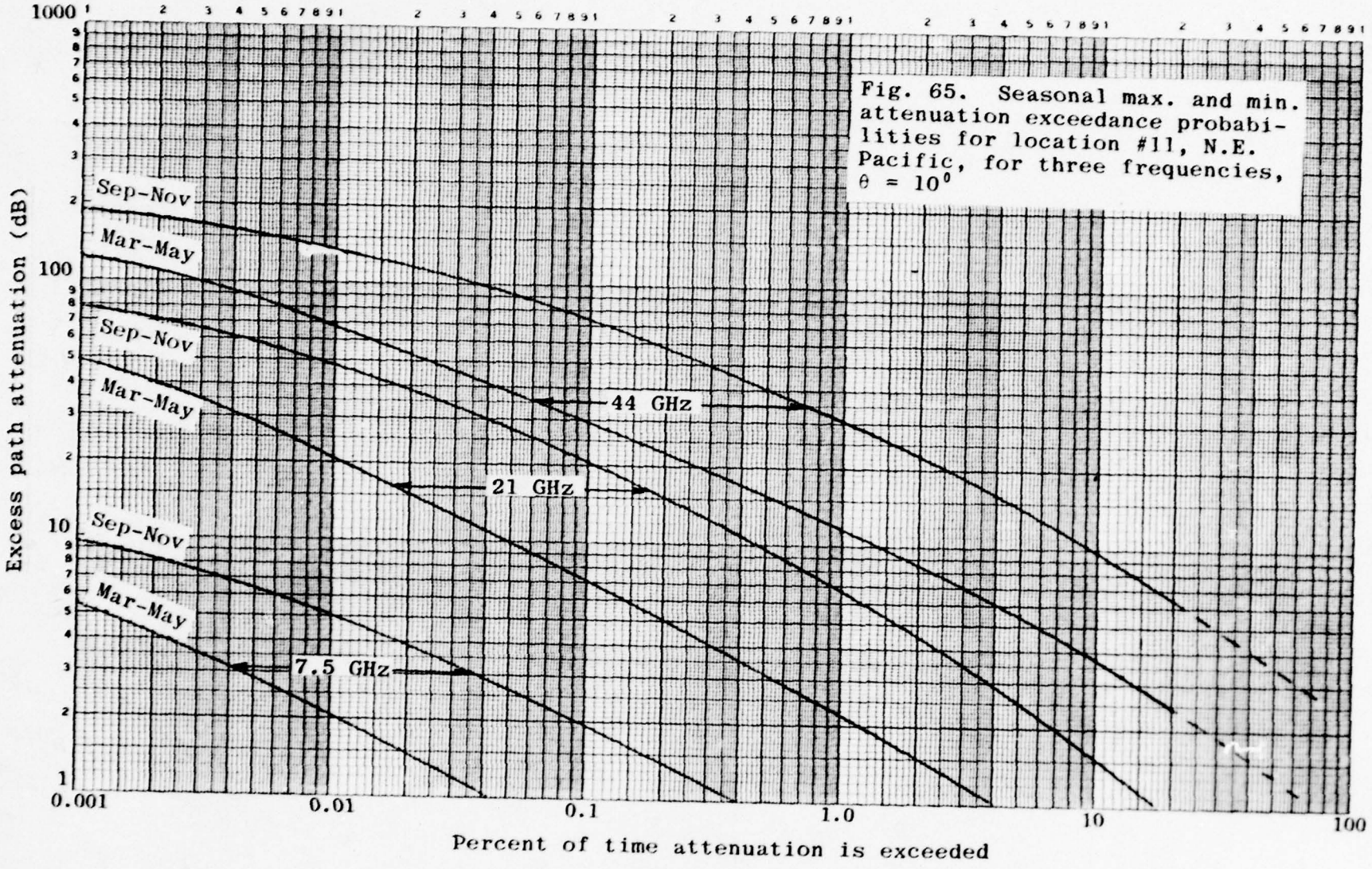

Fig. 65. Seasonal max. and min. attenuation exceedance probabilities for location #11, N.E. Pacific, for three frequencies, $\theta = 10^0$

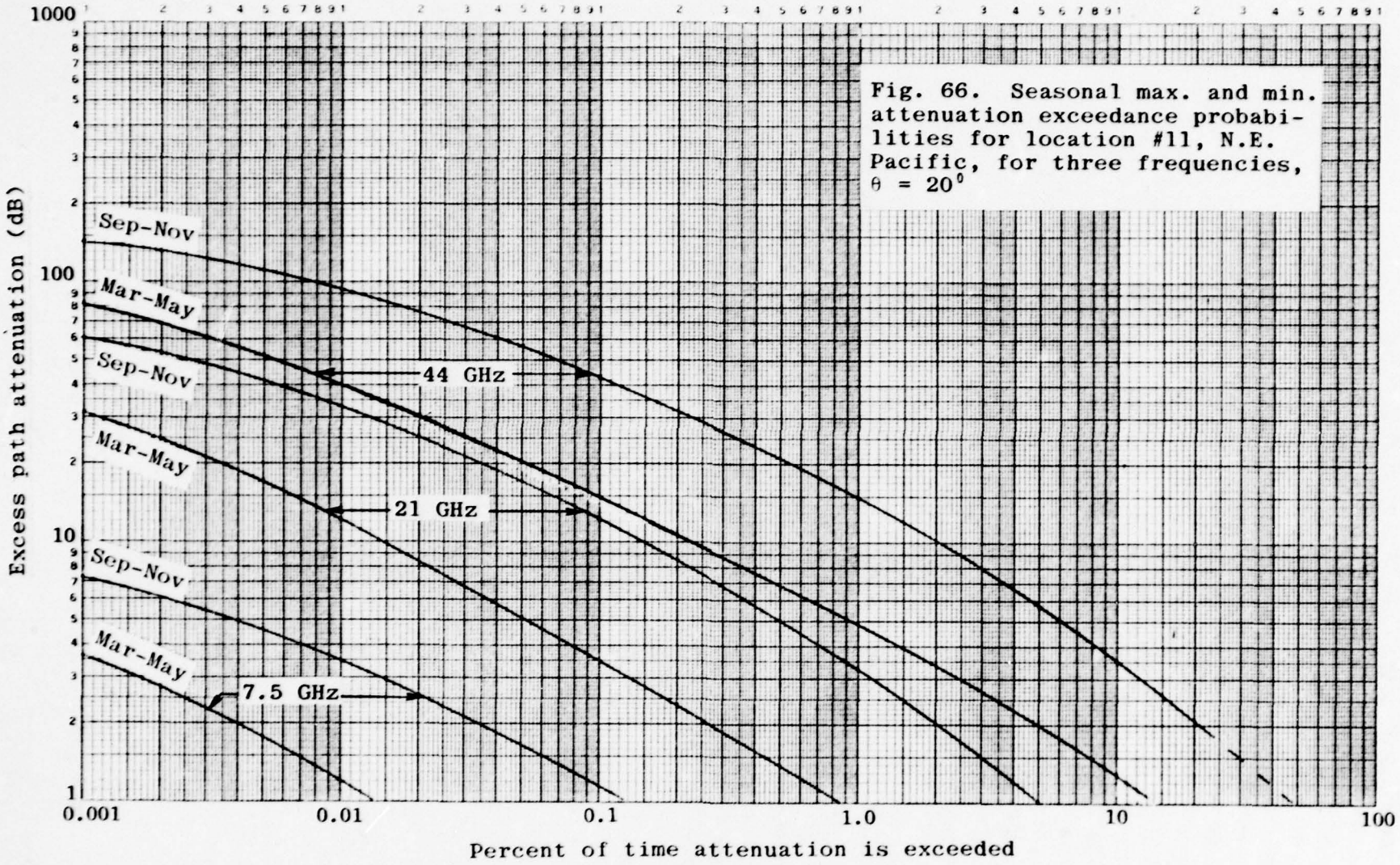

Fig. 66. Seasonal max. and min. attenuation exceedance probabilities for location #11, N.E. Pacific, for three frequencies, $\theta = 20^0$

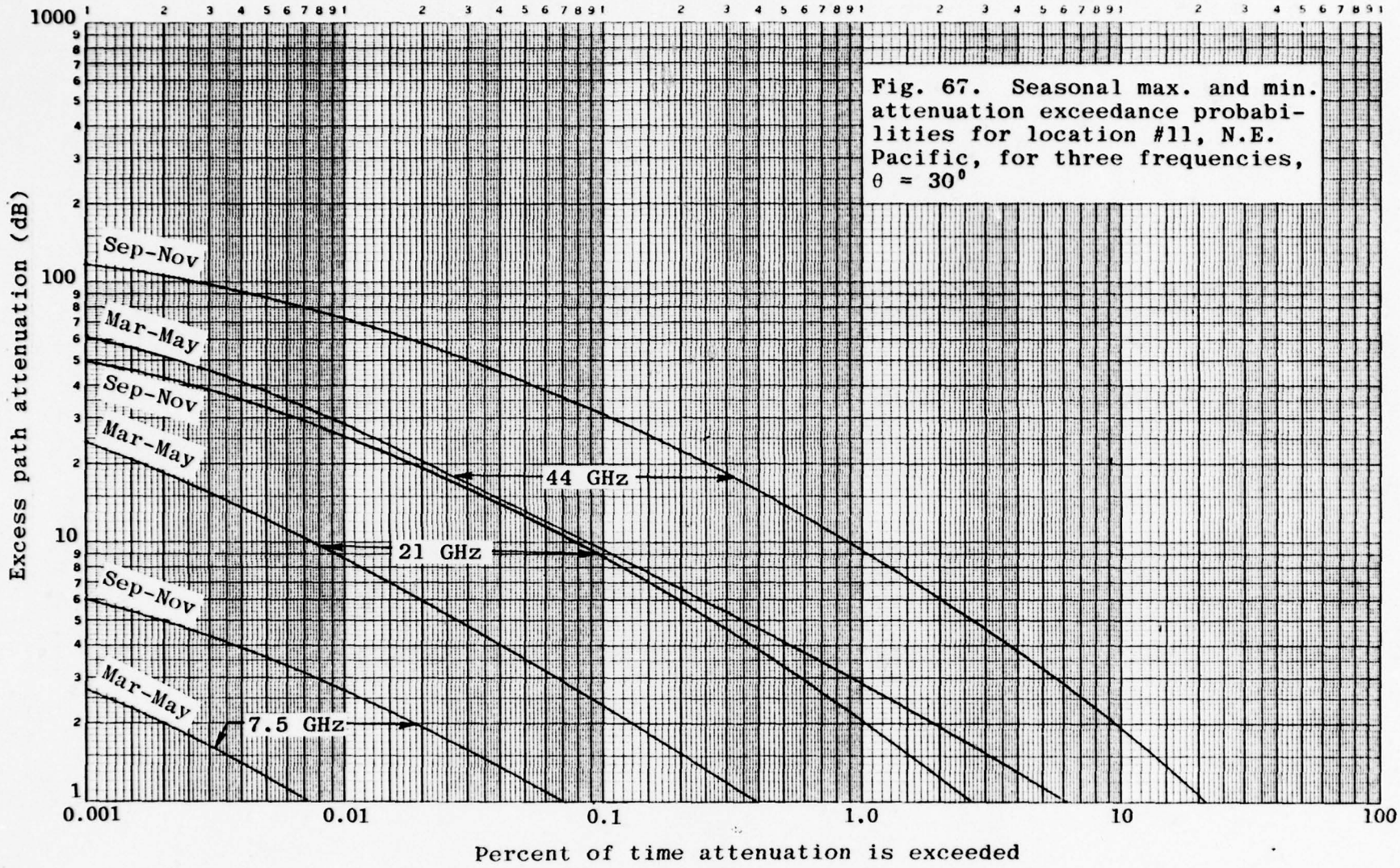

Fig. 67. Seasonal max. and min. attenuation exceedance probabilities for location #11, N.E. Pacific, for three frequencies, $\theta = 30^0$

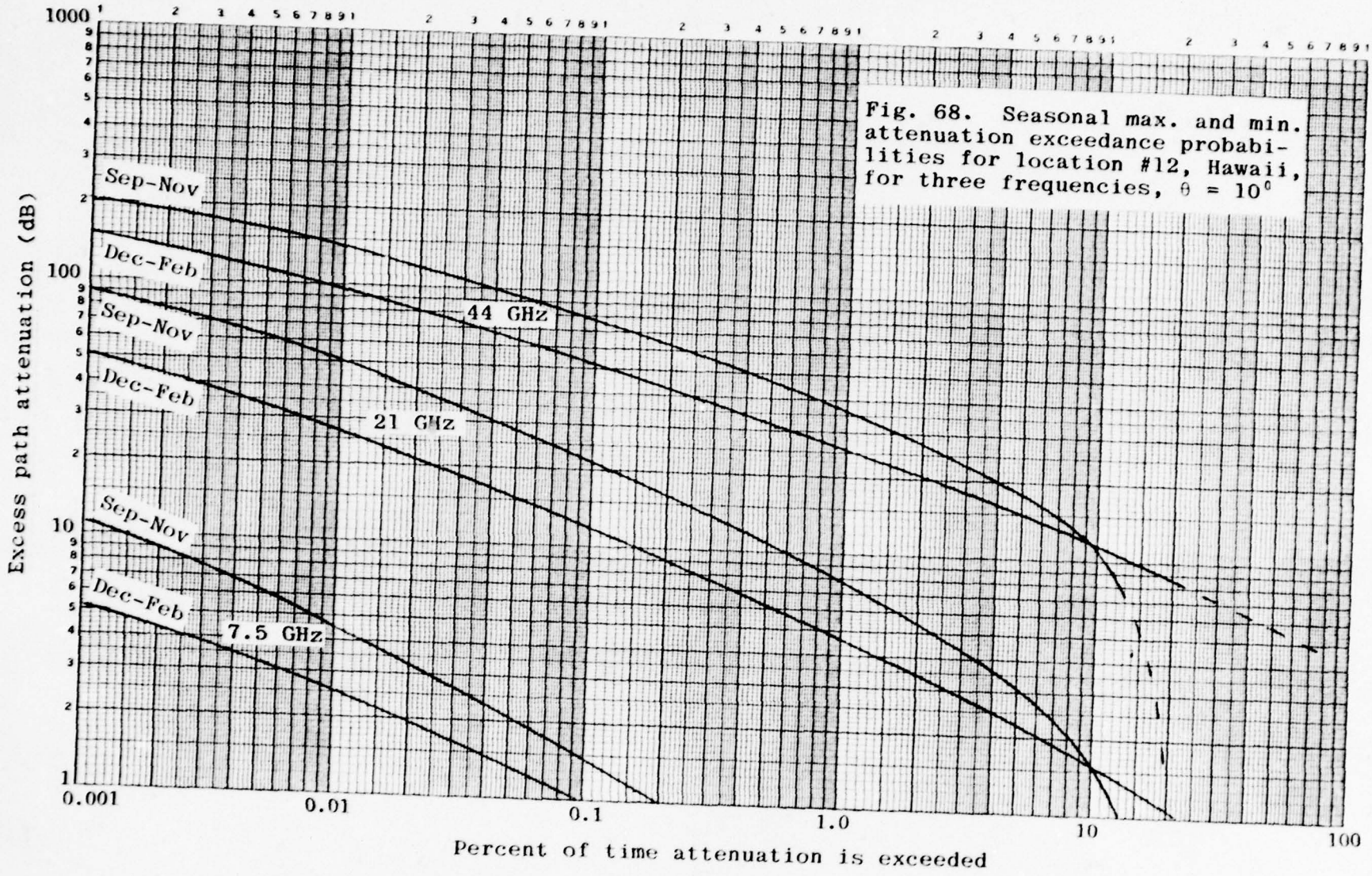

Fig. 68. Seasonal max. and min. attenuation exceedance probabilities for location #12, Hawaii, for three frequencies, $\theta = 10^0$

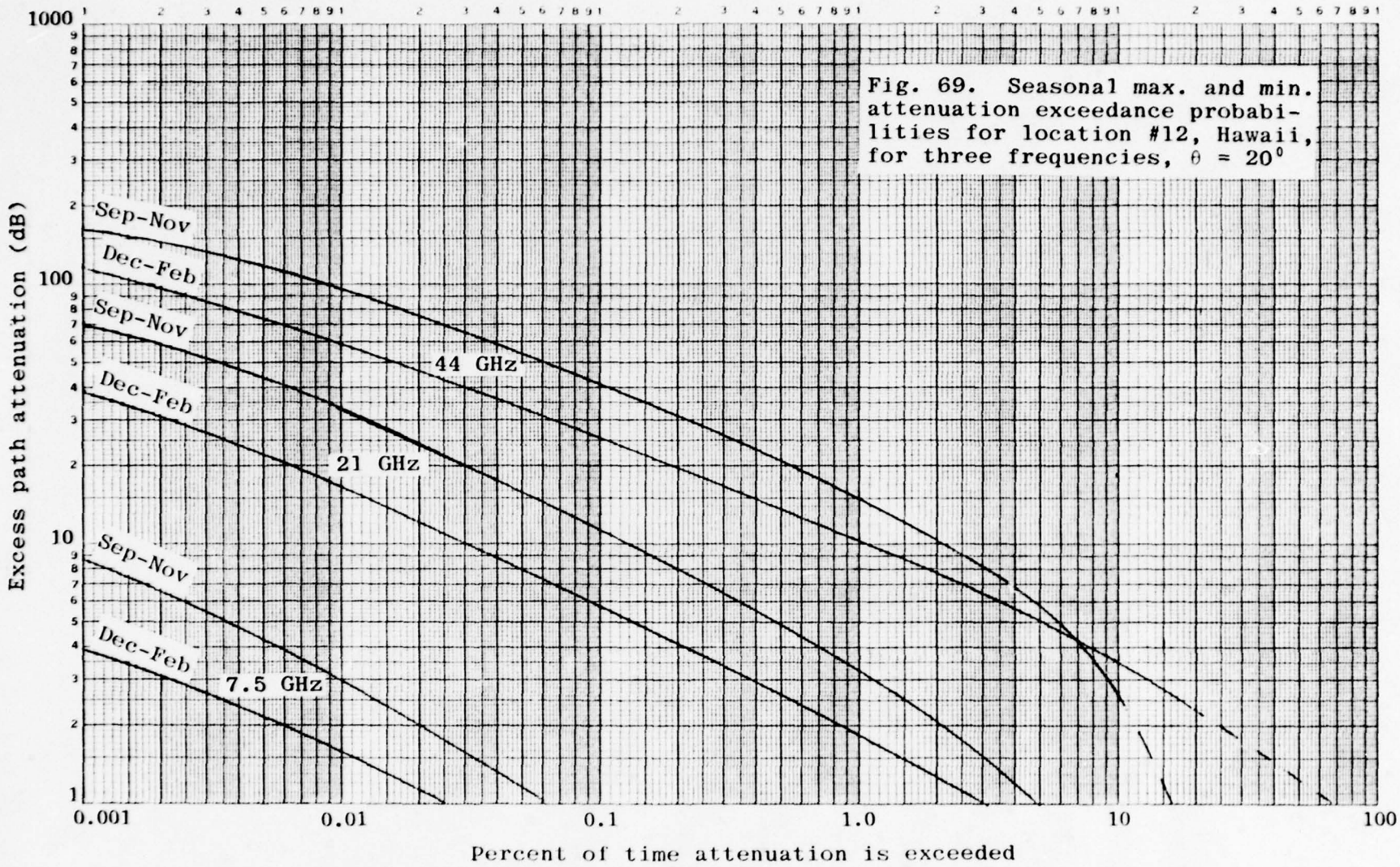

Fig. 69. Seasonal max. and min. attenuation exceedance probabilities for location #12, Hawaii, for three frequencies, $\theta = 20^0$

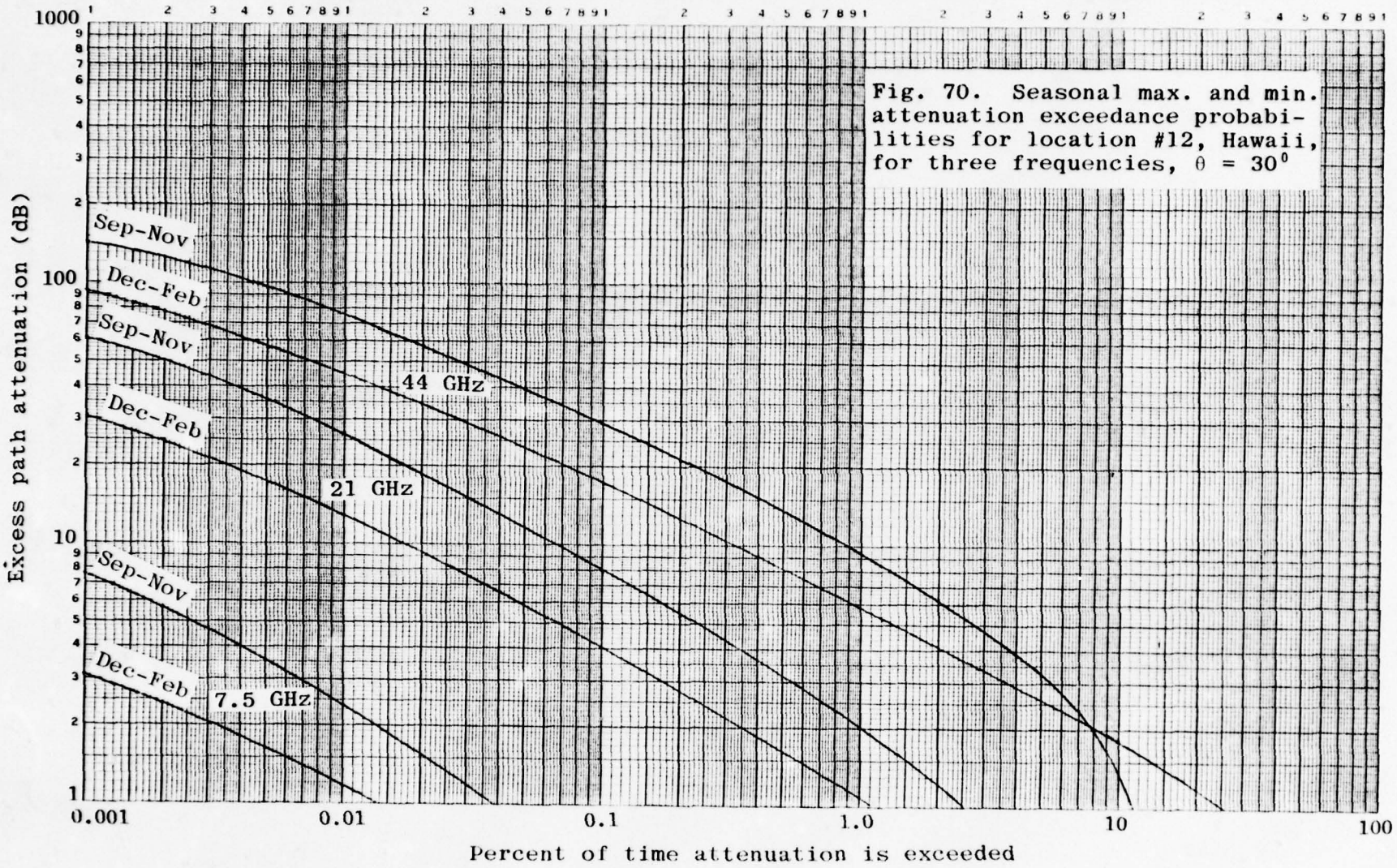

Fig. 70. Seasonal max. and min. attenuation exceedance probabilities for location #12, Hawaii, for three frequencies, $\theta = 30^0$

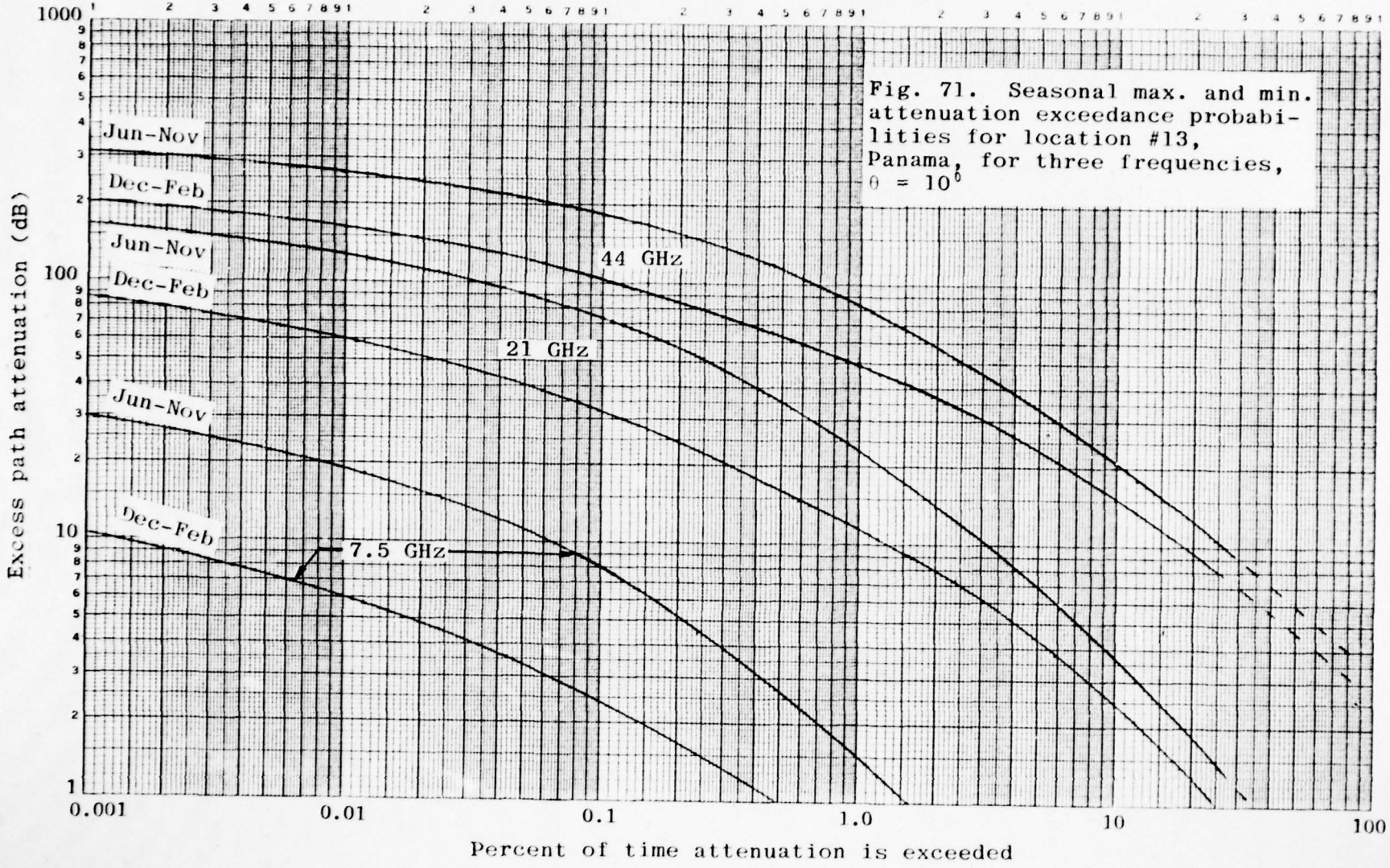

Fig. 71. Seasonal max. and min. attenuation exceedance probabilities for location #13, Panama, for three frequencies, $\theta = 10^0$

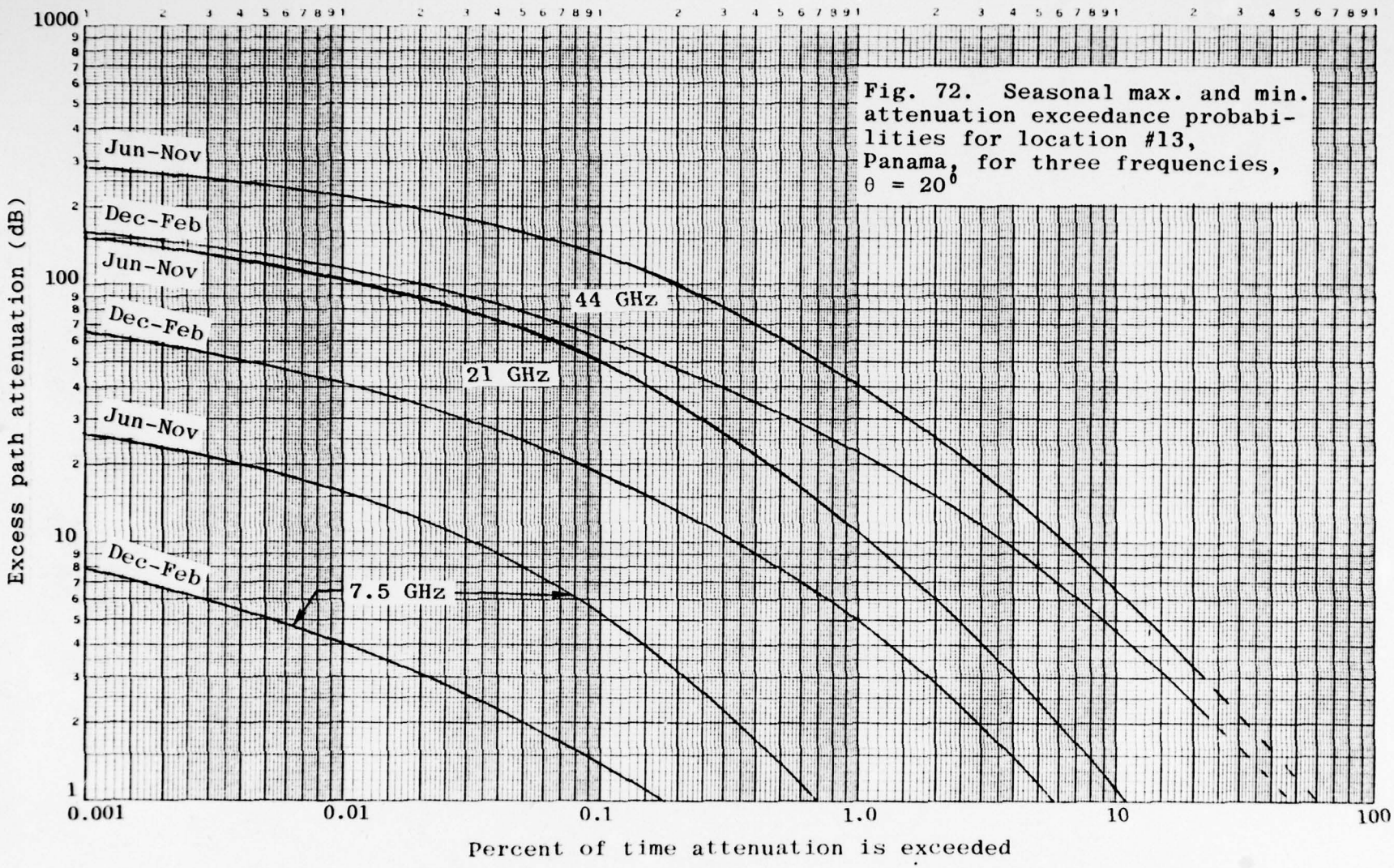

Fig. 72. Seasonal max. and min. attenuation exceedance probabilities for location #13, Panama, for three frequencies, $\theta = 20^0$

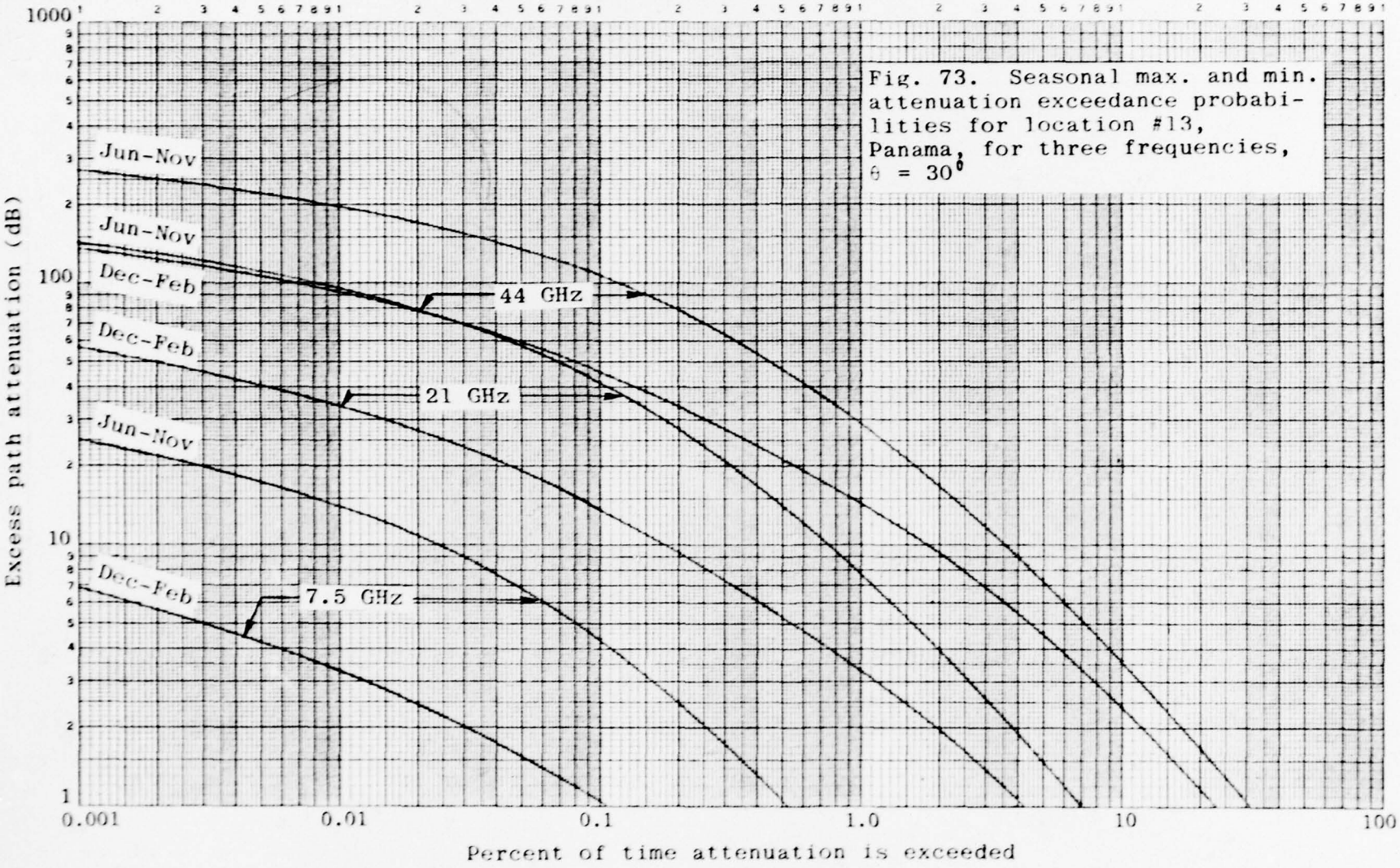

Fig. 73. Seasonal max. and min. attenuation exceedance probabilities for location #13, Panama, for three frequencies, $\theta = 30^0$

Attenuation values greater than 100 dB are shown merely for completeness, not because of their significance for system design. Values less than 1 dB were calculated and used to accurately locate the 1 dB intercepts, although such low values are of no interest in themselves.

Wherever possible, the curves have been extrapolated to the right toward 100 percent of the time. These dashed extensions go beyond the point where surface rainfall can be measured; they crudely indicate the fact that the attenuation due to clouds will be dominant in those regions, although these effects have not yet been analyzed. We guess that the clouds may cause the attenuation to flare out and drop off even less sharply than indicated at the highest frequencies and lowest elevation angles considered in this study. However, for those arid locations with an F type precipitation (Locations 3, 4, 6 and 12) where there is known to be a large number of cloudless days, the curves dip sharply downward.

Five locations -- namely 13, 8, 11, 1 and 4 in order of decreasing attenuation -- have been picked to present more fully the variation with frequency and the variation with elevation angle. Figures 74 and 75 show the frequency dependence, for 10^{o} and 30^{o}, all at the 1 percent exceedance level. Figures 76 and 77 show the elevation angle dependence, for 21 and 44 GHz, again at the 1 percent level. There are no surprises here, the trends all being similar to those shown in Figures 13-18.

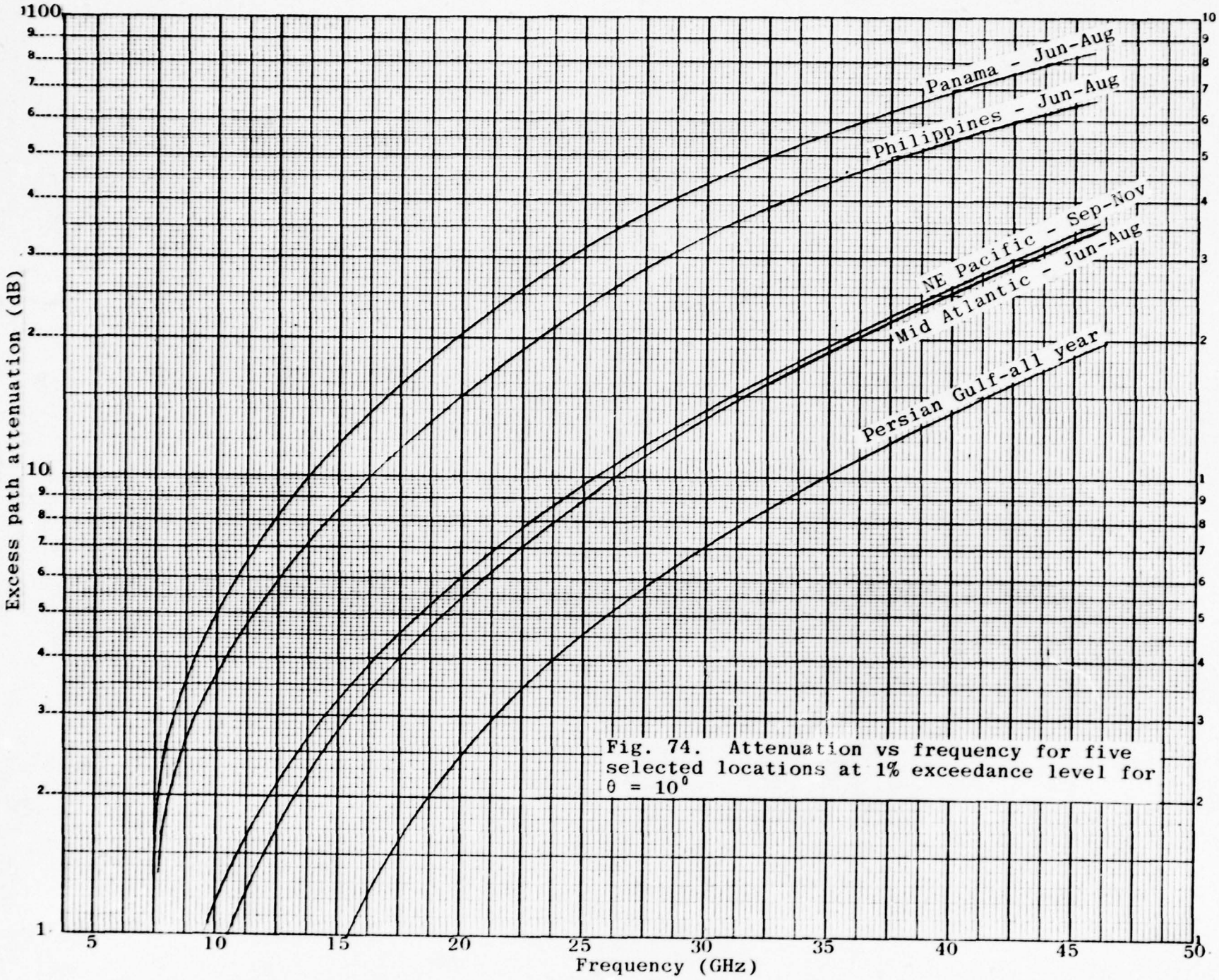

Fig. 74. Attenuation vs frequency for five selected locations at 1% exceedance level for $\theta = 10^0$

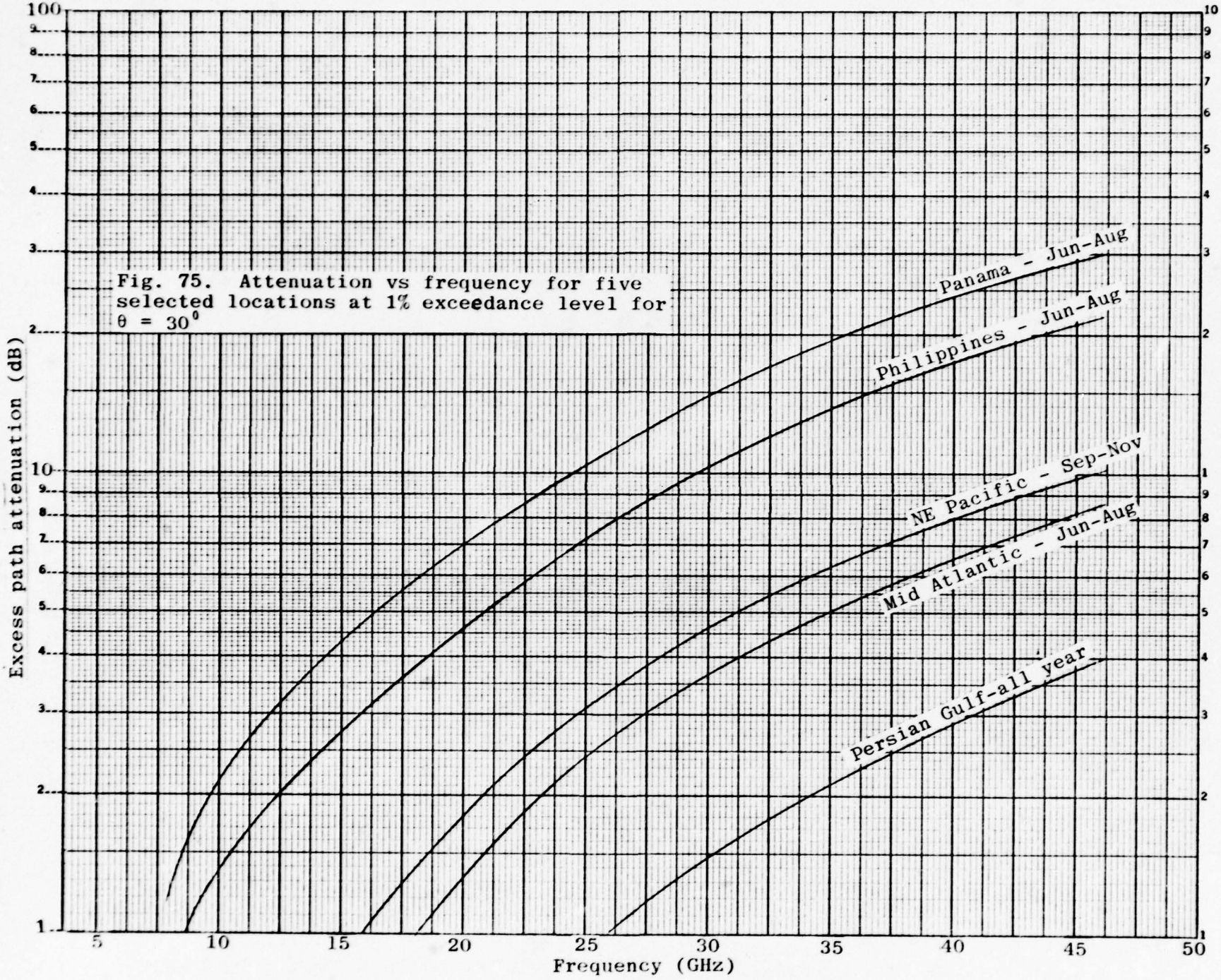

Fig. 75. Attenuation vs frequency for five selected locations at 1% exceedance level for $\theta = 30^0$

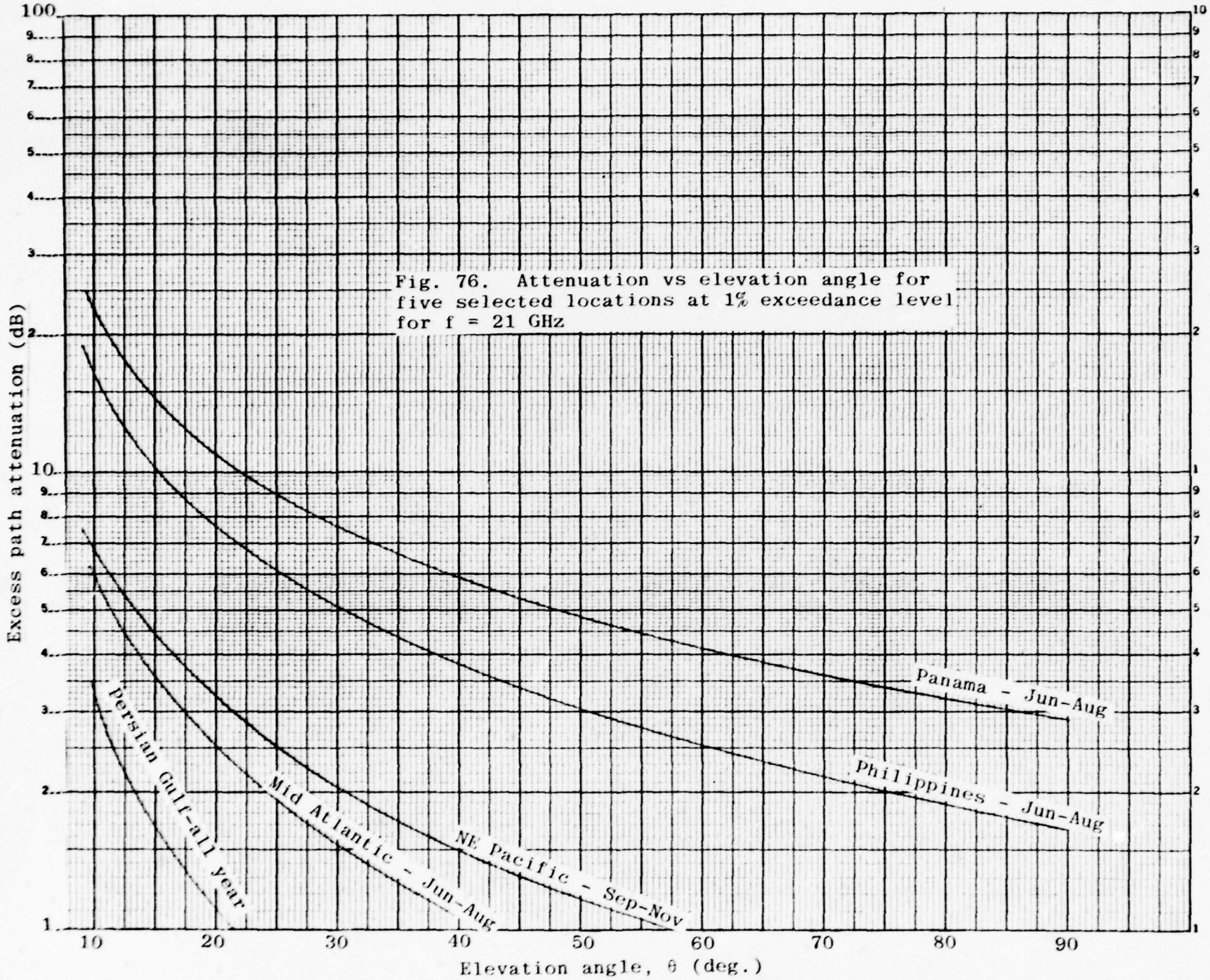

Fig. 76. Attenuation vs elevation angle for five selected locations at 1% exceedance level for f = 21 GHz

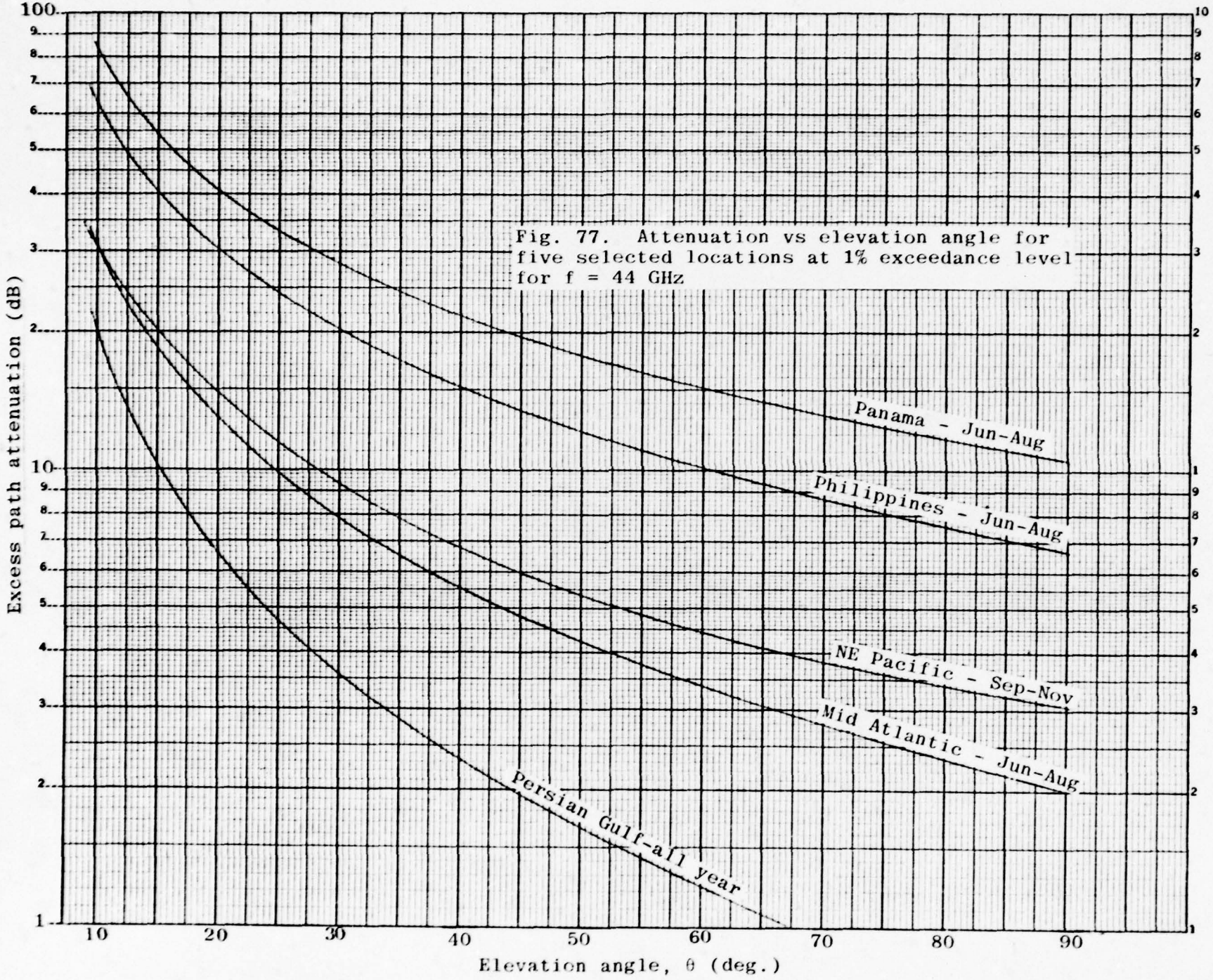

Fig. 77. Attenuation vs elevation angle for five selected locations at 1% exceedance level for f = 44 GHz

5.0 OUTAGE DURATION STATISTICS

To evaluate the impact of a cumulative outage time on communications requires knowledge of the outage duration statistics. The system design alternatives are radically different depending on whether typical outage durations are microseconds, seconds, minutes or hours.

5.1 Local Precipitation Frequency Correction Factor

We need to make an additional adjustment to the precipitation-rate distributions to account for time and space variations in precipitation frequencies within the precipitation-rate regions. Recall that the frequency distributions were extended to 0.1 (and 0.05) mm/hr precipitation rates based on assumed characteristic precipitation frequencies for each region. At any given location and season, the actual "point-season" precipitation frequency often differs from the assumed characteristic value; and the distribution used in the attenuation calculations should reflect that difference. A first approximate adjustment is to move the affected frequency distribution left or right (in Fig. 34) according to the ratio of point-season precipitation frequency to characteristic precipitation frequency. Equivalently, the percent of year values in the left column of Table 7 are multiplied by the precipitation frequency ratio, k'.

Section 4.1 presented a local precipitation-rate correction factor, k, which we obtained by comparing the average daily precipitation for a specific location (shown in Table 4), with the characteristic values we assumed (see Table 6). This k factor amounts to a vertical adjustment of the precipitation rate distribution curves (Fig. 34) to give the correct value of the integral under those curves. This method of correcting for the locally measured rainfall was designed to give more accurate predictions of path attenuation for the selected location. However, in analyzing the outage duration statistics, we realized that an analogous local precipitation-frequency correction factor, k', should have been developed at the same time. To completely utilize existing local

data, as differentiated from the nominal or characteristic estimates of our model, Tables 4 and 6 can be compared with regard to precipitation frequency as well as with regard to average daily precipitation amount. In other words, using the two coordinates of Figure 25, we can allow for the fact that local point-season data may differ in both coordinates from the nominal values. This amounts to shifting the distribution curves of Figure 34 both vertically and horizontally, so as to correct both the time scale and the integral value to match the specific locality.

In view of the evolutionary nature of this research and the lack of time and resources to rerun all the previous calculations, we devised a graphical method for applying this second correction to the previous results in the few cases being pursued in this section. The application of this second correction (k') on top of the first one (k) (instead of doing them simultaneously) makes a direct linear change in the time scale, and hence is of great importance to the outage duration analysis. Fortunately, its effect on the attenuation values is only second order. Depending on the actual slope of the distribution curves, the correction may be either up or down. It usually constitutes not more than 2 to 5 dB and always constitutes less than 10 dB in the cases we have examined. Accordingly, the attenuation results in Figures 35 to 77 have errors of a few dB at most, but the outage times in Tables 10 to 12 are fully corrected for both effects. The precipitation-frequency correction factor, Precipitation-frequency Ratio k', is derived and its value shown for each of three locations in Tables 10 to 12. At the low precipitation rates of Tables 10 to 12, the application of k' to the precipitation rate in the way we have done (to maintain the value of the integrated rainfall) appears overly conservative. A weighted correction which increases the high precipitation-rate end more than the low end may be more accurate. The result would be a small or even negligible correction at the low precipitation-rate end of the distribution, i.e., attenuations $\leq$15 dB. For the present, we use the attenuation values corresponding to an unweighted uniformly increased precipitation rate.

5.2 Link Margin Exceedance Probabilities

The three locations to be considered in detail are #8, the Philippines in summer; #11, the NE Pacific in the fall; and #1, the Mid-Atlantic in summer. At these locations Figures 56-58, 65-67, 35 to 37 give the percent of the time that various levels of attenuation in dB are exceeded. We can interpret such numbers as the percent of the time that outages will occur given that amount of system margin in dB. These values are listed in Tables 10-12 for these three locations. Each table covers two frequencies (21 and 44 GHz) and two elevation angles (10^{o} and 30^{o}), for link margins of 5 to 30 dB in 5 dB steps. These time percentages are easily converted to hours per season simply by multiplying by 2192 (one-fourth of the number of hours in a year, which is 8766). We use the time percentages to enter the appropriate precipitation rate distribution curve, i.e., H, C' or C as the case may be, of Figure 34 to obtain the nominal precipitation rate for that climate type. This in turn can be converted to the precipitation rate at the specified location by multiplying the abscissa by the correction factor k' and the ordinate by k/k' for these three point-season combinations. Precipitation rate, mean freezing heights and path length are also given in Tables 10 to 12 in order to assist the reader in visualizing each of the conditions.

5.3 Estimating Precipitation Durations

An outage of a communications link can be related to the occurrence of a precipitation rate of a particular magnitude, given a particular freezing height. In the present model, freezing height is assumed constant over a three-month season at any given location. Therefore, the minimum precipitation rate associated with an outage is that rate that is equalled or exceeded with the same frequency as the expected occurrence frequency of the outage. For example, in Table 12a, the (adjusted) attenuation exceedance time at 44 GHz with a 10 dB link margin is 8.7%, which corresponds to a precipitation rate $\geq$0.25 mm/hr.

Table 10. EXCEEDANCE TIMES FOR VARIOUS MARGIN LEVELS: LOC. #8, PHILIPPINES, JAN-AUG, RAIN TYPE H

Point-season precipitation frequency = 0.11
Mid-region precipitation frequency = 0.20
Precipitation frequency ratio, k' = 0.55

(a) Elevation angle $\theta = 10^0$, $\overline{FH} = 4.9$ km, L = 28.2 km

44 GHz			Link	21 GHz		
Percent of time	Hrs. per Season	Rain Rate (mm/hr)	Margin (dB)	Percent of Time	Hrs. per Season	Rain Rate (mm/hr)
15.0	330	0.04	5	2.4	53	1.2
7.8	170	0.19	10	1.07	23	3.5
4.8	105	0.41	15	0.60	13	6.4
3.3	73	0.73	20	0.40	8.7	10.0
2.4	53	1.17	25	0.27	6.0	14.0
1.8	40	1.75	30	0.19	4.2	19.0

(b) Elevation angle $\theta = 30^0$, $\overline{FH} = 4.9$ km, L = 9.8 km

44 GHz			Link	21 GHz		
Percent of time	Hrs. per Season	Rain Rate (mm/hr)	Margin (dB)	Percent of Time	Hrs. per Season	Rain Rate (mm/hr)
2.2	47.0	1.5	5	0.58	12.7	6.5
1.15	25.0	3.0	10	0.25	5.4	16.0
0.75	16.0	5.0	15	0.15	3.3	25.0
0.54	11.9	7.2	20	0.11	2.3	34.0
0.41	9.0	9.9	25	0.08	1.8	42.0
0.32	7.0	12.8	30	0.065	1.4	50.0

Table 11. EXCEEDANCE TIMES FOR VARIOUS MARGIN LEVELS: LOC. #11, NE PACIFIC, SEP-NOV, RAIN TYPE C'

Point-season precipitation frequency = 0.16
Mid-region precipitation frequency = 0.35
Precipitation frequency ratio, k' = 0.46

(a) Elevation angle $\theta = 10^0$, $\overline{FH}$ = 3.0 km, L = 17.3 km

44 GHz			Link Margin (dB)	21 GHz		
Percent of time	Hrs. per Season	Rain Rate (mm/hr)		Percent of Time	Hrs. per Season	Rain Rate (mm/hr)
12.0	260	0.25	5	0.78	17.0	3.9
4.5	97	0.85	10	0.25	5.5	9.8
2.2	47	1.6	15	0.11	2.5	15.4
1.2	27	2.6	20	0.07	1.5	21.5
0.8	18	3.7	35	0.04	0.9	30
0.6	13	5.1	30	0.03	0.6	41

(b) Elevation angle $\theta = 30^0$, $\overline{FH}$ = 3.0 km, L = 6.0 km

44 GHz			Link Margin (dB)	21 GHz		
Percent of time	Hrs. per Season	Rain Rate (mm/hr)		Percent of Time	Hrs. per Season	Rain Rate (mm/hr)
1.20	28	2.6	5	0.15	3.3	14.0
0.50	11	5.8	10	0.07	1.5	25.0
0.25	5.4	9.6	15	0.03	0.63	38.0
0.15	3.4	13.7	20	0.016	0.35	52.0
0.10	2.2	18.1	25	0.010	0.22	67.0
0.07	1.6	21.7	30	0.0065	0.14	83.0

Table 12. EXCEEDANCE TIMES FOR VARIOUS MARGIN LEVELS: LOC. #1, MID-ATLANTIC, JUN-AUG, RAIN TYPE C

Point-season precipitation frequency = 0.13
Mid-region precipitation frequency = 0.30
Precipitation frequency ratio, 'k' = 0.43

(a) Elevation angle $\theta = 10^0$, $\overline{FH}$ = 4.2 km, L = 24.2 km

44 GHz			Link	21 GHz		
Percent of time	Hrs. per Season	Rain Rate (mm/hr)	Margin (dB)	Percent of Time	Hrs. per Season	Rain Rate (mm/hr)
31.0	680	<.10	5	0.45	10.0	2.6
8.7	190	0.25	10	0.15	3.2	7.5
3.7	80	0.62	15	0.076	1.7	13.5
1.9	42	1.08	20	0.035	0.8	20.0
1.1	23	1.65	25	0.019	0.42	28.0
0.6	13	2.4	30	0.012	0.26	37.0

(b) Elevation angle $\theta = 30^0$, $\overline{FH}$ = 4.2 km, L = 8.4 km

44 GHz			Link	21 GHz		
Percent of time	Hrs. per Season	Rain Rate (mm/hr)	Margin (dB)	Percent of Time	Hrs. per Season	Rain Rate (mm/hr)
1.5	32.0	1.3	5	0.1	2.2	11
0.35	7.6	3.0	10	0.021	0.45	19
0.16	3.6	5.2	15	0.010	0.23	28
0.09	1.9	7.8	20	0.006	0.14	38
0.06	1.3	10.8	25	0.004	0.08	49
0.04	0.9	14.0	30	0.003	0.06	60

If the frequency distributions of precipitation-rate exceedance durations were known, then we could assume their corresponding attenuation exceedance duration distributions to be the same. That is, using the same example as above, if the duration statistics for a precipitation rate ≥ 0.25 mm/hr were known, then the duration statistics for a 44 GHz attenuation ≥ 10 dB would also be known (at the given location, season, and antenna elevation angle).

Only one precipitation-rate duration frequency distribution was found in the literature [13]; an exhaustive survey might discover more. Those precipitation-rate duration statistics come from an analysis of 10 years of data recorded by a precipitation gauge at McGill University, Montreal. Tabulated values from Reference 13 are plotted in Figure 78 and it is seen that the distribution of durations is very nearly lognormal. We therefore drew a straight-line lognormal approximation through the points. Also reproduced in Figure 79 are two fade (outage) duration frequency distributions for earth-space links. According to Lin (Reference 14), these are two of nine that he calculated, all of which were nearly lognormal.

How may a general method for predicting precipitation-rate exceedance durations (hence, outage durations) be constructed from such meager information? What follows is a tentative first step toward building a general method for deriving duration statistics.

The basic building block is the McGill University precipitation-rate duration distribution. That distribution applies to <u>all</u> precipitation; therefore, it is assumed to apply to precipitation rates in excess of 0.05 to 0.1 mm/hr. The McGill distribution represents the long-term, year-around, precipitation regime at Montreal. How the distributions for other precipitation regimes (e.g., more or less convective than Montreal) would differ from the McGill distribution is unknown at this point. One can speculate that the slope of the distribution would vary slightly -- slightly flatter for all convective precipitation, probably pivoting about some point in the short-duration ($\sim$1 min) end of the distri-

bution. Without corroborating data, however, we tentatively assume that the slopes of the duration distributions for all precipitation regimes can be approximated by that for Montreal.

One rule can be laid down with reasonable certainty:

- As the threshold precipitation rate increases, the lower the probability of long durations and the higher the probability of short durations.

This follows from the fact that the higher precipitation rates are largely associated with convective precipitation "cells," most of which are limited in size (~1 to 10 km diameter) and are temporally and spatially transient. Given the above rule and the assumed constancy of the duration distribution slope, it follows that, for increasing threshold precipitation rates, the lognormal duration distributions would be parallel to the McGill distribution but be displaced (in Figure 78) downward or leftward.

A tenuous basis for estimating the duration distributions for high-attenuation threshold precipitation rates is provided by Lin's two fade duration distributions (also plotted in Fig. 78). First, note that the distribution for the 19 GHz link with 5 dB fade margin (England) is almost exactly parallel to the McGill precipitation-rate duration distribution. We find this encouraging. The fact that the New Jersey 30 GHz, 21 dB distribution departs in slope is not too bothersome at this primitive stage, because it includes data from two winters and only one summer. It can be rationalized that the distribution is biased toward wintertime stratiform precipitation, the resulting slope being consistent with our previous speculation on this subject. In his article[14], Lin also provides the occurrence frequency distributions of rain attenuation for these two sets of data, from which it is estimated that the corresponding threshold precipitation rates for both locations are 5 $\pm$ 1 mm/hr. This estimation was made as follows: (1) From Lin's data, the percent of raining time that 5 dB attenuation was exceeded in the England measurements was 0.85%. In the

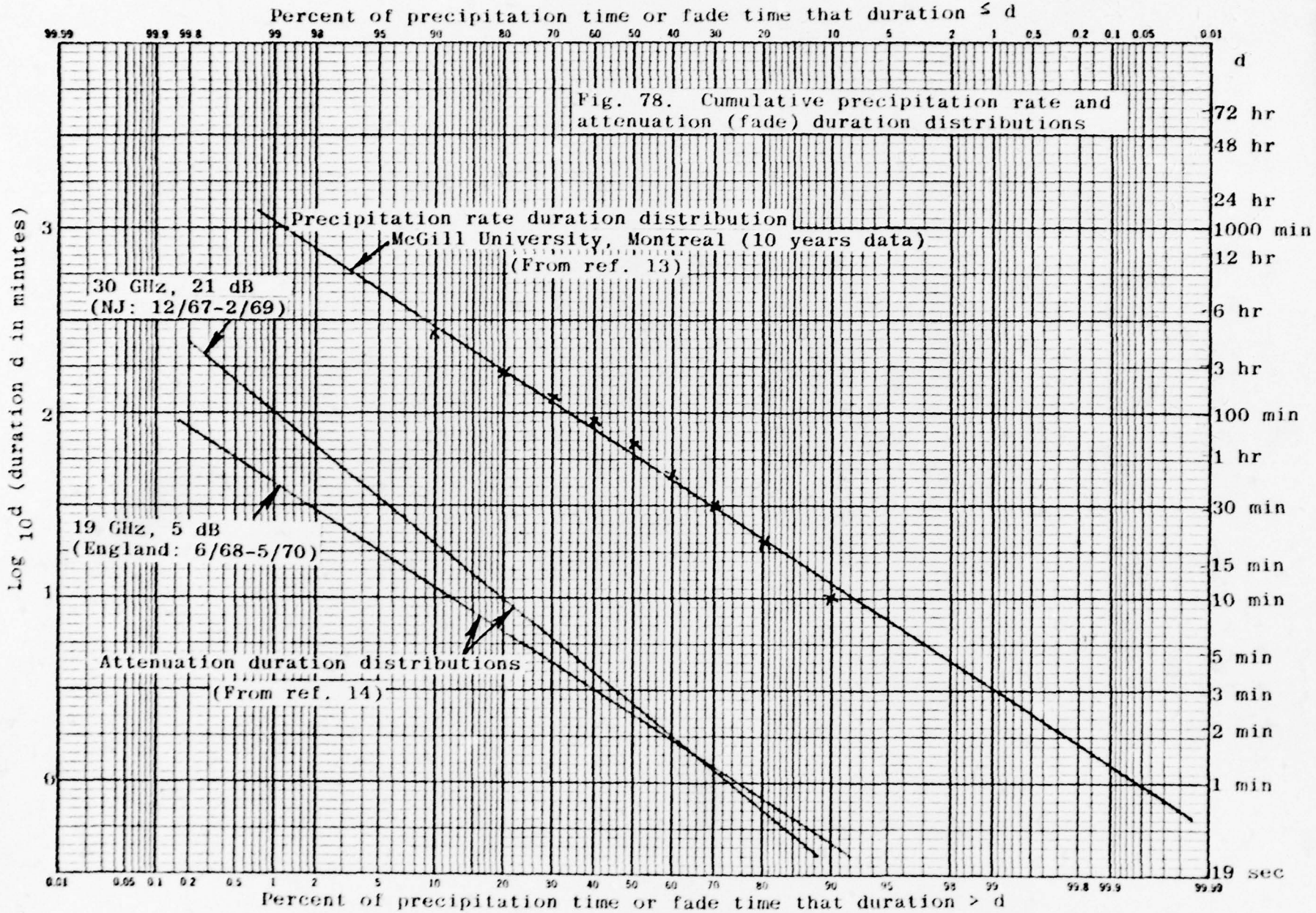

Fig. 78. Cumulative precipitation rate and attenuation (fade) duration distributions

New Jersey measurements, 21 dB was exceeded 3% of raining time. (2) From Table 6, the overall precipitation frequency in England (type-C climate) is about 0.3, and in New Jersey (type-D) climate about 0.15. (3) Multiplying the corresponding pairs of percent of raining time values by the fraction of time that it rains gives the percent (or fraction) of total time that the attenuation exceeded the fade margins, 0.255% and 0.45% respectively. (4) Figure 34 is then entered at 0.255% and 0.45% on the abscissa, and precipitation rates corresponding to the types C and D distributions, respectively, are read off the ordinate: 4.2 mm/hr and 5.6 mm/hr.

The obvious anchoring assumptions are then made: the McGill distribution represents the precipitation-rate duration frequency distribution for a threshold (minimum observable) precipitation rate assumed to be 0.08 mm/hr.* The England attenuation duration distribution represents the precipitation-rate duration frequency distribution for a threshold precipitation rate of 5 mm/hr. We arbitrarily assumed a logarithmic spacing and interpolated parallel distributions for other threshold precipitation rates. The resulting estimated precipitation-rate duration frequency distributions for threshold precipitation rates of 0.05 to 100 mm/hr are shown in Figure 79, which presents a set of universal curves.

Figure 79 can be used with the data in Tables 10, 11 and 12 to estimate outage duration probabilities for specific conditions. This has been done at 44 GHz, and the results appear as probability density functions in Figures 80 to 82. Tables 13, 14 and 15 present the same information in still another form, in terms of the median and mean outage durations and the average number of outages per day during the rainy season.

---

*An arbitrary compromise between the 0.05 and 0.1 mm/hr minimum precipitation rates previously discussed.

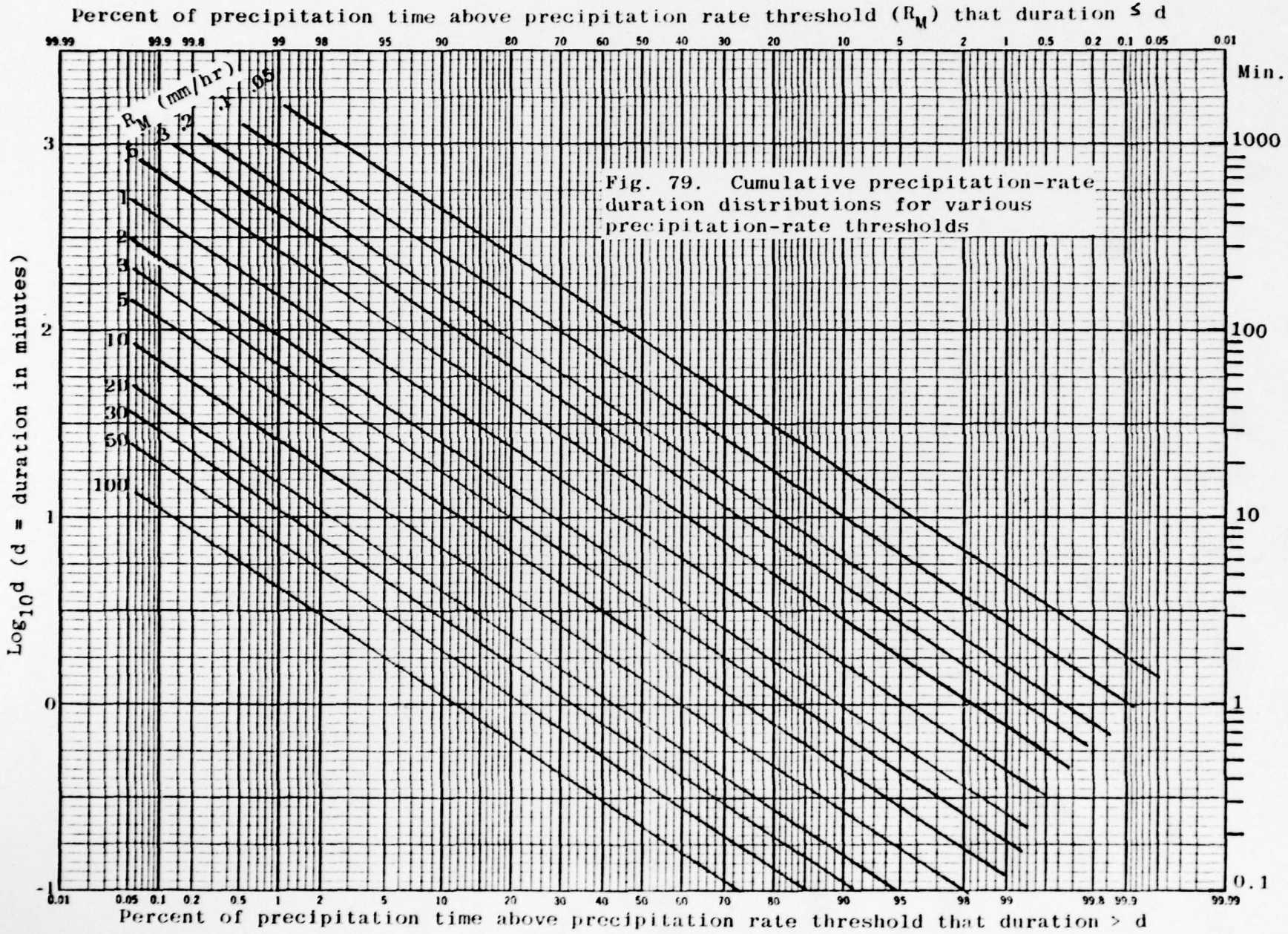

Fig. 79. Cumulative precipitation-rate duration distributions for various precipitation-rate thresholds

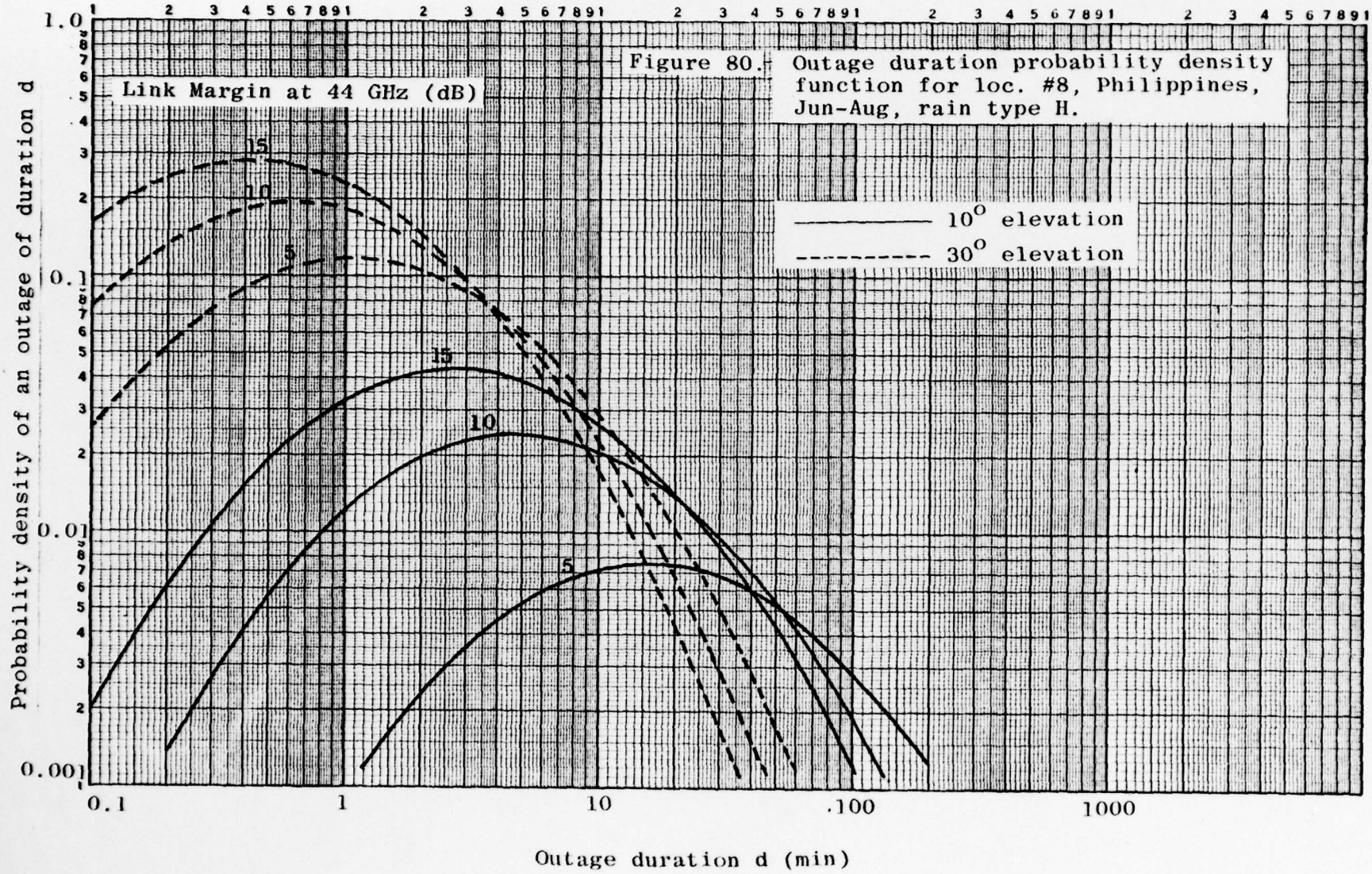

Figure 80. Outage duration probability density function for loc. #8, Philippines, Jun-Aug, rain type H.

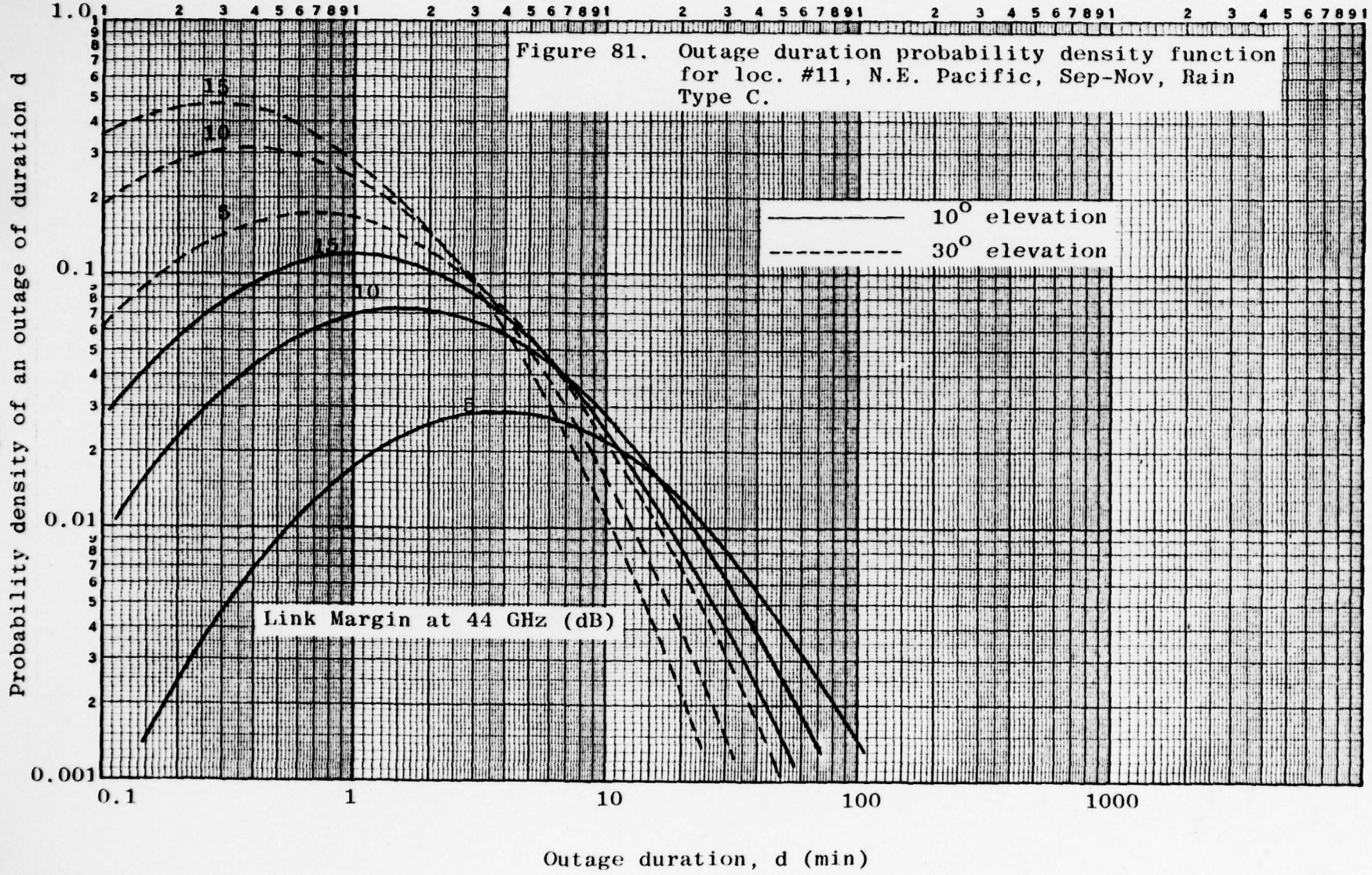

Figure 81. Outage duration probability density function for loc. #11, N.E. Pacific, Sep-Nov, Rain Type C.

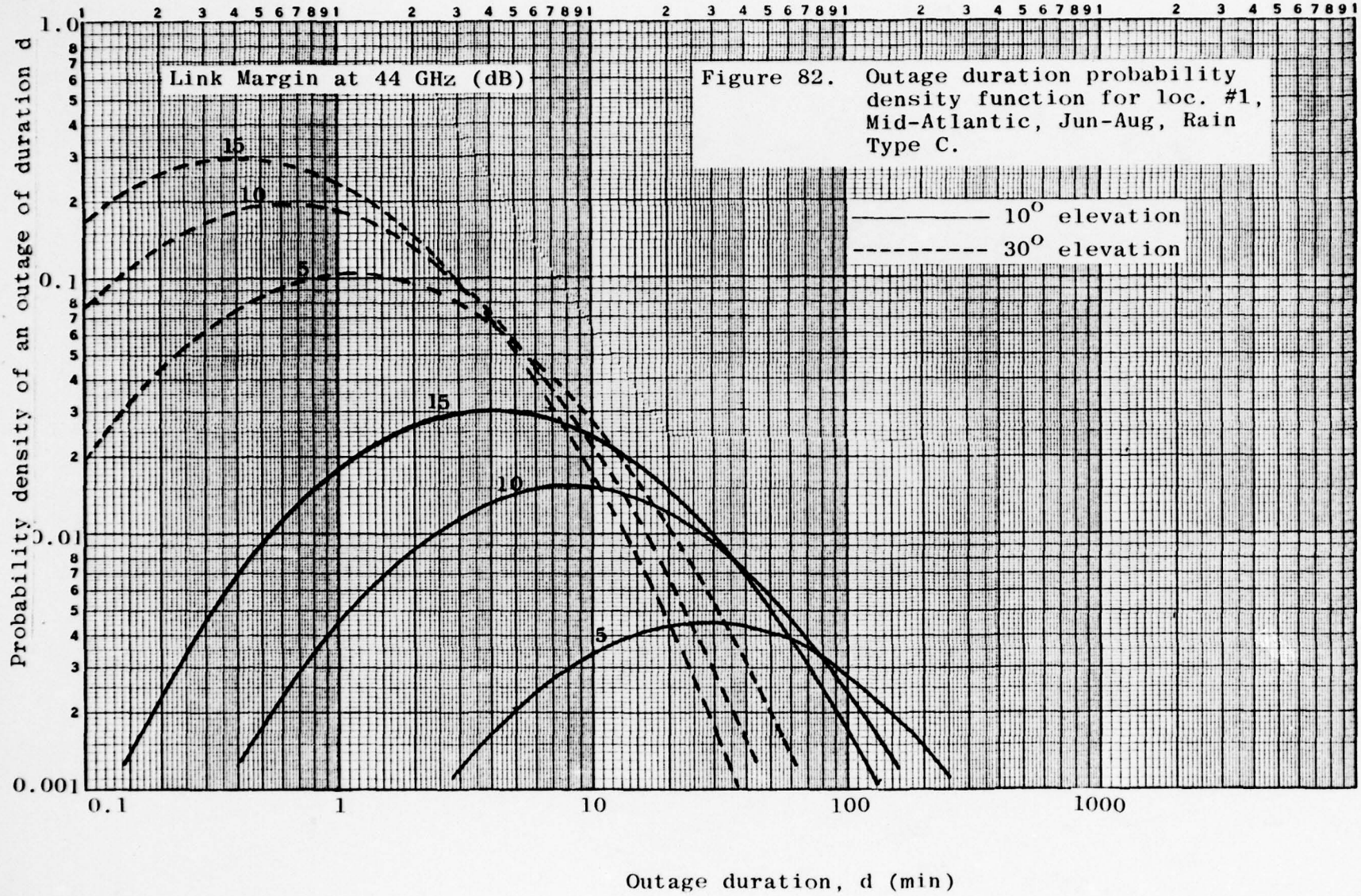

Figure 82. Outage duration probability density function for loc. #1, Mid-Atlantic, Jun-Aug, Rain Type C.

Table 13. MEAN OUTAGE DURATION AND AVERAGE NUMBER OF OUTAGES PER DAY FOR LOC. #8, PHILIPPINES, JUN-AUG, RAIN TYPE H

ELEVATION ANGLE (Deg.)	LINK MARGIN (44 GHz) (dB)	R_M (mm/hr)	P (%)	MEDIAN OUTAGE DURATION* d(min)	MEAN OUTAGE DURATION* d(min)	CUMULATIVE DAILY OUTAGE* (min)	AVG. NUMBER OF OUTAGES* PER DAY
10	5	0.04	15.0	95.2	232.1	216.0	0.9
10	10	0.19	7.8	29.6	72.2	112.3	1.6
10	15	0.41	4.8	16.6	41.2	69.1	1.7
30	5	1.5	2.2	6.3	15.3	31.7	2.1
30	10	3.0	1.15	3.7	9.1	16.56	1.8
30	15	5.0	0.75	2.6	6.2	10.8	1.7

* Rounded off to one decimal place

Table 14. MEAN OUTAGE DURATION AND AVERAGE NUMBER OF OUTAGES PER DAY FOR LOC. #11, NE PACIFIC, SEPT-NOV, RAIN TYPE C'

ELEVATION ANGLE (Deg.	LINK MARGIN (44 GHz) (dB)	R_M (mm/hr)	P (%)	MEDIAN OUTAGE DURATION* d(min)	MEAN OUTAGE DURATION* d(min)	CUMULATIVE DAILY OUTAGE* (min)	AVG. NUMBER OF OUTAGES* PER DAY
10	5	0.25	12.0	24.1	58.7	172.8	2.9
10	10	0.85	4.5	9.6	23.5	64.8	2.8
10	15	1.6	2.2	6.0	14.6	31.7	2.2
30	5	2.6	1.20	4.0	9.8	17.3	1.8
30	10	5.8	0.50	2.2	5.4	7.2	1.3
30	15	9.6	0.25	1.6	3.9	3.6	0.9

* Rounded off to one decimal place

Table 15. MEAN OUTAGE DURATION AND AVERAGE NUMBER OF OUTAGES PER DAY FOR LOC. #1, MID-ATLANTIC, JUN-AUG, RAIN TYPE C

ELEVATION ANGLE (Deg.)	LINK MARGIN (44 GHz) (dB)	R_M (mm/hr)	P (%)	MEDIAN OUTAGE DURATION* d(min)	MEAN OUTAGE DURATION* d(min)	CUMULATIVE DAILY OUTAGE* d(min)	AVG. NUMBER OF OUTAGES* PER DAY
10	5	0.1	31.0	47.9	116.8	446.0	3.8
10	10	0.25	8.7	24.1	58.7	125.3	2.1
10	15	0.62	3.7	13.5	32.9	53.3	1.6
30	5	1.3	1.5	7.0	17.0	21.6	1.3
30	10	3.0	0.35	3.7	9.1	5.0	0.6
30	15	5.2	0.16	2.5	6.0	2.3	0.4

* Rounded off to one decimal place

6.0 CONCLUSIONS AND FUTURE WORK

We began this analysis by examining Crane's precipitation-rate model for earth-to-satellite excess path attenuation because it constituted the best available model. Temperature and drop-size distribution were found to be small effects. We therefore, used 20°C near the equator (latitudes $\leq 30^{\circ}$) and used 0°C for all higher latitudes. The Laws and Parsons low rain-rate drop-size distribution was used for precipitation rates $R_p < 40$ mm/hr and the Laws and Parsons high rain-rate drop-size distribution was used for $R_p > 40$ mm/hr. We smoothed the transition region between the two curves. The excess path attenuations due to precipitation showed no surprising behavior as a function of the eight climate regions (actually defined by eight cumulative precipitation-rate distributions), as a function of frequency, or as a function of elevation angle. However, comparison of Crane's map for the ocean climate regions with world-wide data on ocean precipitation frequency, thunderstorm days and cloud cover showed important differences in detail. For example, we felt that more of the oceans should be type F subtropical arid; that the polar tundra type A extends too far south into the North Atlantic; and that the Mediterranean should not be type D, continental. Examination of the seasonal variation among these parameters and also in total precipitation made it evident that separation into four seasons was almost as important as the separation into eight precipitation rate climates. By combining the data in an annual model, previous work smeared the basic climate types.

Crane makes the correction for spatial correlation as a precipitation-rate-dependent correction to the attenuation. The correction has the form $\gamma(D)R_p^{-\delta(D)}$ where R_p is the one-minute surface point rain rate for a given exceedance probability P. At very high rain rates, the $R_p^{-\delta(D)}$ factor dominates. This results in a flat or even rising attenuation at steep elevation angles. This phenomenon, however, manifests itself for $P < 0.01$ percent of

the time or under conditions for which the excess path attenuation A >100 dB. These conditions ($P < 0.01\%$; A >100 dB) are not the focal point of this study. The domain of primary interest in this study is $1\% \leq P \leq 20\%$ and corresponds to A < 50 dB. At the low precipitation rates corresponding to $P \geq 1\%$, excess path attenuation is dominated by the path length factors $L(\theta)\gamma(D)$. One sees the results of this in the elevation angle plots of Figures 13, 14 and 15. The steep slopes for regions G and H (Figure 18, 10^{o} elevation) arise from the spatial correlation correction factor $\gamma(D)$ augmenting the long path lengths in the tropics. Thus the seasonal mean freezing height ($\overline{FH}$) becomes a key parameter. Investigation showed $\overline{FH}$ to vary strongly with longitude as well as latitude. From Dec-Feb to Jun-Aug, the precipitation-rate climatic regions shift south by 5 to 10^{o} latitude; $\overline{FH}$ shows an even greater shift. The arid subtropical areas expand in the summer hemisphere and contract in the winter hemisphere. Wetness, particularly in the subtropics and tropics, varies considerably from season to season.

6.1 Conclusions

To cope with the large increase in detail, we found it necessary to expand Crane's single map of the climate regions to seasonal geographic maps accompanied by seasonal maps of $\overline{FH}$ (a total of eight maps). This permitted us to show all the detail we had available. To extract all of the data in Crane's cumulative precipitation rate distributions, we replotted them on a log-log scale and smoothed the curves. We based the plot on Crane's tabulated data on $R_p(P)$. Integration under these curves to determine total precipitation showed the need for certain new precipitation-rate distributions for the oceans. We defined three new precipitation rate distributions, A', B' and C'. C' is a small, high precipitation-rate region within region C, while A' and B' replace Crane's regions A and B over the oceans. For the nine precipitation rate regions in our oceanic model, we generated two types of descriptions: a narrative one and a quantitative one. The quantitative description defined each precipitation-rate distribution as a rectangular

block in the precipitation frequency (frequency-of-occurrence) and average daily precipitation (mm/day) domain.

Then we selected thirteen locations covering seven of the nine precipitation-rate regions. The two regions not represented are the mildest region A' (see Fig. 34, page 61) and a small region E (found only in one season, see Fig. 28, page 52). For these locations, we tabulated the seasonal precipitation and precipitation frequency (also the number of thunderstorm days). Using the average daily precipitation rate (mm/day) and frequency of precipitation for the season, local correction factors k and k' were calculated. P becomes k'P and R_p becomes $\frac{k}{k'}R_p$ as a result of these local corrections. This makes the frequency of occurrence and total precipitation (the integral under the precipitation rate distribution) correct for the specific locality and season.

The graphs of section 4.0 contain the k correction factor but not k'. The data from Tables 10-12 have been corrected for frequency-of-occurrence and its effect on R_p at the link margin by using k'P and $\frac{k}{k'}R_p$. For 13 locations around the world, the seasonal extremes of attenuation have been plotted for 44, 21 and 7.5 GHz and for elevation angles of 10, 20 and 30°.

The 0.001 percent of the year end of the curve involves rare events; thus high variability from year to year can be expected. On the other hand, the 1 to 10 percent of the year end of the curves involves commonplace events. Thus the year-to-year variability in this portion of the curves should be much smaller. Inspection of the 13 graphs at 5 percent of the time and 20° elevation shows that about 13 dB is sufficient link margin during the rainy season anywhere in the world at 44 GHz. We have presented cumulative outage duration distributions using Lin's conclusion that they are log-normally distributed. The same results for the three locations of Tables 10, 11 and 12 appear as probability density functions in Figures 80 to 82. Tables 13, 14 and 15 present the same information in still another form, in terms of the median and mean outage durations and the average number of outages per day during the rainy season.

The highest rainfall regions, i.e., the regions of highest precipitation rate and greatest frequency of occurrence, will require better satellite coverage than other regions. These high rain-rate regions are in the tropics and subtropics. Constellations using an adequate number of geostationary or low-inclination-orbit satellites can provide such coverage. Fewer satellites in view and thus more links operating at low elevation angles (around 20^{o}) can be tolerated at high latitudes since the precipitation rate is so much less. At high latitudes, the mean freezing height is at ground level for part of the year and much of the precipitation falls as dry, relatively lossless snow.

6.2 Future Work

The following problems require analysis; we need to :

- Develop a cloud attenuation model which approaches the rain attenuation for high P by coming down in P from the clear weather side.

Path attenuation does not drop off to zero as R_p falls to zero because of the clouds. At 20^{o} elevation and 44 GHz, cloud effects may be significant for $5 \leq P \leq 20$ percent of the time.

- Extend the seasonal model of this study to the continental areas. The large amount of data available on continental weather and the greater importance of local variation make this a more complex study than the development of the oceanic model.
- Validate the continental model through the use of available data from satellite beacons, radiometers and suntrackers.
- Refine and extend the oceanic model. This includes further work on:
  - Minimum observable precipitation rate
  - Limits on regional attenuations
  - Drop size distribution effects
  - Year to year variation
    Mean and worst year in 5 to 15 years

- Detail within the geographically largest regions
- Sensitivity analysis for integration and attenuation calculation (convective fraction)
- Effect of supercooling
- Outage duration distribution by rain type
- Inter-outage distribution within a storm
- Estimating number of rainy days per season, i.e., interoutage distribution between storms
- Deterministic rainfall, e.g. occurring at a fixed time of day
- Automating all corrections to characteristic R_p
- Effect of rain on sky temperature, system degradation
- Applications software for link designers
- Adequacy of a seasonal $\overline{FH}$ versus a distribution of FH
- Correlation between FH and occurrence of precipitation
- Derivation of purer oceanic precipitation rate distributions for a seasonal model
- Developing a systematic and accurate way to integrate the precipitation rate curves and to apply the correction factors
- Making the daily amount (average daily precipitation during a season) and the frequency of occurrence corrections simultaneously
- Verifying model does account for the fact that tropical rain does not extend up to the $\overline{FH}$

REFERENCES

1. Feldman, N.E. and S.J. Dudzinsky, Jr., A New Approach to Millimeter-Wave Communications, The Rand Corporation, R-1936-RC, April 1977.

2. Hogg, D.C. and T. Chu, "The Role of Rain In Satellite Communications", Proc. of the IEEE, September 1975, pp. 1308-1331.

3. Mundie, L.G. and N.E. Feldman, The Feasibility of Employing Frequencies Between 20 and 300 GHz for Earth-Satellite Communications Links, The Rand Corporation, R-2275-DCA, May 1978.

4. Crane, R.K., "A Global Model for Rain Attenuation Predication", Eastcon Conference Proceedings, 1978.

5. Crane, R.K., "Rain Attenuation Prediction", Draft Submission to the CCIR Special Preparatory Meeting in Geneva, 1978, Document F5/003, April 25, 1978.

6. Olsen, R.L., et. al., "The aR^b Relation in the Calculation of Rain Attenuation", IEEE Transactions On Antennas and Propagation, Vol. AP-26, No. 2, March 1978, pp. 318-329.

7. Möller, F., "Viertelsjahrskarten des Niederschlags für die ganze Erde, Petermanns Geographische Mitteilungen, Justus Perthes, Gotha, 1951, pp. 1-7.

8. Crutcher, H.L. and O.M. Davis, U.S. Navy Marine Climate Atlas of the World, Volume VIII, The World, NAVAIR 50-1C-54, Naval Weather Service Command, March 1969.

9. Sadler, J.C., L. Oda and B.J. Kilonsky, Pacific Ocean Cloudiness from Satellite Observations, UHMET 76-01, Dept. of Meterology, Univ. of Hawaii, Octover 1976.

10. World Meteorological Organization, World Distribution of Thunderstorm Days; Part 2: Tables of Marine Data and World Maps, Secretariate of the WMO, Geneva, 1956.

11. United States Air Force, Handbook of Geophysics, Revised Edition, The Macmillan Co., New York, 1960.

12. Crutcher, H.L. and J.J. Meserve, Selected Level Heights, Temperatures and Dew Points for the Northern Hemisphere, NAVAIR 50-1C-52, Naval Weather Service Command, January 1970.

REFERENCES (cont'd)

13. Drufuca, G and I. Zawadzki, "Statistics of Raingage Data", J. Appl. Meteorol., Vol. 14, No. 8, Dec. 1975, pp. 1419-1429.

14. Lin, S.H., "Statistical Behavior of Rain Attenuation", The Bell System Technical Journal, Vol. 52, No. 4, April 1973, pp. 557-581.